Chem. Erde **63** (2003), 185–246
Urban & Fischer Verlag
http://www.urbanfischer.de/journals/chemerd

CHEMIE der ERDE GEOCHEMISTRY

INVITED REVIEW

The Kaidun Microbreccia Meteorite: A Harvest from the Inner and Outer Asteroid Belt

Michael Zolensky[1,*] and Andrei Ivanov[2]

[1] Astromaterials Research and Exploration Science, NASA Johnson Space Center, Houston, TX, USA
[2] Vernadsky Institute, Moscow, Russia

Received: 16. 5. 2003 · Accepted: 14. 7. 2003

Abstract

We summarize the results of two decades of research into the complex Kaidun microbrecccia meteorite. This meteorite contains an unprecedented accumulation of materials from many different asteroids, principally carbonaceous and enstatite chondrites, but also many other frequently strange materials. The following well-known meteorite types are definitely present in Kaidun: EH3–5, EL3, CV3, CM1-2, and R chondrites. Also present in Kaidun are new C1 and C2 type lithologies, unique alkaline-enriched clasts, impact melt products, phosphide-bearing clasts, vein- and cavity-filling materials, new enstatite-bearing clasts, and Ca-rich achondrite materials. Many further materials have yet to be characterized.

Obviously, the Kaidun parent object accumulated materials from across the entire main asteroid belt. Many of these materials were subjected to varying levels of physical processing, heating, shock, melting, and aqueous alteration.

Kaidun is important because it contains many asteroidal materials we have not seen before, providing a more complete view of the diversity of materials in the asteroid belt than has been provided by other meteorites. This is possible because of the small, generally sub-millimeter-size of the component clasts in Kaidun – it is far easier for these smaller objects to scatter throughout the solar system than it is for larger, conventionally-sized meteorites.

We suggest that the final parent object where Kaidun was assembled was a large body with a C-type asteroid signature – possible asteroid 1-Ceres or the martian moon Phobos.

Key words: Kaidun, Asteroids, Carbonaceous Chondrites, Enstatite Chondrites, R Chondrites, Oxygen Isotopes

*** Corresponding address:**
Michael Zolensky, Astromaterials Research and Exploration Science, NASA Johnson Space Center, Houston, TX 77058 USA
Tel.: 001-281-483-5128; Fax: 001-281-483-5347; e-mail: michael.e.zolensky@nasa.gov

0009-2819/03/63/03-185 $ 15.00/0

Introduction

Meteorites remain the key source of information about the birth and early history of our solar system. Over the past millennia (and predominantly over just the past two centuries) we have accumulated several tens of thousands of meteorite samples for study and adulation, and so one might imagine that by this time we must have been provided with samples of just about every body in the solar system. Unfortunately, the dynamics of meteorite delivery to Earth are so selective that we actually have samples of, at best, on the order of 100 bodies (including Mars and Earth's moon) (Meibom and Clark 1999). Thus, it is with keen anticipation that every newly-fallen or recognized meteorite is examined, as each one carries the potential of providing critical information on an entirely new extraterrestrial body.

Against this background it is easy to appreciate the value of a new meteorite that provides samples of not merely one, but rather many previously unsampled solar system bodies. This is the opportunity presented by the Kaidun meteorite

The Kaidun meteorite fell in the Peoples Republic of South Yemen on 3 December 1980, into a military base of the USSR, at a time of civil war. One can only imagine the effects of the incoming fireball on the troops. A single stone was recovered immediately after its fall, which largely prevented terrestrial alteration of the meteorite due to hydration, oxidation, and hydrolysis. We are extremely fortunate that Kaidun: (1) was an observed fall, (2) fell into a desert country, (3) was recovered immediately, and (4) was immediately transported to Moscow for detailed study rather than disappearing into a private collection or suffering a worse fate.

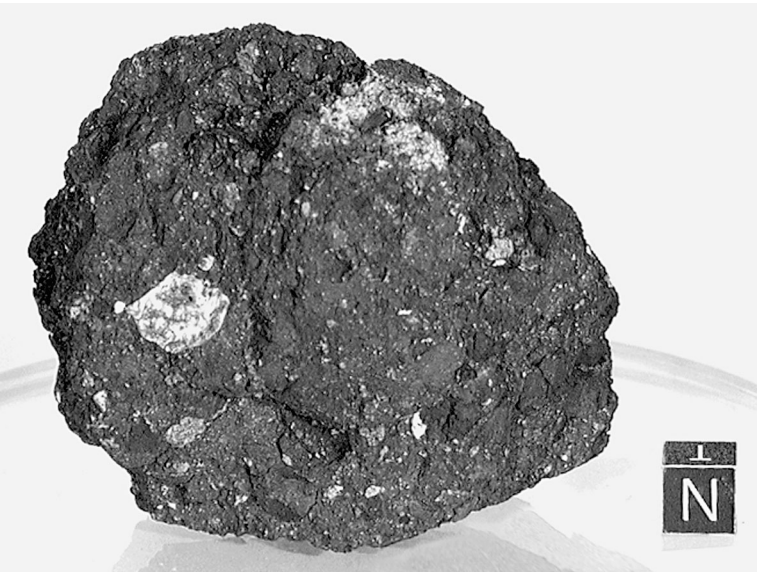

Fig. 1. Image of the entire recovered Kaidun meteorite. The small block at lower right measures 1 cm on edge.

The meteorite split upon hitting the ground, and then being very weak, was crushed during transportation. The total mass of the received material was about 850 g, which included several fragments of varying sizes, numerous small fragments and crumbs. The largest of the remaining pieces weighed 507 g and was half covered with fusion crust (Fig. 1).

The Kaidun meteorite is a complex microbreccia (cover; Fig. 2). While a brecciated structure is rather characteristic of many stony meteorites (Binns 1967; Keil 1982; Rubin 1983), the Kaidun meteorite contains only mm-sized clasts – an apparently unique feature.

Usually chondritic breccias are monomict ones and their components differ only in the extent of their shock and/or thermal alteration. However, many chondritic breccias contain fragments of foreign material (xenoliths), usually fragments of chondrites of other groups (e.g., Keil 1982; Olsen et al. 1988). Usually these xenoliths are ordinary or carbonaceous chondrite materials. Enstatite chondrites, for example, have not been found as xenoliths.

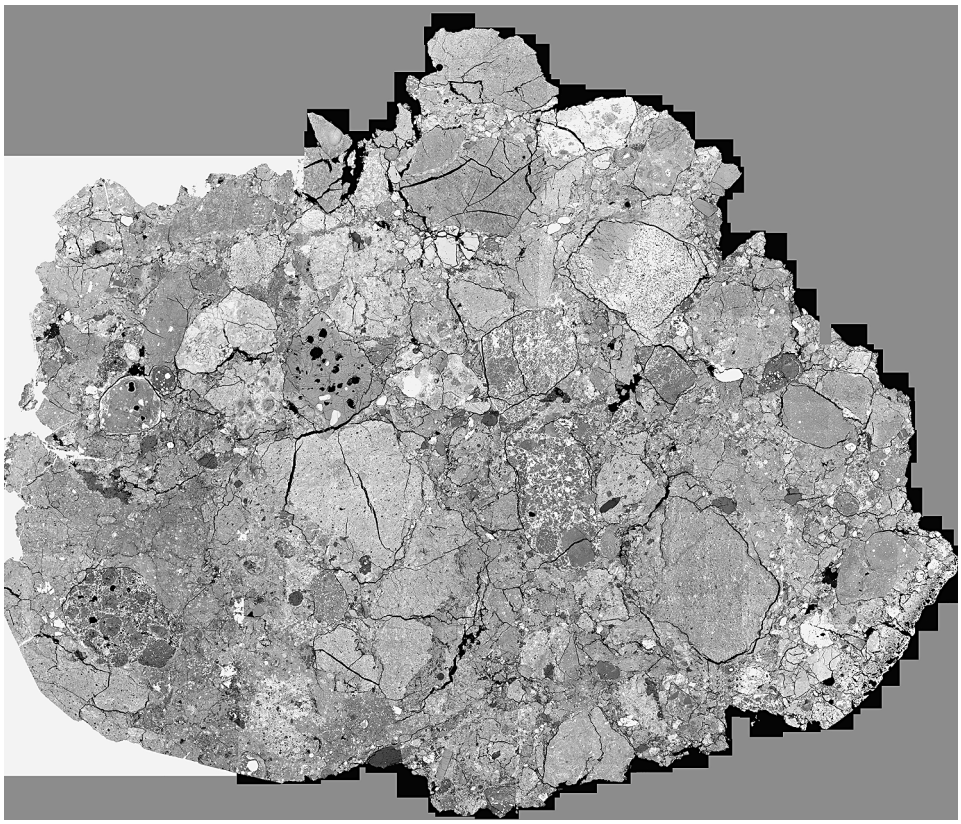

Fig. 2. BSE image of one Kaidun thin section, showing the remarkable number of diverse lithologies. Image measures 4 cm across.

The Kaidun meteorite is different from all other meteorites. The extremely high heterogeneity of this meteorite was shown during its preliminary investigation. Work quickly demonstrated that Kaidun consists of a mixture of "incompatible" types of meteoritic material – carbonaceous and enstatite chondrites, i.e. corresponding to the most oxidized and the most reduced samples of meteorite materials. With further investigation, we gradually realized that Kaidun contains samples of *many* parent body types. Almost every new section of Kaidun is found to contain some new material, frequently lithologies not previously encountered in any meteorite, and sometimes entirely new minerals.

This review paper suffers from four critical, but inevitable, limitations, which faithful readers need to constantly bear in mind.

(1) The reported results come from only about 20 years of intermittent work by principally ourselves and a few close collaborators. However, samples of Kaidun are slowly migrating through the meteoritical community.

(2) The limited number of investigators who have worked on Kaidun necessarily means that only a few opinions are represented among the discussions. Fortunately, the principal authors disagree on many points of interpretation, and so the reader is presented with some variety of opinion.

(3) Kaidun contains an unprecedented diversity of materials for a single meteorite (and not a very large one at that), and to make matters worse practically every new sample that is prepared of Kaidun is found to contain something completely new and perplexing. Therefore, there is space in this paper for only a summary of results from a few key lithologies.

(4) The total mass of the Kaidun meteorite was less than 1 kg, and consequently the samples of each of the lithologies within Kaidun are rather smaller than desirable to completely characterize them. For example, the apparent lack of chondrules in most of the Kaidun lithologies could be due merely to statistically small sampling.

Bulk Compositions and Classifications

There are serious problems with any attempt to classify Kaidun lithologies, even major ones, based upon bulk chemical and isotopic compositions. A major complication unique to this meteorite is the fact that it is a fragmental breccia of very different chondrite materials, with most component clasts measuring a few mm in size or less – often *much* less. For example, the O isotopic data for many Kaidun samples (Fig. 3) plot between the fields of E, CI and CM chondrites, indicating that these are intimate mixtures of these chondrite materials. Inspection of any Kaidun thin section verifies this hypothesis (Fig. 2).

Detailed analyses have been made on Kaidun samples which appeared (at mm scales) to be rather homogeneous. Unfortunately, these data sets frequently indicate quite the opposite. For example, Kaidun aliquot 40.22 was analyzed both by INAA (Fig. 4) as well as for O isotopes (Clayton et al. 1994) (Fig. 3). It was a sample of one of the dominant lithologies in Kaidun, based upon general appearance under a binocular microscope. As can be seen in a comparison of Figs. 3 and 4, the bulk composition for many lithophile and siderophile elements are similar to both CM and CR chondrites, although the sample is enriched in the violatile lithophiles Mn, P, and Na, and depleted in Ti. However, the O

isotopic composition of 40.22 lies above the fields for both CM and CR chondrites, though it is closest to CR. One might conclude from these observations that 40.22 is most likely CR chondrite material. The problem with this is that we have seen no petrographically recognizable clasts of CR material within Kaidun, using the criteria developed by Weisberg et al. (1993). Similarly, bulk data for light elements and isotopes are of no assistance here. As reported by Kerridge (1985), the bulk Kaidun N composition is 1890 µg/g and the ^{15}N isotopic composition is +165. This is most compatible with ranges for CR chondrites (510–850 µg/g and +165–190, respectively), but are also within the ranges of CM chondrites (345–1150 µg/g and +13–335, respectively) and CI chondrites (1250–1855 µg/g and +31–52). Unfortunately, no samples of 40.22 were subjected to mineralogic analysis, so this particular issue will probably remain unresolved. Sample 40.22 could be CM or could be CR. On balance, the apparent lack of recognizable CR material in the available thin sections suggests that classification as CM or as an ungrouped chondrite is most appropriate.

In the following text we briefly describe the principal Kaidun lithologies we have encountered to date. Lest the reader think that this is an exhaustive listing of Kaidun lithologies, we caution that practically every new thin section we have made of this meteorite has revealed something new and strange.

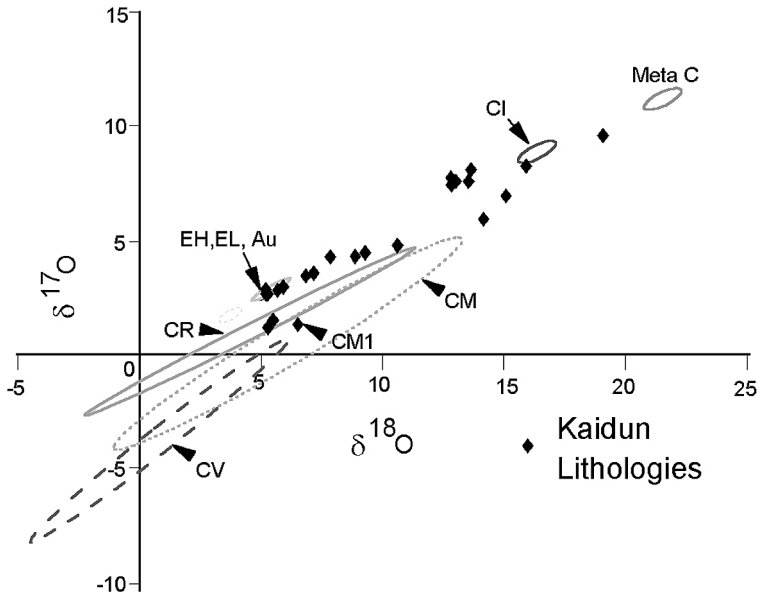

Fig. 3. Plot of the oxygen isotopic compositions of 24 separate Kaidun samples (black diamonds), compared to the fields for CR, CV, CM, CI, metamorphosed C (Meta C) chondrites, enstatite chondrites (EH, EL) and aubrites (Au). Of the Kaidun samples plotted here, only the CM1 lithology is explicitly identified here. It is clear from this diagram that most of the analyzed Kaidun samples actually consist of mixtures of CI (or C1), CM (or C2, but apparently not CR), and enstatite chondrite materials. This conclusion is supported by our mineralogical analyses. Lithologies like CV and R are too rare in Kaidun to have a significant leverage effect on the bulk compositions. One Kaidun sample lies between the CI and metamorphosed C chondrites, and may be metamorphosed (?).

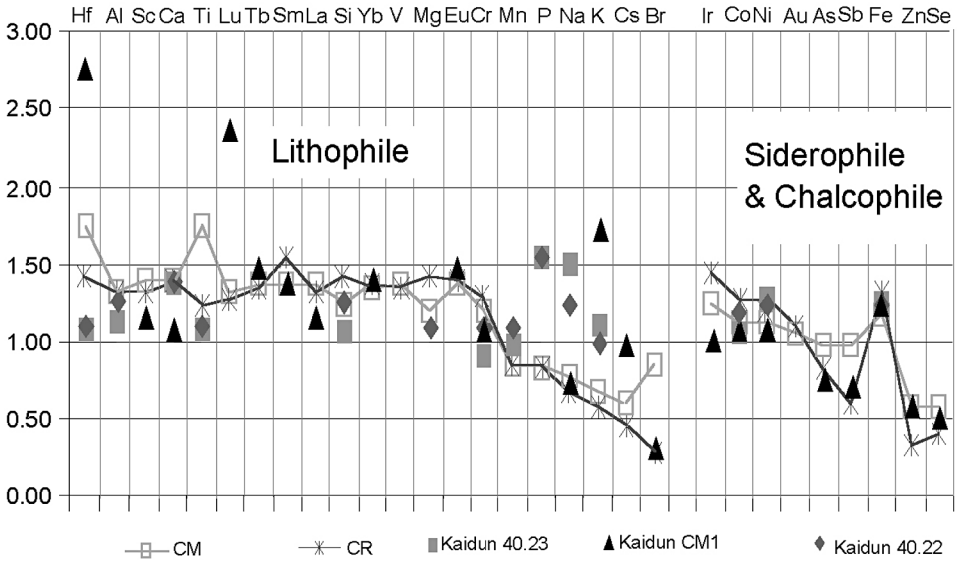

Fig. 4. Bulk chemical compositions of three separate Kaidun samples, normalized to average CI chondrites and plotted according to decreasing 50% condensation temperature. These Kaidun samples were originally chosen because they appeared to resemble CI, CM1 and CR chondrites (only the CM1 is identified). It is clear that the Kaidun samples are most similar, but not identical, to CR and CM chondrites. Data from David Mittlefehldt.

Enstatite Chondrite Lithologies

One of the many intriguing peculiarities of the Kaidun breccia is the presence of many different enstatite chondrite lithologies, which together make up a large fraction of the entire meteorite. These lithologies differ in their chemical compositions – both EH and EL chondrites are present – as well as in their detailed petrography.

EH Chondrite Lithologies

Three EH lithologies (#01.3.06 EH3–4; #40,7,1 EH5 – previously called Kaidun III; #02.04 EH5) have been studied rather exhaustively (Ivanov 1989a; Ivanov et al. 1986, 1996a,b, 1997, 1998). They are rather similar in mineralogy and mineral compositions, but display noticeable differences in petrography (Figs. 5, 6).

- Mineralogy

Enstatite, plagioclase, silica, Fe,Ni, schreibersite, troilite, niningerite and unusual Fe,Cr-sulfides are present in all EH lithologies. Carbon and perryite are rather usual. Oldhamite, sphalerite, djerfisherite, schöllhornite, daubreelite, roedderite and Ca,Fe-phosphate are rare. Such mineral associations are typical for EH chondrites (Keil 1968). A particularly interesting feature is that hydrated phases are abundant in all EH lithologies in Kaidun, in contrast to all other examples of EH chondrites which are entirely anhydrous.

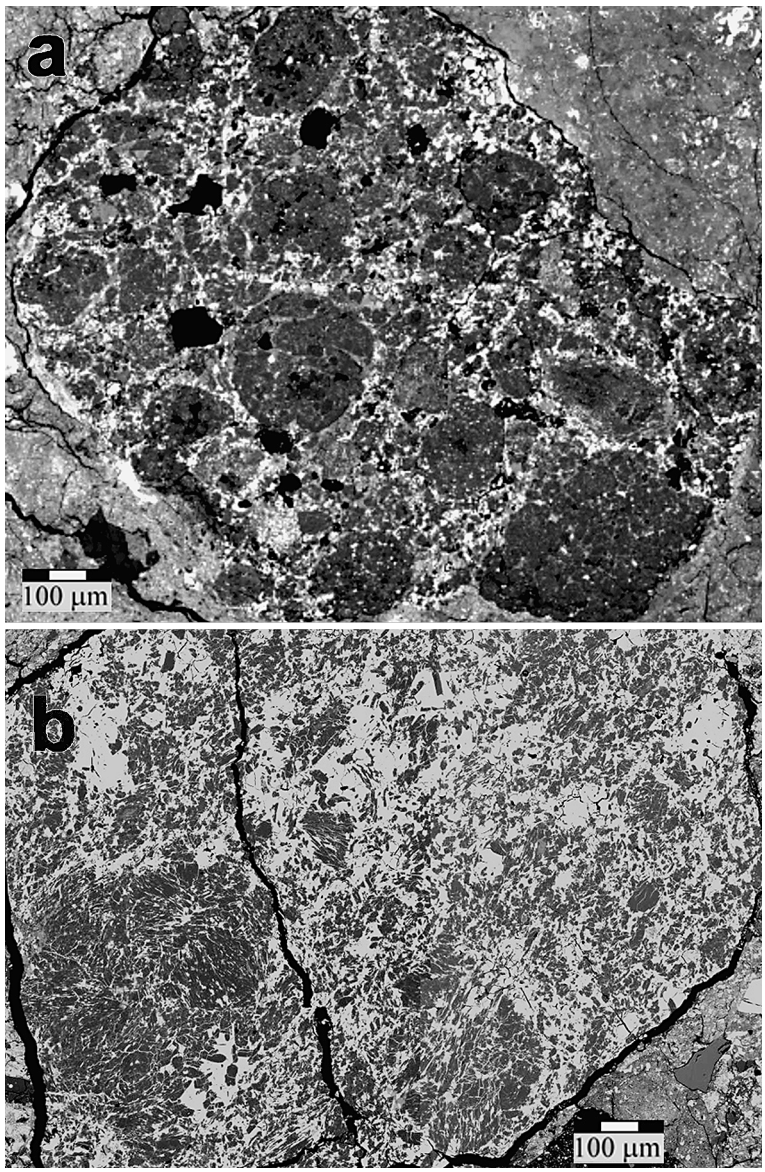

Fig. 5. Low-magnification BSE images of typical enstatite chondrite lithologies in Kaidun. Metal is the major white and enstatite the major black phase in these images. (a) EH3 lithology. (b) EH5 lithology; note chondrule at lower left of image.

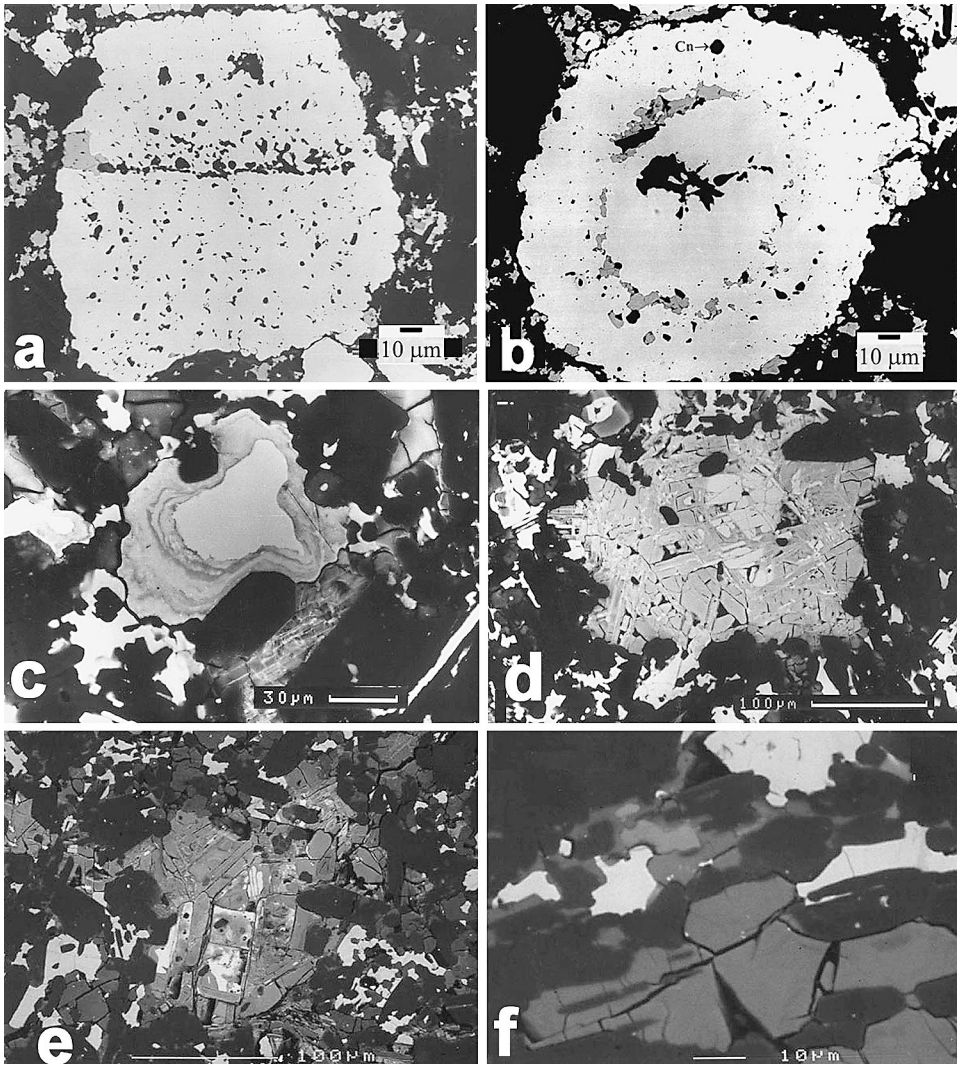

Fig. 6. BSE images of metal nodules from EH3–4 fragment #01.3.06. (**a**) A nodule of type I has a globular structure, which is reflected in a chain-like disposition of the inclusions and in rugged festooned contours of the nodule. (**b**) A nodule of type II shows a massive core and globular mantle. Dark areas in the center of the nodule core are holes. Gray grains in the transition zone between the massive core and globular mantle are sulfides (mainly troilite, rare grains of niningerite and oldhamite are also present); black is silica. Cn = carbon inclusion. (**c**) and (**d**): Altered grains of schreibersite (**c**) and Fe-Ni metal (**d**) at the rim of the EH5 fragment #40.7.1. (**e**) and (**f**) Grains of Fe-rich hydrated phases in the EH5 fragment #02.04. (**e**) A large Fe-Ni grain in the marginal part of the fragment is replaced by the hydrated phase of type I (gray). (**f**) Grains of a hydrated phase of type III (gray) in the central part of the fragment. Grains contain elongated enstatite crystals (dark). Light areas are troilite.

Enstatite (usually En >98) is the principal mineral in this lithology, of course. Plagioclase or glass of plagioclase composition (Ab >95) fills small interstices between enstatite grains in chondrules and is found in the matrix.

Silica usually is present as small grains together with plagioclase. However, it shows different cathodoluminescence colors in different lithologies: pink luminescence in #01.3.06 and weak gray-blue turned red after exposition of an electron beam in #02.04. This appears to suggest that silica in #01.3.06 is quartz and in #02.04 is cristobalite (Frondel 1975).

Fe-Ni metal forms large aggregates of different types and abundances in the matrix (Figs. 5, 6a,b). Metal is rather similar in all lithologies in Ni contents (5.5–5.8 wt.%) but with varying Si contents (2.8 wt.% in #40.7.1, 3.1–3.3 wt.% in others). Rare metal grains in chondrules are poorer in Si (1.6–2.1 wt.%). Schreibersite is usually present in the matrix in association with kamacite. It is rich in Ni (18.8–19.7 wt.%) in all lithologies.

Troilite is the dominant sulfide. It typically has relatively constant contents of Mn (< 0.1 wt.%), Ti (~0.35 wt.%) and Cr (0.8–1.0 wt.%). Niningerite is also a typical matrix mineral. Its composition is similar in all Kaidun EH lithologies and shows high Mn contents (10.3–11.8 wt.%) that are characteristic of the most common group of EH niningerites (Ehlers and El Goresy 1988).

A new unusual Fe-Cr sulfide (Fig. 6c,d) is present in all Kaidun EH lithologies (Ivanov 1989a, Ivanov et al 1986b, 1996b, 1997, 1998) and is also found in other EH chondrites (Lin et al 1990). This phase is close to daubreelite in stoichiometry but has consistently low analytical totals of 92–94 wt.%. In contrast to normal daubreelite this sulfide shows strong optical anisotropy. This phase is characterized by its Na content (~0.3 wt.%). Compared to the composition of normal daubreelite from other enstatite chondrites (Keil 1968, Ehlers and El Goresy 1988, Kimura et al 1993), the new phase has low Mn contents (≤0.3 wt.%). There is also a noticeable difference in the metal/sulfur ratio, which is higher in the new phase (0.80 on average) in comparison with such ratios in daubreelite of the enstatite chondrites (0.73–0.77) (Keil 1968; Ehlers and El Goresy 1988). This suggests that OH may be present in the new phase.

One grain of Fe-Cr sulfide was found in Kaidun lithology #02.04 whose composition differs markedly from the others. This grain is associated with an enstatite crystal within a large troilite grain. The Fe-Cr sulfide grain is strongly enriched in Mn (1.6 wt.%) and lacks Na. The metal/sulfide ratio in this grain is 0.73, i.e. matches that of daubreelite in the enstatite chondrites.

- Lithology #01.3.06

This lithology is characterized by the presence of unusual metal nodules in the matrix (Fig. 6a,b) (Ivanov et al 1996a,b, 1997). They are large (up to 300 µm across) and can be divided into three petrographic types. Type I nodules (Fig. 6a) have irregular shapes, are relatively small size, and have a globular structure. They consist of grains (globules) of metal up to 20 µm across with small (usually < 5 µm) inclusions at the edges. The globular structure of the nodules is reflected in a chain-like distribution of the inclusions and in the rugged, festooned contours of the nodules. Type II nodules (Fig. 6b) are more rounded or ellipsoidal and typically have a zoned structure. The central cores of these nodules are massive kamacite, while the mantles have globular structures and contain inclusions. The transition zone between core and mantle contains sulfide and silicate grains. Type III nodules also have a rounded shape, but no internal structure. They are noticeably bigger, up to 20 µm.

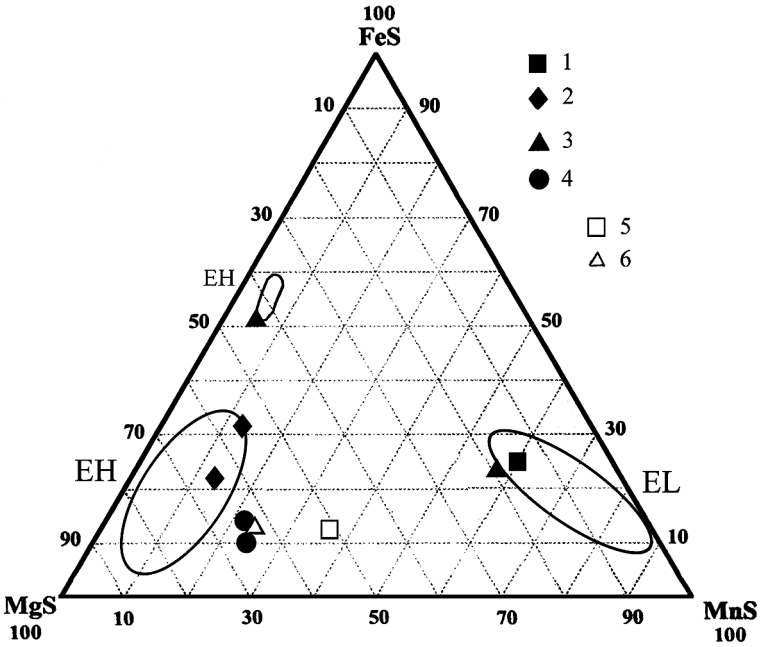

Fig. 7. Compositions of cubic sulfides from the Kaidun meteorite. The compositions of EL and EH sulfides are shown by ellipses (Lin et al. 1990; Patzer et al. 2001). 1 – Kaidun EL fragment; 2 – Kaidun EH fragments; 3 – separate grains from Kaidun carbonaceous breccias; 4 – Kaidun sulfide-enstatite aggregates. The compositions of E sulfides (5) from Y793225 chondrite (Lin et al. 1990) and an exotic grain (6) from Qingzhen (Ehlers and El Goresy 1988) are shown. The compositions of sulfides from the Kaidun sulfide-enstatite aggregates and c are similar in this plot. However, they differ noticeably in Ca contents: about 5 wt.% in the Kaidun aggregates and <1 wt.% in the Qingzhen grain.

The inclusions in the nodules are subdivided into five chemical types: (A) virtually pure silica; (B) glass of albite composition; (C) a mixture of silica and sodium sulfide; (D) enstatite; and (E) roedderite. The inclusions of the A, B, and C types are fairly common in the nodules, and inclusions of type D are rare, and a type E inclusion was encountered only once. Inclusions of multiphase composition also occur. Nodules can contain inclusions of different types. No relationship was noted between the compositions, shapes and sizes of the inclusions.

Of special interest are the type C inclusions. Their compositions are characterized by analytical totals close to 100 wt.%, an S/Na atomic ratio close to unity, a high (50–65 wt.%) content of SiO_2, and the invariable presence of Fe. Inclusions in metal nodules were previously found in a number of ordinary and carbonaceous chondrites (Perron et al 1990; Zanda et al 1990; Zanda 1992) and in the EH3 chondrite Y-691 (Kimura 1988; Ikeda 1989). The inclusions in the studied Kaidun lithology and in the E chondrite Y-691 are morphologically and chemically similar, except that the Kaidun lithology contains inclusions that are a mixture of SiO_2 and sodium sulfide (Fig. 8).

There are no known chemical compounds which fit the composition of the type C inclusions (Fig. 8). In the Na-S system, the only compound whose Na/S atomic ratio is equal to unity is Na_2S_2 (Samsonov and Drozdova 1972). These inclusions are likely to contain a mixture of SiO_2 and Na_2S_2. This is the first known occurrence of a simple alkali-metal sulfide in nature.

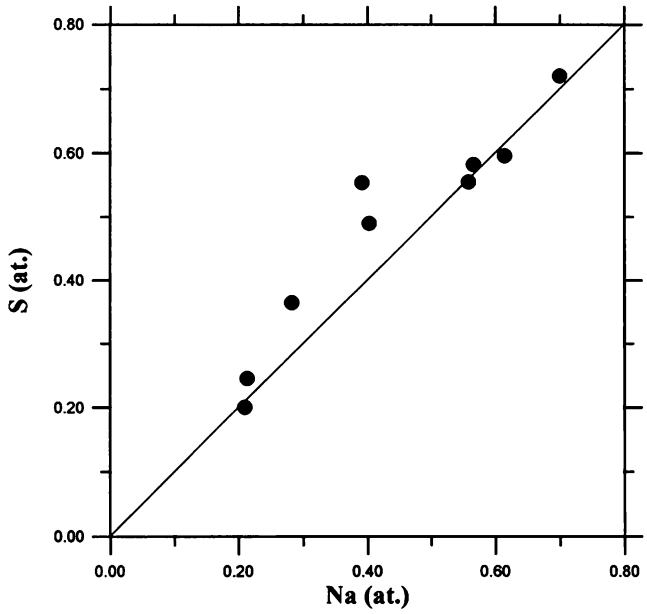

Fig. 8. Sodium vs. sulfur atomic percent in the type C inclusions in metal nodules from EH3–4 fragment #01.3.06. The diagonal line shows the Na/S ratio equal to 1.

The formation of inclusions in metal nodules of various chondrite types is commonly attributed to the separation of components of the inclusions from the metal phase due to cooling or metamorphism (Perron et al 1990; Zanda et al 1990). These processes are possible in the case of the type A inclusions (silica). However, such processes cannot easily explain the formation of the entire compositional range of the inclusions and, especially, the presence of the type C inclusions (containing sodium sulfide), two components of which (Na and S) condense at relatively low temperatures and do not occur in the metal in appreciable amounts. Moreover, metal recrystallization is expected to produce a granular (granoblastic) rather than a globular texture.

An alternative mechanism of the formation of the inclusions is the condensation process itself. The CWPI model (Petaev and Wood 1998) shows the possibility of sodium sulfide formation and preservation by condensate isolation. Inclusions may have formed not only by direct condensation, but also by gas-solid reactions.

The type I metal nodules were probably formed as the result of agglomeration of individual kamacite grains (globules), which were similar to those present in the matrix. Condensates that formed thin films on the surfaces of the grains have been preserved in the nodules. The aggregation of metal grains in the nodules and the compaction of the latter led to a redistribution of condensed material and to the formation of the inclusions, which were arranged as chains along the boundaries of the globules. The condensed material may have recrystallized, but it retained its composition in the closed system within the nodules. The structure of nodules of types I and II suggests that the processes of their formation were more complicated and include the remelting of previously formed metal aggregates. A more detailed treatment of the formation mechanism of inclusions and nodules in this Kaidun lithology is presented by Ivanov et al. (1996b).

- Lithology #40.7.1

This lithology is characterized by a coarse-grained structure (Ivanov et al. 1986). Large Fe-Ni metal grains show a morphology of polycrystalline octahedra, similar to the structure of metal grains in the St. Mark's EH5 chondrite. The formation of this morphology is connected with isolation of carbon in the form of graphite plates along the octahedral faces of metal during cooling (Grokhovsky and Ivanov 1986).

This lithology, as well as most EH lithologies in Kaidun, contains Fe-rich hydrated phases, which appear to be products of aqueous alteration of opaque phases (Figs. 6e,f; 9). This process was studied in detail on one grain of schreibersite and one of metallic iron (Ivanov et al. 1993). The maximum sizes of grains are 100 and 250 µm, respectively. Both grains are located near the peripheries of lithology clasts, suggesting that asteroidal fluids had only begun to seep in and alter the EH clasts. Altered parts of both schreibersite and metallic iron are characterized by high variations of practically all elements.

The altered zone of the schreibersite grain displays a stripe structure in optical and BSE images. The main components of the altered zone are iron oxides or iron oxyhydroxides. The light bands in BSE images have high Ni and S contents (Fig. 6e,f). Contents of lithophile elements are very low, no more that 2 wt.% of each. The dark bands in the BSE images are characterized by high contents of lithophile elements (e.g., SiO_2 up to 21.0, Al_2O_3 up to 10.4, MgO up to 8.7, Cl up to 1.8 wt.%).

All parts of the schreibersite altered zone have a very constant S/Ni atomic ratio close to 2, suggesting that this is some stoichiometric compound, possibly vaesite (NiS_2) or violarite ($FeNi_2S_4$). This phase is the main component of the light bands in the BSE images.

The altered zone of the metallic iron grain shows highly variable compositions, with high contents of impurities (e.g., SiO_2 up to 23.8, Al_2O_3 up to 3.5, MgO up to 4.7, Cl up to 6.4 wt.%); these compositions does not correspond to a single mineral phase. There are systematic changes in the contents of most components – as one goes from areas adjacent to relict metal to the rim, the S, Ni, and Cl contents decrease, while SiO_2, Al_2O_3, MgO, CaO and Na_2O increase.

As already mentioned, in some samples of this lithology clear boundaries are present between altered and unaltered material (Fig. 9), which reveal the reaction boundary of the aqueous fluid (or water table) on the parent asteroid – a petrographic feature perhaps unique to Kaidun. Another interesting feature of this material is the high variation of many minor elements in the alteration products. This compositional variation clearly indicates the unequilibrated character of the alteration process.

- Lithology #02.04

This lithology contains well-defined chondrules set within a fine-grained matrix. Chondrules vary in size from 0.15 to 0.4 mm. In addition to typical enstatite-plagioclase chondrules, a single chondrule whose main minerals are a SiO_2-phase (probably cristobalite) and enstatite was also found. This unusual chondrule contains two types of enstatite – $Fs_{0.6}Wo_{0.15}$ and $Fs_{1.4}Wo_{3.5}$.

Some chondrules have areas of enstatite containing abundant micrometer- to submicrometer-sized opaque inclusions ("dusty grains"). The dusty areas are 10–100 µm in size. Relatively large opaque grains (up to 5 µm) from these areas are composed of Fe-Ni sulfide or Fe-Ni metal, with Ni contents varying widely (1.2–8 wt.%). The submicrometer spherical grains are generally metallic iron with a low nickel content. Dusty enstatite grains also occur in the matrix. One more textural component of the lithology is rounded-to-ellipsoidal areas of kamacite-enstatite intergrowths up to 0.7 mm in size.

A distinctive feature of the lithology is the presence of Fe-rich hydrated phases of different compositions (Ivanov et al 1998), which can be classified into three types (Fig. 10). The type I and II phases show significant variations in the contents of virtually of all their elements. These phases, particularly those of type I, have high Cl contents (up to 2.4 wt.%) and the quantitative predominance of Na_2O over K_2O. The type I phases are also high in Ni and S (up to 23.5 and 16.5 wt.%, respectively), with the quantity of the former being usually about twice of the latter. The Al_2O_3 and

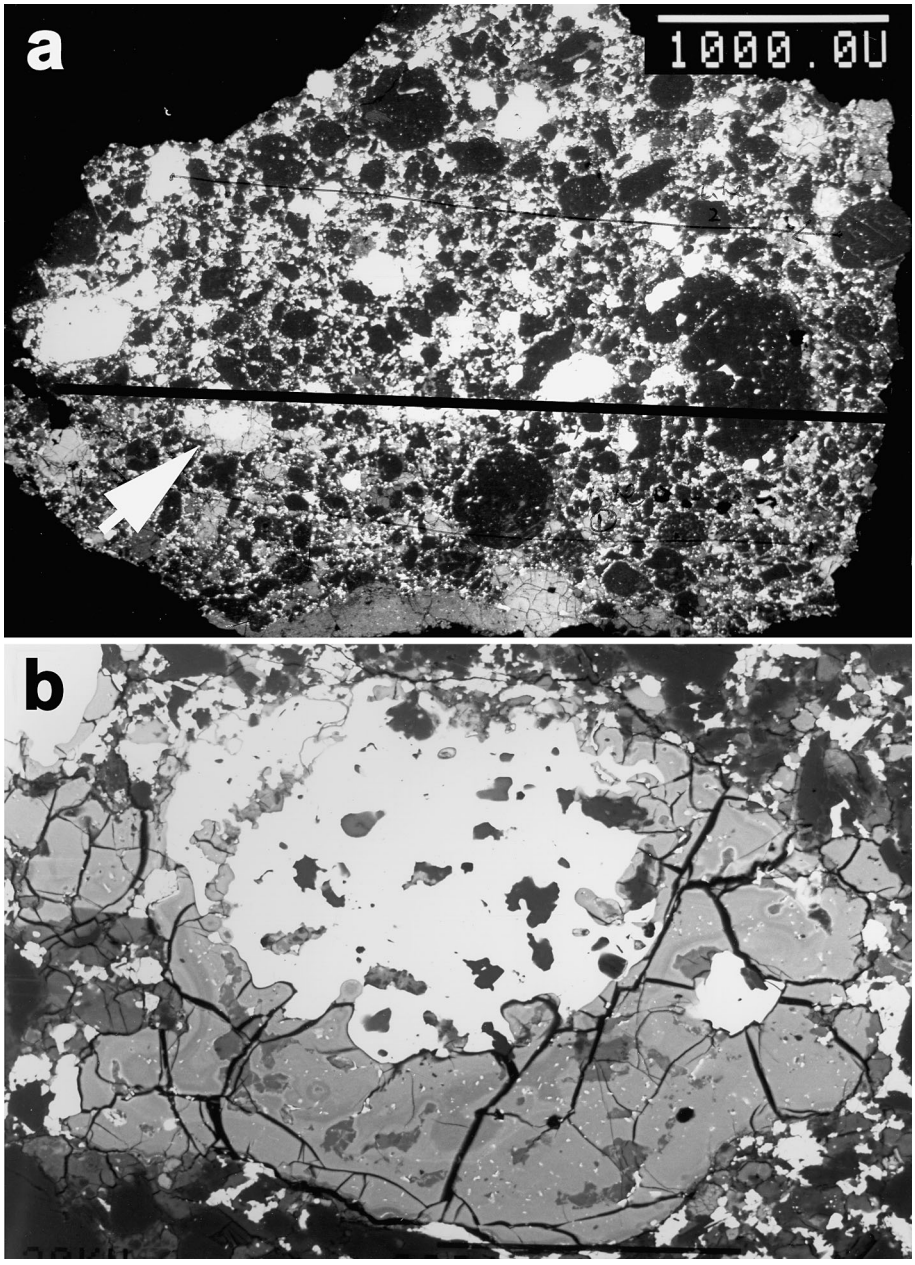

Fig. 9. BSE images of a unique partially-aqueously altered EH lithology. (a) The entire clast. Above the black line the sample is pristine, below the line all phases are completely aqueously altered. (b) Closeup of altered chondrule [see arrow in (a)]. Metal and silicates are completely altered to iron-oxyhydroxides and silica gel (grey). Troilite has been transformed to pyrrhotite (white).

MgO contents are low (< 1.5 wt.%). The type II phases are relatively low in Ni and S (no higher than 0.9 and 1.7 wt.%, respectively), whereas the contents of Al_2O_3 and MgO are fairly high (up to 21.0 and 16.5 wt.%, respectively). Significant compositional variations occur in the type I and II phases, both between different grains and within single grains. Hydrated Fe-Ni-S bearing compounds usually occur at the edges of clasts of this lithology; they are common at the margins of metal grains.

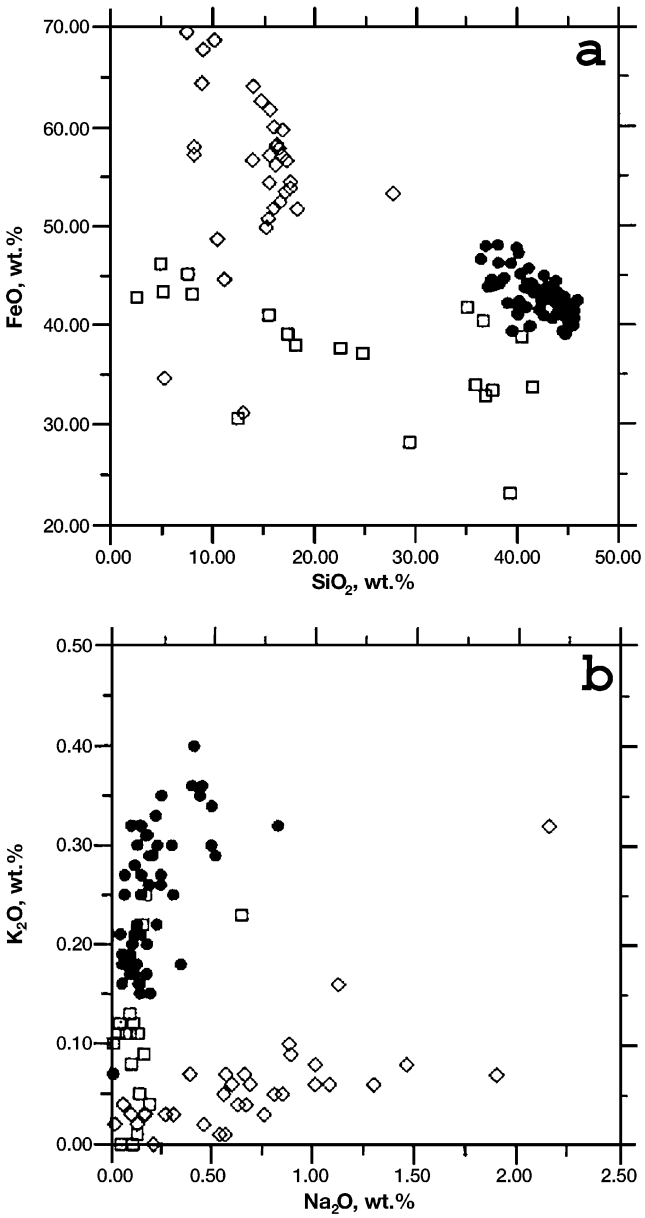

Fig. 10. Covariations in the contents (wt.%) of (**a**) FeO and SiO_2 and (**b**) K_2O and Na_2O in Fe-rich hydrated phases in EH5 fragment #02.04. Diamonds = type I phase, squares = type II phase, circles = type III phase.

The type III phases are notably different from those of the other types. Their compositions vary insignificantly in major components (FeO and SiO_2), and the concentrations of minor components are typically low. The Cl contents are almost always below the microprobe detection limit. The contents of Na_2O and K_2O are nearly equal, or slightly favor the latter (Fig. 10). These phases are usually represented by irregularly shaped grains up to a few tens of micrometers in size, often with small inclusions of elongated enstatite grains. No regularities in the spatial distribution of the type III phases were found.

The compositions and petrographic associations of type I and II phases in this lithology are essentially identical to those of the opaque minerals in lithology 40.7.1 described above. This indicates that the type I and II phases are the products of aqueous alteration of metallic iron (and, perhaps, schreibersite) on the meteorite parent asteroid. Differences in the composition of phases of different types, as well as the compositional variability of each of these types, can be related to differences in the modal composition of the altered zones (for example, aggregates of metallic iron and schreibersite), local variations in the properties of the fluids (compositions, temperature, and pH), and different degree of alteration. The broad compositional variability of the type I and II phases testifies to the incomplete and unequilibrated nature of the processes that formed these minerals.

The type III phases differ from those of types I and II in several ways. First and foremost, their compositions are nearly constant, a fact that seems to point to a relatively long-lasting interaction between metal and an altering agent or high intensity of alteration. Other remarkable features of this phase, in contrast to those of types I and II, are their low contents of minor elements, particularly the absence of Cl, and the predominance of K_2O over Na_2O. It is worth noting that the type III phases are equally distributed over the whole thin section area, unlike the type I and II phases, which occur in the marginal parts of clasts.

The characteristics described above suggest that the hydrated type III phases are not related to the type I and II inclusions. We suggest that the former formed by alteration of metallic iron grains during an early, preaccretionary period.

The compositions of the type III Fe-rich hydrated phases require that alteration of the metallic iron was accompanied by addition of significant silica and alkalies under the influence of a vapor with a fractionated Na/K ratio. Alkaline metasomatic alteration with various Na/K ratios have been proposed for a Kaidun calcium-aluminum-rich inclusion (CAI) (Ulyanov et al 1994). This report suggests that the metasomatic processes occurred before the final assembly of the two parts of the inclusion.

The type III Fe-rich hydrated phases have constant composition. Moreover, their compositions are nearly stoichiometric and may be approximated by the formula $FeSiO_3.n\ H_2O$, which would be a previously unknown mineral.

EL3 Chondrite Lithology

The mineralogy and petrography of this material was described by Ivanov et al. (1986). This lithology has a clear unequilibrated texture – well-defined chondrules set within a fine-grained matrix. The chondrules vary from <0.3 up to 6 mm in size, and their fragments and large (up to 1 mm) xenomorphic metal-sulfide-schreibersite intergrowths are set within matrix consisting of black opaque material containing grains of enstatite, olivine, kamacite and troilite.

The chondrules are sharp and well-defined, typical of type 3 chondrites, and comprise about 45 vol.% of the lithology. Enstatite-rich radial chondrules are the most abundant type. Also present are olivine-pyroxene microporphyritic chondrules with idiomorphic olivine grains in the center, and enstatite-rich barred chondrules. Ferromagnesian glass of variable composition, albitic glass, silica and diopside are present in the chondrules as rare accessory phases. The opaque minerals are represented by Fe-Ni metal, Fe-Ni sulfides and schreibersite.

- Mineral Chemistry

Enstatite is the most widespread mineral of this material and shows the same composition in various textural types ($Fs_1Wo_{0.5}$; FeO/MnO = 6.5). Both ortho- and clinoenstatites were found in both chondrules and matrix. The presence of two varieties of enstatite is characteristic of EH chondrites, while in EL chondrites only orthoenstatite has been found (Keil, 1968; Petaev and Skripnic 1983). The composition of enstatite corresponds to that in EH chondrites, which in comparison with EL chondrites is characterized by higher contents of FeO and, usually of MnO and lower CaO (Keil, 1968).

Olivine present in microporphyric chondrules and in matrix has a similar composition (Fa < 0.5). Olivine has previously been found in some EH chondrites but has not been found in any EL chondrites (Petaev and Skripnik 1983). Compared to olivine in the EH chondrites Indarch and Kota-Kota (Leitch and Smith 1982), olivine of the Kaidun material is characterized by lower contents of the trace oxides Al_2O_3, Cr_20_3, MnO and CaO.

Albitic glass ($An_{5.2}$) is present in small grains in the chondrules and in the matrix. This composition is generally characteristic of the EH group, although the FeO content (1.0 wt.% on average) is somewhat higher.

Primary ferromagnesian glass occupies interstitial locations in the chondrules and is characterized by noticeable compositional diversity. Compared to olivine and enstatite, this glass is enriched in Al_2O_3, CaO, Na_2O and K_2O. Small grains of a SiO_2-phase were found in several chondrules of different types.

Diopside ($En_{58}Wo_{42}$) was found as single grain about 20 µm in size in radial chondrules. Its composition is practically identical to that of diopside in the Happy Canyon EL7 meteorite (Olsen et al. 1976).

Fe-Ni metal is the main opaque mineral in this lithology. This kamacite is present in chondrules, matrix, and in metal-sulfide-phosphide intergrowths. The composition of kamacite in all components is practically the same (Ni = 7.4, Co = 0.5, Si = 0.63 wt.%). The Si-content of metal is the lowest of all studied E chondrites. Schreibersite forms two groups that differ in nickel contents (17.4 vs. 9.7 wt.%). On the whole, the schreibersite composition is more variable than in typical enstatite chondrites.

Fe-Ni-Cr sulfide has various petrographic associations, and differs from simple troilite in other enstatite chondrites by its high chromium content, sometimes reaching 5 wt.%. The distribution of chromium within individual grains is very non-uniform due to the presence of thin lamellae of a chromium-rich phase. The content of copper and zinc in the sulfide is also variable: its contents within individual grains vary from <0.03 to about 0.15 wt.%. Ferroalabandite is encountered in association with kamacite and troilite. Its composition [$(Mn_{0.62}Fe_{0.27}\ Mg_{0.11})S$] is close to that for typical EL chondrites.

- Classification

The bulk chemical composition of this lithology (reported by Ivanov et al., 1986) as well as the presence of alabandite, which is a typomorphic mineral of EL chondrites, and the relatively low Si contents in metallic iron, all indicate that this clast belongs to the EL chondrites. However, this EL lithology in Kaidun exhibits several unusual characteristics. A number of its characteristics have been generally observed only in EH chondrites. These include the presence of both ortho- and clinopyroxene, the composition of enstatite, the rather high spread of FeO contents (0.1–1.9 wt.%), the presence of both olivine and silica, albitic glass, ferromagnesian glass of variable compositions, and clear chondritic textures. It is significant that these characteristics were observed in only Qingzhen, Parsa, Yamato-691 and some other EH3 chondrites (Rambaldi et al. 1983a,b; Nehru et al. 1984; Prinz et al. 1984a,b). This Kaidun lithology was thus the first identified example of an EL3 chondrite (Ivanov et al 1986).

Individual Enstatite Aggregates

The heterogeneous Kaidun breccia contains, along with fragments of fairly recognizable chondrite and achondrite lithologies, aggregates that consist mostly of pure enstatite and have variable textures and accessory mineral phases. Here we describe enstatite aggregates of two different types. Such aggregates have apparently not previously been reported in meteorites.

Enstatite Aggregate with Sulfide-Oxide Inclusions

The only aggregate of this type was found within section #d2C (Ivanov et al. 2002). The aggregate is equant in shape with an apparent diameter of 0.5 mm. Its boundary is sharp, without any traces of interaction between it and the remainder of the materials in the section (Fig. 11a,b).

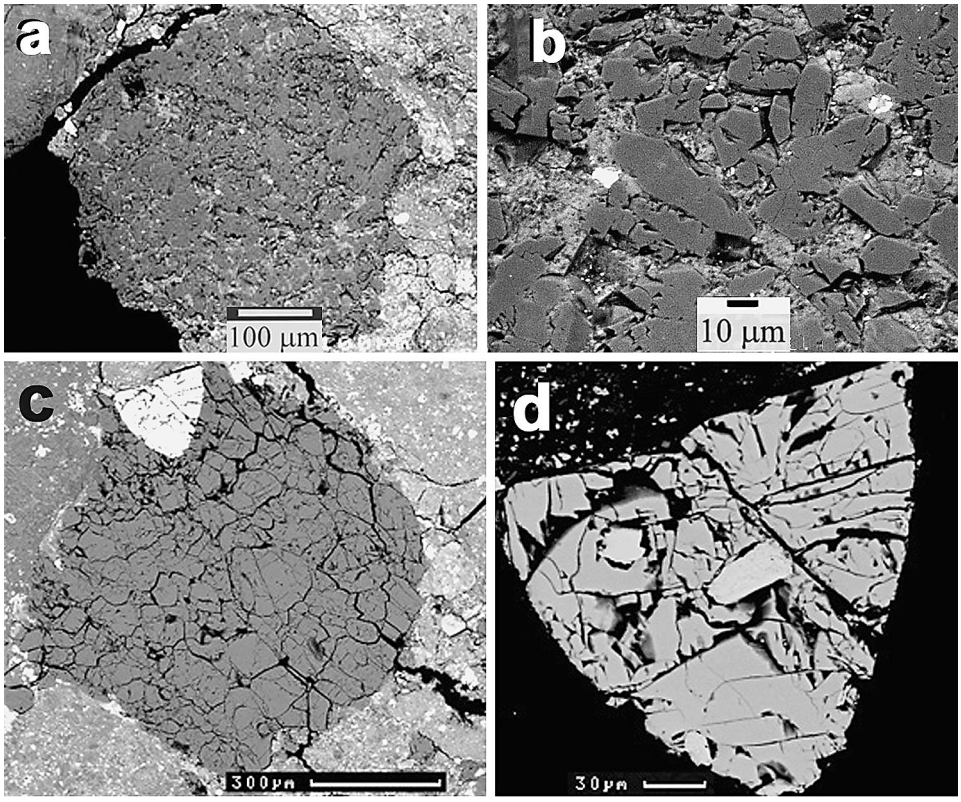

Fig. 11. BSE images of the enstatite aggregate with sulfide-oxide inclusion #d2C. (**a**) The aggregate surrounded by a carbonaceous matrix. Dark gray is enstatite, pale gray is calcite and the hydrated phases, and bright specks are sulfide-oxide inclusions. (**b**) a part of the aggregate with druse-like aggregate of enstatite crystals. The interstitial hydrated phase contains two large sulfide-oxide inclusions. (c) and (d) BSE images of the sulfide-enstatite aggregate #d6R (**c**) and its sulfide nodule (**d**) consisting of niningerite (gray) and heideite (white).

- Texture and Composition

Enstatite is the dominant phase of the aggregate, occurring as euhedral prismatic crystals up to 50 µm long, which often compose aggregates, sometimes with a radiating texture. Enstatite shows significant compositional variations for FeO (Fs = 0.3–2.4), Al_2O_3, and MnO, as well as in the FeO/MnO ratio (1.9–13.6). Forsterite is rare and occurs in subordinate amounts, usually enclosed within enstatite crystals. Its composition varies very little (Fa = 0.5–0.6, FeO/MnO = 2.4–5.7).

Interstices between crystals are filled with Ca-carbonate and hydrated ferromagnesian phases of complex compositions. The hydrated phases are characterized by low totals (83.3–90.7 wt.%) and fairly broad variations in the concentrations of most components, particularly SiO_2 and Al_2O_3. The Ca-carbonate contains 1.2 wt.% MgO, 1.1 wt.% MnO, and 0.44 wt.% FeO on average.

A distinctive feature of the aggregate is the occurrence of numerous small (up to 7 µm) inclusions of Fe-, Mn-, Ti-, and Cr-sulfides and oxides within the interstitial hydrated phases (Figs. 11a,b). The inclusions are often rounded, and their cores consist mainly of oxides, and the peripheries are dominated by sulfides. Elemental maps show that Ti is concentrated in the core and Mn in the rim of the inclusions, whereas Cr is evenly distributed. Calculated compositions of these inclusions (after subtraction of the host material from the microprobe analyses) demonstrate that the rims consist mainly (70–95%) of ferroan alabandite with average composition $(Mn_{0.47}Fe_{0.44}Mg_{0.09})S$ (Ivanov et al 2002b).

- Genesis

The broad variations in the chemistry of enstatite, the dominant phase of the aggregate, suggest that it was not melted after its original crystallization. The occurrence of radiating aggregates of enstatite crystals in this object are consistent with this suggestion. The compositions of the enstatite and forsterite are characterized by low FO/MnO ratios (in average 6.4 and 3.5, respectively) and in this respect approaches the compositions of low-iron manganese-enriched (LIME) silicates which were proposed, by Klöck et al. (1989), to have formed by condensation from a cooling gas of solar composition. It follows that enstatite in this aggregate may be a nebular condensate.

The interstitial hydrous phases and carbonates are probably due to parent body aqueous alteration. The small sulfide-oxide inclusions in the hydrated phases are concentrically zoned, with Ti oxide occurring at the center of the inclusions. This inner structure obviously suggests the origin of the objects in a number of stages and indicates that oxides, notably Ti oxide, were the first to form.

There are no reasons to believe that Ti oxide was produced by aqueous alteration. However, taking into account the abovementioned probable condensation origin of enstatite, the dominant mineral of the aggregate, and the fact that the Ti minerals were among the earliest condensation products in the cooling solar nebula, it is realistic to suggest that Ti- and Cr-rich phases are also condensation products. These objects in the aggregate can, perhaps, be regarded as an analogue of the oxide inclusions (MgO, TiO_2, CaO, and Al_2O_3) found in calcium-aluminum-rich inclusions (CAI) (Greshake et al 1996).

The formation of ferroan alabandite rims of small inclusions can be explained by processes connected with late-stage aqueous alteration of the aggregate.

Sulfide-Enstatite Aggregates

Three aggregates of this type, #d1L, #d2B and #d6R, were found in three different large thin sections of the meteorite (d1, d2 and d6). These particular serial sections show an unusually large number of different lithologies, even for Kaidun.

- Texture and composition

These aggregates consist of enstatite without any other silicates (Figs. 11c,d). They have sizes from 0.6 to 1.5 mm rounded to irregular shapes and a porous, granular texture with grain size of about 100 µm. The aggregates contain predominantly rounded nodules of niningerite up to 650 µm in size with abundant inclusions of heideite of variable sizes (up to 80 µm) and shapes (usually irregular). One very small (< 5 µm) grain of oldhamite was found in niningerite. Some products of heideite oxidation, (Fe,Ti,Si) oxides or hydroxides, an Mn,Ti-rich phase and some Ca carbonates were found in niningerite.

Enstatite is consistently Fs < 1, with very low concentrations of other elements. Niningerite (Fig. 11d) is chemically homogeneous in a given aggregate, although it varies in composition between different aggregates. However, these niningerites have a significantly different composition than those in Kaidun EH fragments as well as in other EH chondrites (Keil 1968; Leitch and Smith 1982; Ehlers and El Goresy 1988). Niningerites in these aggregates have the most Ca of any niningerite recorded (up to 6 wt.%) and among the highest contents of Mn (up to 18.5 wt.%) and Ti (about 0.3 wt.%) (Keil 1968; Rubin and Keil 1983; Ehlers and El Goresy 1988). The composition of niningerite from the Kaidun aggregates can be approximated by the formula

$$(Mg_{0.56–0.58}Mn_{0.22–0.24}Fe_{0.10–0.11}Ca_{0.08–0.10})S.$$

Heideite was previously found in the Bustee aubrite (Keil and Brett 1974; Kurat et al. 1992; McCoy 1998). In comparison with this, heideite from Kaidun is enriched in Cr and Mn. Its composition can be approximated by the formula

$$(Fe_{0.88–1.00}Cr_{0.41–0.44})_{1.29–1.41}(Ti_{1.80–1.85}Fe_{0.15–0.20})_2S_4.$$

The trace element contents of aggregate #d1L (Kurat et al 1977) show that the sulfides from the aggregates are enriched in all trace elements, except Be, relative to co-existing enstatite, demonstrating strongly chalcophilic behavior of common lithophilic elements.

- Genesis

The similarities in texture and mineral composition of the sulfide-enstatite aggregates suggest a common origin. The preferential partitioning of Sc, Li, Sr, and some other elements, which are typical for pyroxenes, into sulfides indicates low redox and high S-fugacity formation conditions (Kurat et al. 1997).

Niningerite is a hallmark phase of EH chondrites, and its presence within the aggregates suggests a genetic connection to EH material. On the other hand, the discovery of niningerite in the Shallowater and Bustee aubrites (Keil et al 1989; McCoy 1998) permits a possible connection with aubrites. This situation requires additional study.

An unusual feature of the sulfide-enstatite aggregates is their high Ca contents in niningerite. According to Skinner and Luce (1971), Ca contents of niningerite and alabandite depend on temperature of formation. The estimation of minimal temperatures of enstatite chondrite formation is 600–800 °C (Skinner and Luce 1971). Taking into consideration experimental data of Skinner and Luce (1971) for CaS contents in niningerites and alabandites for different equilibrium temperatures, a minimal equilibrium temperature of formation of niningerate from Kaidun aggregates is estimated about 850–900 °C. It appears that this niningerite is the highest-temperature niningerite known.

The presence of an oldhamite grain in a nodule in clast #d2B is also of special interest. Oldhamites in aubrites are interpreted as either primitive (Kurat et al. 1992) or partly metamorphosed (Lodders 1996) condensates, or as products of crystallization of sulfide melts in both aubrites (Wheelock et al. 1994) and unequilibrated enstatite chondrites (Crozaz and

Lundberg 1995; Hsu 1998). It seems that formation of sulfide nodules in the Kaidun aggregates is in rather good agreement with a model (Wheelock et al. 1994) of oldhamite formation by crystallization during cooling of two immiscible sulfide melts (Ca-rich and Mg,Fe,Mn,Cr-rich, respectively). For Kaidun aggregates, a melt highly enriched in Ti resulted in formation of heideite instead of the usual troilite. Cooling of this melt was apparently very quick, resulting in incomplete separation of high-Ca and high-Mg,Fe,Mn components. It appears that the very high contents of REE and other trace elements in the aggregate's niningerite is also connected to incomplete separation from sulfide melt of an oldhamite component which is usually a main depository for these elements.

The homogeneity of sulfides in nodules and their rounded shapes are in good agreement with formation during melting, and the high Ca contents in niningerite indicate a high cooling rate. It appears likely that these processes occurred in a preaccretionary environment. The high enrichment of sulfide in comparison with enstatite by lithophilic elements as well as the texture of the enstatite aggregates exclude the possibility of their formation from coexisting melts.

The characteristics of enstatite aggregates of both types indicate that they are products of nebular condensation and were not substantially altered during any of the aqueous events recorded by the many other Kaidun lithologies.

Carbonaceous Chondrite Lithologies

Carbonaceous chondrite lithologies appear to dominate Kaidun. Some of these, such as the CV3 and CM1 lithologies, are easily recognized materials. However, there are also numerous type 2 and 1 materials which do not appear to have analogues in other meteorites.

CV3 Lithology

This lithology is described here for the first time from Kaidun. The largest sample is shown in Fig. 12 (section d3), and is a clast measuring about 2 mm across. The bulk of this lithology consists wholly of chondrules, chondrule fragments, olivine-rich aggregates, lithic fragments and a sulfide aggregate, set within finer-grained, olivine-rich matrix. Matrix consists of 15 µ- to sub-micron size olivine (Fa52–41), low-Ca pyroxene, and pyrrhotite.

- Mineralogy and Petrography

The matrix of this lithology is dominated by irregular to platy-shaped olivine grains (Fig. 12b) with a rather uniform, composition ($Fa_{41–52}$). The compositional range of this matrix olivine is essentially identical to that found in the oxidized CV3 chondrites Allende and Grosnaja (Krot et al. 1995). These olivines have the unusual, platy, often curved morphology typical for some CV3 chondrites and many of their dark inclusions. Krot et al (1995) suggested that this morphology was formed by pervasive aqueous alteration of anhydrous CV3 material, forming platy phyllosilicates from glass, olivine and pyroxene, followed by thermal metamorphism that produced olivine pseudomorphs after the phyllosilicates.

Even the largest clast of the Kaidun CV3 lithology is rather too small to expect a good statistical sampling of large components such as CAIs and chondrules. The material we have seen contains very abundant aggregates of zoned to unzoned olivine ($Fa_{7–43}$), high and low-ca pyroxene ($Fs_{8–33}$; Fs_4Wo_{44}), plagioclase, and Fe-Ni sulfides. Some of these objects are clearly small chon-

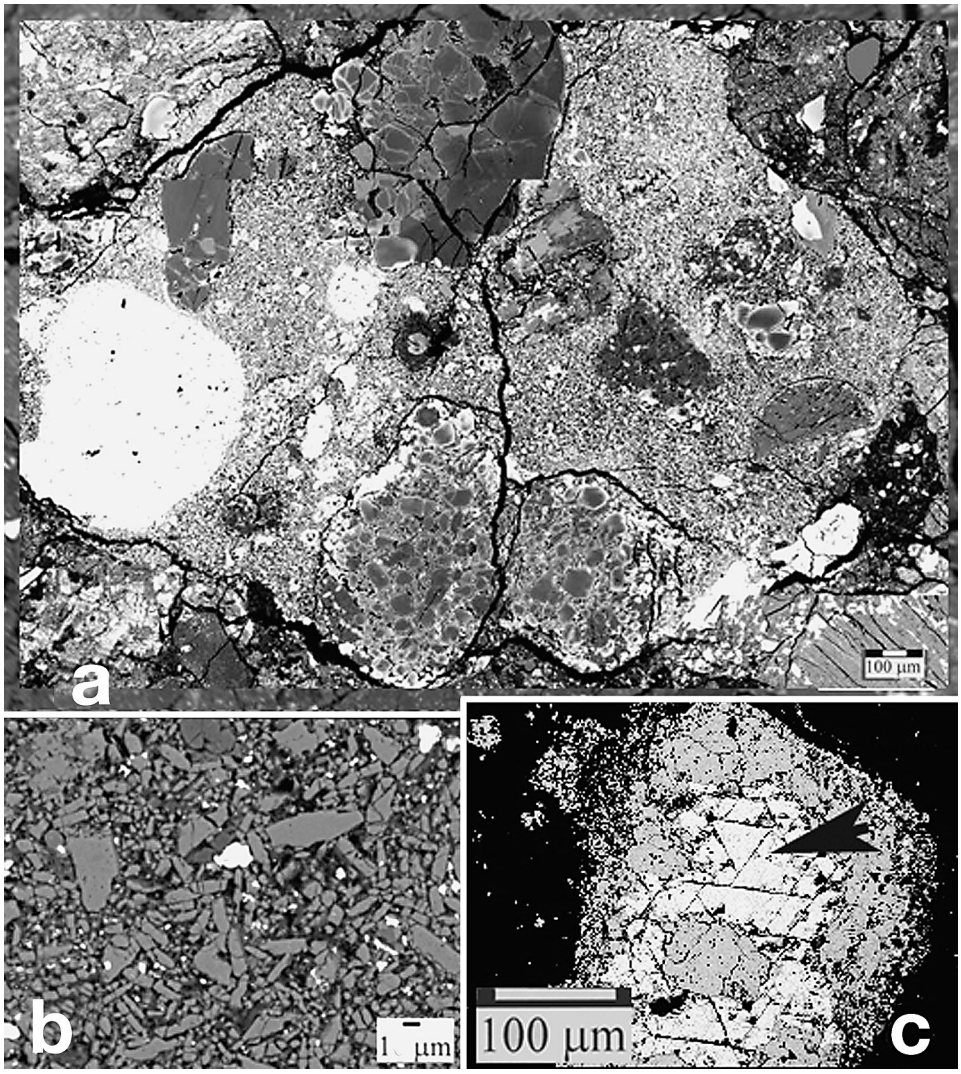

Fig. 12. BSE images of the CV3 Kaidun lithology. (a) Low-magnification image of an entire CV3 clast. Note the obvious olivine zoning, indicating the unequilibrated nature of the lithology. (b) High-magnification view of the olivine matrix, revealing the typical curved olivine crystallites. (c) Details of the pyrrhotite (white) and pentlandite (grey) aggregates (evident at the left side of (a)). Note that the pyrrhotite appears to have octahedral cleavage or parting (arrowed), which must have been inherited from an earlier, now pseudomorphed phase.

drules, while others are clearly fragments of larger radial pyroxene and porphyritic olivine chondrules (Fig. 12). An aggregate consisting wholly of pyrrhotite and pentlandite is clear evidence of the oxidized nature of this material. An intriguing feature of the pyrrhotite is that it displays apparent cleavage or parting along octahedral faces (Fig. 12c). This suggests that this phase is pseudomorphous after metal or magnetite.

- Classification and Genesis

We have no bulk composition for this lithology, and it may not be possible to obtain this. However, all features of the mineralogy and petrography of this lithology are consistent with a classification as CV3, of the oxidized sub-group.

The CV3 lithology has apparently experienced parent body aqueous alteration, followed by a period of thermal metamorphism sufficient to transform phyllosilicates to olivine, but insufficient to homogenize zoned olivine. Such temperatures must have been in the range 400–700 ºC (Lipschutz et al. 1999). It is interesting that the matrix olivines within this lithology suggest a wet past, as do so many other Kaidun lithologies, however it is impossible to determine on which asteroid the aqueous alteration occurred. It is clear that the proposed metamorphism witnessed by this lithology was not experienced by the bulk of Kaidun materials, and so plausibly occurred on a previous parent asteroid.

CM2 Lithology

This Kaidun lithology is described here for the first time. The largest sample of this lithology is shown in Fig. 13 (section d3). It consists of matrix of fine-grained serpentine and pyrrhotite. Set within this matrix are submillimeter-sized chondrules, all of which are incompletely altered to serpentine and pyrrhotite (Fig. 13). We briefly describe each of these components below.

- Mineralogy and Petrography

Matrix serpentine displays variously fibrous, platy and cylindrical morphologies typical for serpentine-containing carbonaceous chondrites (Fig. 14a), including the CM2s (Zolensky et al. 1993). We did not observe any saponite among the matrix, which is again typical for CMs.

The compositional range of serpentine from the Kaidun CM2 lithology, when displayed on a Fe-Mg-(Si+Al) diagram (Fig. 15), essentially spans the compositional range for serpentines from CM chondrites. Such variable serpentine compositions are typical of the CM chondrites that have experienced an intermediate degree of aqueous alteration (McSween 1987; Zolensky et al. 1993; Browning et al. 1993).

Pyrrhotite is very abundant within the matrix of this lithology, appearing as individual grains and clusters, and is present everywhere including within chondrules, olivine aggregates, and phyllosilicate lumps. We did not find any tochilinites, which are generally found in CM2 chondrites, and we suggest that this is due to heating to at least 350° – this is known to transform tochilinite to pyrrhotite or troilite (Gooding and Zolensky 1987; Zolensky et al. 1989).

- Chondrules and Other Large Components

Set within the matrix-supported fabric of this lithology are numerous porphyritic chondrules, olivine aggregates and probable lithic clasts. The chondrules and aggregates have thin, fine-grained rims. The olivine has the composition Fa_{1-22}; low-Ca pyroxene is present also in minor amounts. Pyrrhotite is present everywhere. Glass may be present, but we have not obtained reliable microprobe analyses of this due to the ubiquitous presence of serpentine replacing anhydrous silicates. This serpentine has approximately the same composition as that in the matrix and can often be seen replacing olivine crystals with perfect fidelity (Figs. 13b,c). The chondrules range from 0.2 to 0.4 mm in average diameter. This range is consistent with chondrules in both the CM and CR chondrites (King and King, 1978).

Aggregates of olivine crystals, often zoned, are present. These are partially replaced by serpentine.

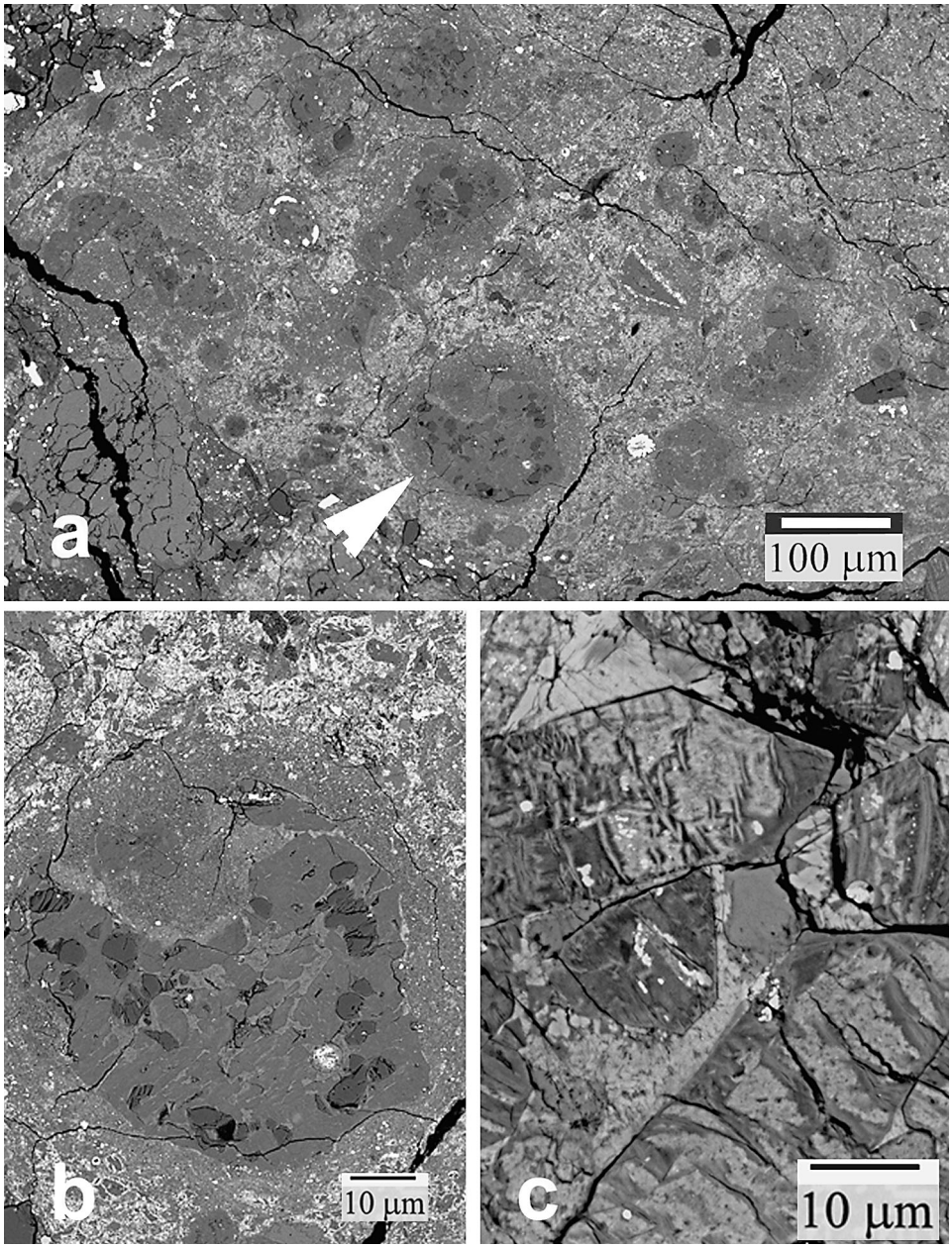

Fig. 13. BSE images of the CM2 lithology in Kaidun. (a) View of an entire clast. (b) Closeup of partially aqueously-altered chondrule arrowed in (a). Residual olivine grains are darkest grey. (c) View of serpentine pseudomorphs after olivine crystals in another aqueously-altered chondrule.

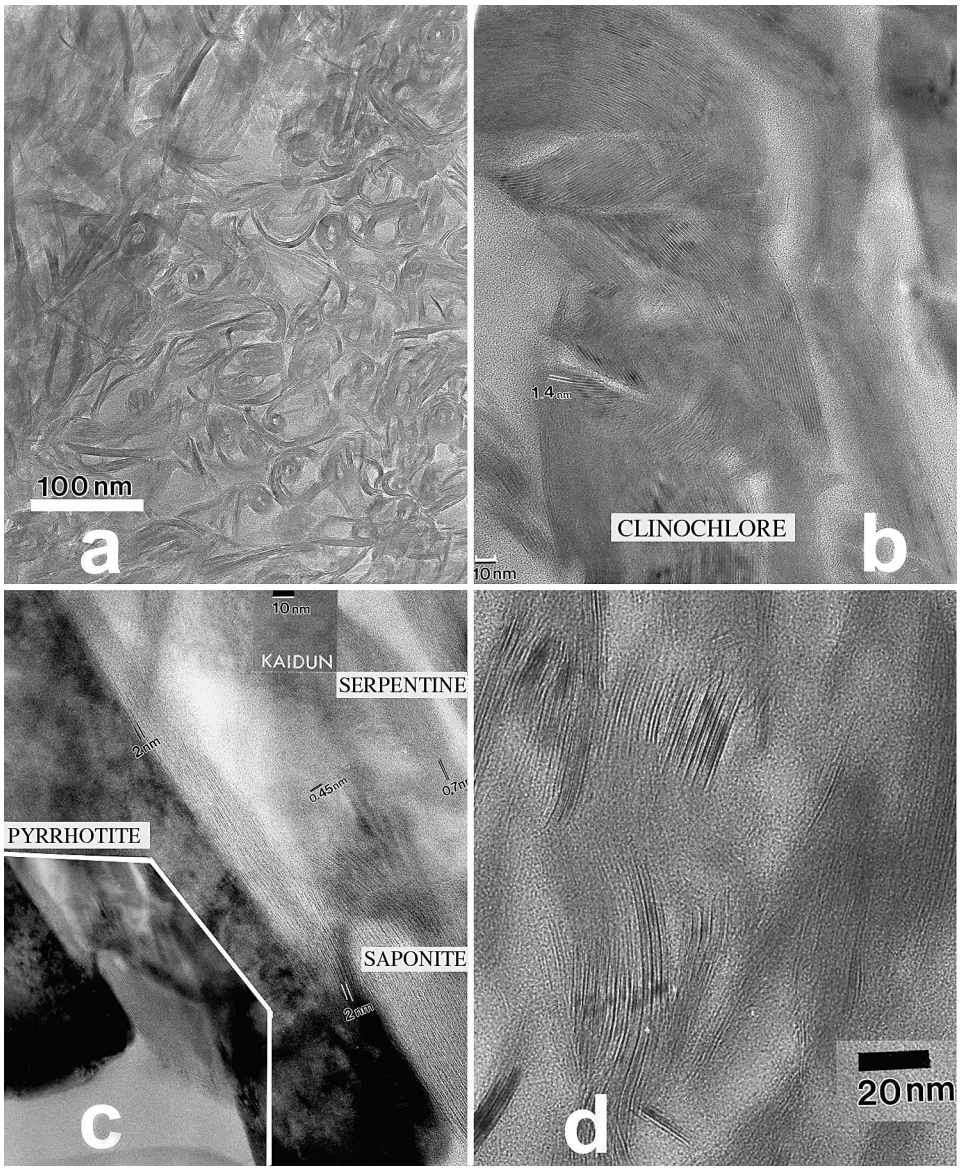

Fig. 14. TEM images of typical Kaidun phyllosilicates. (a) Flaky and cylindrical serpentine (7 Å), (b) Clinochlore (14 Å), (c) Saponite (10–14 Å) and serpentine coating a pyrrhotite crystal. (d) Intergrowths of serpentine and saponite.

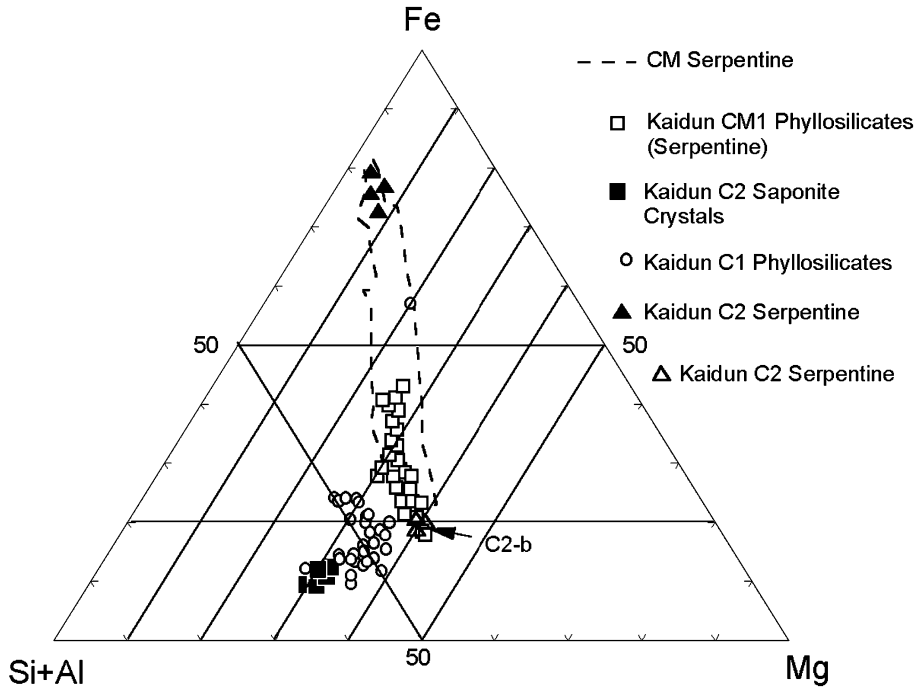

Fig. 15. Compositional variation of phyllosilicates in several carbonaceous Kaidun lithologies, displayed on a Fe-Mg-Si+Al wt.% atom triangular diagram. The dashed field is the variation of serpentine compositions displayed by 15 CM chondrites, a range also spanned by Kaidun serpentines.

- Bulk Chemistry and Classification

We have not attempted collection of bulk composition data for separated clasts of CM2 material, because of their small size. However, analyses of several aliquots of Kaidun carbonaceous material by INAA (David Mittlefehldt, personal communication 2003) are reported in Fig. 4. It is clear from these data that the concentrations of most of the analyzed elements are similar to average CM and CR2 chondrites, with the exceptions of K and Br; K is not particularly well determined by INAA, and Br is notoriously mobile. Our failure to recognize any CR2 chondrite material in Kaidun by petrographic techniques suggests that the bulk of the carbonaceous material is therefore most similar to CM. This conclusion, in turn, suggests that the present lithology is indeed CM2, despite the apparent lack of tochilinites. We can explain the lack of tochilinites by heating on the parent asteroid.

- Genesis

CM2 chondrites are known to have experienced significant degrees of aqueous alteration on asteroidal parent bodies, based on compositional, petrographic and isotopic evidence (Zolensky et al. 1989). The Kaidun CM2 material has shared this genesis, but may also have witnessed some minor metamorphic heating. However, this latter suggestion is very tenuous, being based on the absence of one mineral generally found in CM2s, and so should not be taken too seriously.

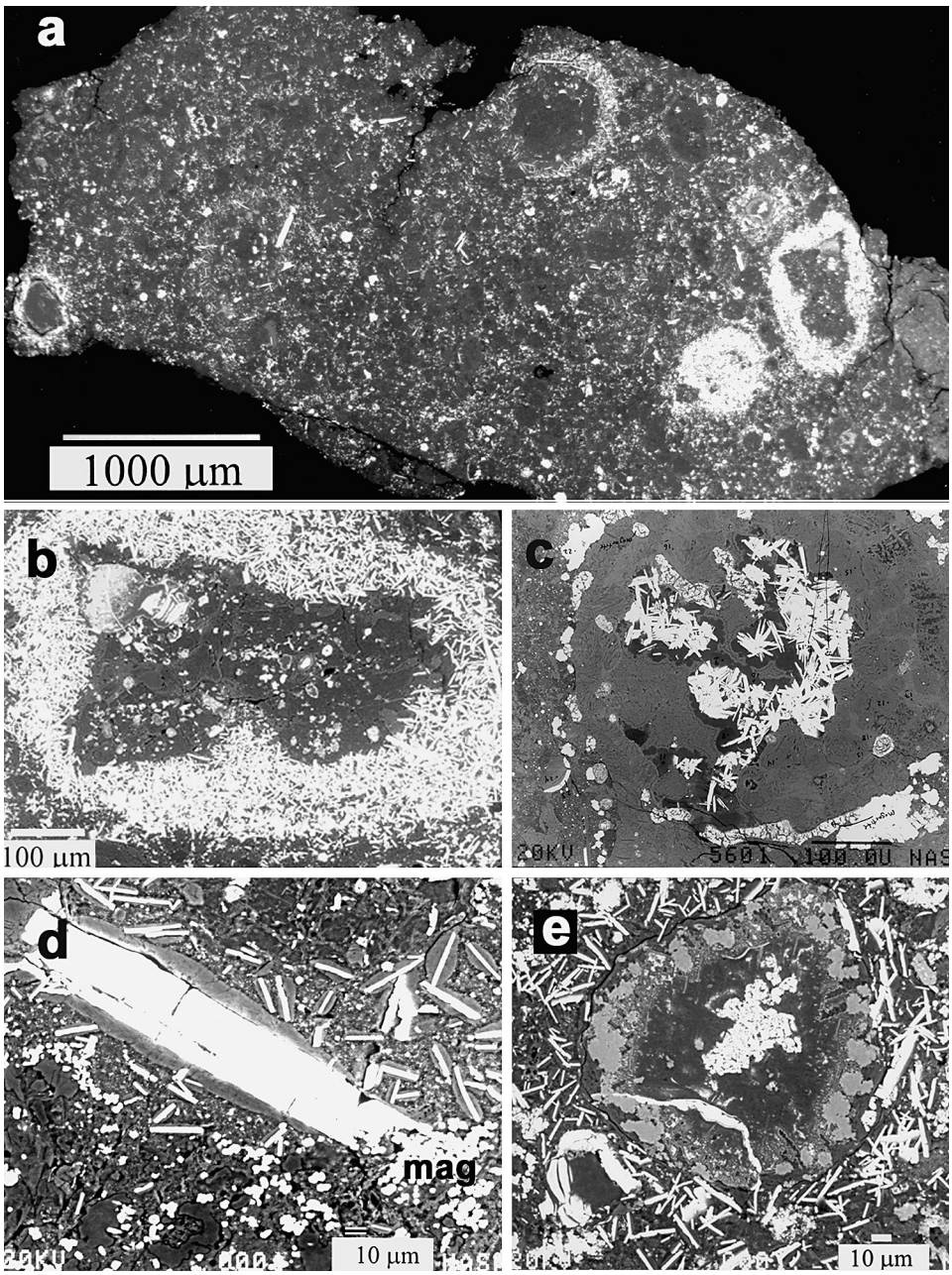

Fig. 16. BSE images of a very common CM1 lithology in Kaidun, type A. (a) Low-magnification image of an entire CM1-A clast. Note the acicular pyrrhotite-rimmed altered chondrules, one of which is shown at higher magnification in (b). (c) A serpentine (grey) and pyrrhotite (white) containing altered chondrule from another example of this CM lithology. Note that here the pyrrhotite is entirely within the chondrule. (d) Phyllosilicate-mantled acicular pyrrhotite grain typical of this CM1 lithology. Note that magnetite (mag) is apparently forming from the breakdown of pyrrhotite at the lower right. (e) Small altered chondrule with a pentlandite core and vein (white), and melanite garnet (medium grey) inner rim.

CM1 Lithology A

This lithology is very abundant in Kaidun, and is found in most Kaidun thin sections (Zolensky et al. 1996). A large sample of this lithology is shown in Fig. 16 (section 01.3.18A). The bulk of this Kaidun lithology consists of fine-grained serpentine, saponite, and minor clinochlore (Fig. 14). Floating in the phyllosilicate-dominated matrix are abundant acicular, mantled pyrrhotites (a very distinctive feature), framboidal magnetite, pentlandite, hydroxylapatite, and rare diopside grains. Set within this matrix are submillimeter-sized complex aggregates containing phyllosilicates, sulfides and melanite garnet, and abundant, homogeneous lumps of phyllosilicates (Fig. 16). Some samples contain phyllosilicates/carbonate veins (Fig. 17). We describe each of these components in turn below.

- Mineralogy and Petrography

The matrix phyllosilicates in this lithology are dominated by Mg-rich serpentine. Saponite and, much less commonly, clinochlore are intergrown with serpentine in most examined samples. Matrix serpentine displays variously fibrous, platy and cylindrical morphologies (Fig. 14a), as it does in most other serpentine-containing carbonaceous chondrites (Zolensky et al. 1997). Intergrown with the serpentine is abundant saponite, with a relatively high interlayer charge; clinochlore is present in small amounts.

The compositional range of the bulk of matrix phyllosilicate, when displayed on a Fe-Mg-(Si+Al) diagram (Fig. 15), is comparable to that exhibited by phyllosilicates in CI1 (Ivuna and Orgueil) and CR2 chondrites (EET 87770 and Renazzo), where serpentine and saponite also dominate (Zolensky et al. 1993). These analyses from the Kaidun CM1 lithology also lie at the Mg-rich end of the compositional range for serpentines from CM chondrites. The matrix consists mainly of Mg-rich serpentine, to an even greater degree than for CI or CR chondrites. Mg-rich serpentine compositions are a hallmark of the CM chondrites which have experienced the most extreme aqueous alteration (McSween 1987; Zolensky et al. 1997; Browning et al. 1993).

One sample of this lithology contains a clast with uniquely coarse-grained saponite – perhaps the coarsest-grained saponite known in nature. This clast contains saponite with mm grain size (rather than the nm grain size that is typical), forming from the alteration of olivine (~Fo_{90}). Residual olivine grains are completely surrounded by white saponite with obvious basal cleavage. Even in a petrographic microscope, crystals of saponite can clearly be traced extending into dissolution embayments in olivine (Fig. 18d), a texture generally observable only in the TEM.

A distinctive component of this lithology is the very abundant acicular pyrrhotite crystals (Fig. 16), which have a very narrow compositional range of $Fe_{0.90}Ni_{0.04}S$ to $Fe_{0.92}Ni_{0.02}S$. These crystals, frequently complexly intergrown, are scattered about within matrix and also rim the complex aggregates (described below). This particular crystal habit has not previously been reported for natural pyrrhotite; laths and pseudo-hexagonal plates are the typical morphologies in carbonaceous chondrites. X-ray diffraction analysis shows that these pyrrhotite laths, which must have once been single crystals, now consist of randomly oriented microcrystallites.

In many of the CM1 samples in Kaidun (but not in all), pyrrhotites are mantled about their long axes by a sheath of phyllosilicate (Fig. 16d), which is in places up to 20 µm thick. Although phyllosilicate sheaths are commonly found about pyrrhotite crystals in carbonaceous chondrites and chondritic interplanetary dust particles (Zolensky and Lindstrom 1992), these are typically on the order of a few to few tens of nanometers in thickness, not the 20 µm observed in Kaidun, and grow parallel to only the basal faces of pyrrhotite crystals. In Kaidun these sheaths are rounded, as if by abrasion, and are not observed to surround the pyrrhotite crystal terminations.

Framboidal magnetite is very abundant within the matrix of this lithology, appearing as individuals and clusters, and are present everywhere except within complex aggregates and phyllosilicate

lumps. In many instances magnetite framboids lie adjacent to embayed pyrrhotite crystals, particularly at pyrrhotite terminations, which suggests that they formed at the expense of the latter phase.

Pentlandite occurs as anhedral grains (curved masses often showing parting), aggregates, and vein fillings. The compositions of this pentlandite range from $Fe_{4.6}Ni_{4.3}S_8$ to $Fe_{4.7}Ni_{4.4}S_8$, which is typical for an assemblage in equilibrium with monoclinic to hexagonal pyrrhotite (Misra and Fleet 1973). Some complex aggregates contain veins of pentlandite (Fig. 16e).

Embedded within matrix are abundant, though small (<10 μm), hollow crystals of hydroxylapatite. Hollow apatites have not been previously reported in meteorites, to our knowledge. The only

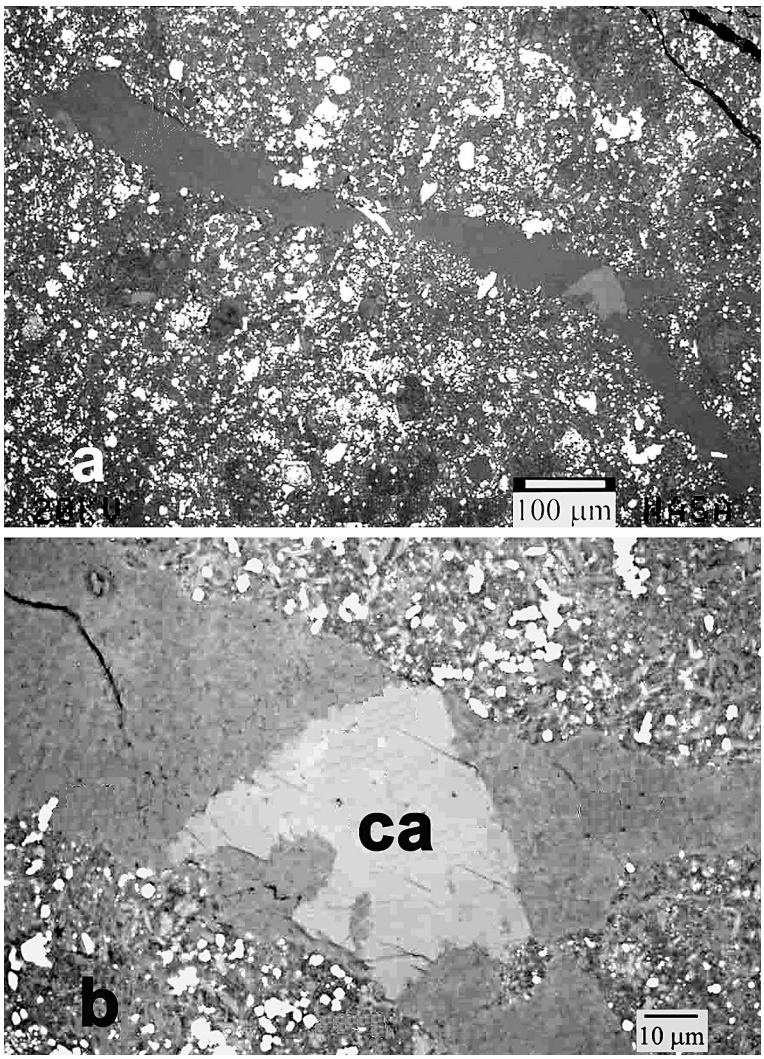

Fig. 17. BSE views of a carbonate/phyllosilicates vein in a C2 clast. (a) Low-magnification view of the entire vein. Medium gray phases are serpentine, white phases are mainly pyrrhotite, and the medium gray phase at lower right is a carbonate grain. (b) High-magnification view of the carbonate grain (ca) from the vein in (a).

anhydrous silicate encountered within the matrix of this lithology was a single fragment of diopside (actually $Fs_{10}Wo_{40}$) measuring approximately 10 µm in greatest dimension.

Sitting in the matrix are a few round aggregates, none larger than 1 mm, consisting dominantly of phyllosilicate, most with outer coatings of acicular pyrrhotite crystals identical to those described above. In some cases these pyrrhotites extend to the center of an aggregate, although this may be a projection artifact. A few of these aggregates contain anhedral lumps of pentlandite in addition to phyllosilicate, as described below. The phyllosilicate in these aggregates is very similar to that in matrix, pyrrhotite sheaths, and phyllosilicate lumps in terms of major element composition.

Several aggregates have discontinuous inner rims of granular melanite andradite garnet (Fig. 16e), with a very unusual composition ($Ad_{75}Uv_{14}Sch_4Py_4Gr_3$) containing significant Cr and Ti. The andradite is locally porous, with inclusions of serpentine and sulfides which are probably due to retrograde metasomatic reactions. The interiors of these complex aggregates contain an assemblage of phyllosilicates and pentlandite.

Some of the CM1-A samples contain carbonates (Fig. 17), which is rather unusual for CM1 (Zolensky et al. 1997). In contrast to CI chondrites, in which dolomite is the major carbonate (Zolensky et al. 1993), calcite is most abundant in Kaidun. Calcite occurs within altered chondrules, CAIs and mineral fragments, and as fragments dispersed throughout the matrix and in veins. Some calcite veins are along the boundaries between lithologies, suggesting that several genera-

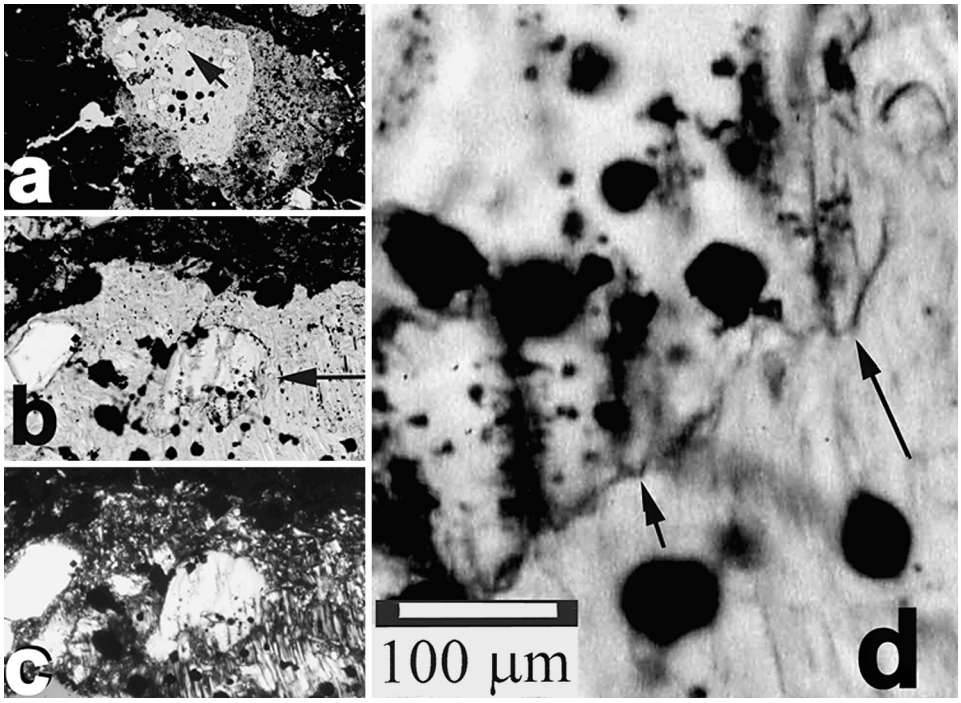

Fig. 18. Unusual C2 lithology with astoundingly coarse-grained saponite. (a) Low-magnification transmitted light image of the saponite/olivine (white) and magnetite (black) aggregate. (b and c) Higher-magnification transmitted light and crossed polar images of (a). Residual olivine grains are white and transparent, and are completely surrounded by white saponite with obvious basal cleavage. Magnetite grains are black. (d) High-magnification transmitted light image of saponite and olivine from the center of (b). Crystals of saponite can clearly be traced extending into dissolution embayments in olivine (arrows).

tions of calcite are present. Calcites show a wide compositional range with minor element concentrations from <0.1 wt.% up to 3.1% MgO, 3.4% FeO and 3.7% MnO. In contrast, minor element abundances in CI calcites are always <0.5 wt.%. Hutcheon et al. (1999) reported the Cr isotope compositions of six Kaidun carbonates. Five carbonates exhibit enrichments in ^{53}Cr with $\delta^{53}Cr$ values ranging up to ~980. The magnitudes of these ^{53}Cr excesses are linearly correlated with the respective $^{55}Mn/^{52}Cr$ ratios, indicative of the in-situ decay of ^{53}Mn and demonstrating that short-lived ^{53}Mn was still present at the time of carbonate formation. The slope of the correlation line on a $^{53}Mn - {}^{53}Cr$ evolution diagram, determined by a weighted least squares fit, corresponds to an initial $^{53}Mn/^{55}Mn$ ratio of $(9.4 \pm 1.6) \times 10^{-6}$. As described by Hutcheon et al. (1999), the initial $^{53}Mn/^{55}Mn$ ratio inferred from the Kaidun carbonate data is among the highest ever measured, exceeded only by values for CAI. The $^{53}Mn/^{55}Mn$ ratio for Kaidun carbonates is comparable to the value measured in Bishunpur and Chainpur chondrules and a recent estimate of the solar system initial value (Lugmair and Shukolyukov 1998). The uncertainty in the present measurement allows a time span of no more than 1 Ma between the formation of Kaidun carbonates and CAIs or chondrules, which appears rather amazing.

• Bulk Chemistry and Classification

The concentrations of most of the analyzed elements in this lithology are similar to average CM chondrites. This Kaidun lithology completely lacks olivine, glass or objects which can unambiguously be called chondrules, and contains only rare, minuscule clinopyroxene (diopside) grains, indicating a classification of C1. The presence of clinopyroxene as the sole anhydrous ferromagnesian silicate is consistent with extensive aqueous alteration, as this is the most stable of the common meteorite-forming anhydrous silicates (Zolensky and Barrett 1994). The matrix of this lithology consists mainly of Mg-rich serpentine, which usually indicates extreme aqueous alteration (McSween 1987; Browning et al. 1993; Zolensky et al. 1997).

The relict chondrules, if that is what they are, range from 0.2 to 0.6 mm in average diameter. This range is consistent with all chondrule-bearing C chondrite types, although it is closest to the CR chondrites which have the largest chondrules (King and King 1978). However, it is possible that small chondrules have been preferentially destroyed during alteration, skewing the chondrule size distribution.

Although Kaidun phyllosilicates in this lithology are distinguished from typical CMs by the presence of abundant saponite, the bulk chemical and oxygen isotopic compositions of this lithology indicate it is indeed CM material, with the latter being very similar to that of Murchison (Clayton et al. 1994). We therefore conclude that this Kaidun lithology is CM1.

• Genesis

This lithology now consists dominantly of clay minerals, including dominantly serpentine, saponite, with minor clinochlore. This phyllosilicate assemblage could have formed under a very wide range of temperatures, on the order of 0–700 °C, with serpentine being stable below 400 °C and saponite below 700 °C (Akai 1990, 1992). The presence of clinochlore is sometimes taken to suggest rather high temperatures, but this contention is uncertain (Deer et al. 1962; Barnhisel and Bertsch 1989). What were the precursor phases for the clay minerals? By analogy to other carbonaceous chondrites these were likely olivine, low-Ca pyroxene and glass. The compositional patterns observed in some of the complex aggregates suggest that they are completely altered type 2 chondrules. Such altered chondrules are common in CMs. Therefore we suggest that the

precursor for this Kaidun lithology was olivine-dominated chondritic material similar, and probably identical, to typical CM2 material.

The most unusual features of this lithology are the presence of melanite and pentlandite veins within complex aggregates, and acicular pyrrhotites within matrix and rimming aggregates. Melanite, and other andradites, can easily form at temperatures below 400 °C, in oxidizing, low CO_2 fluids (as in a skarn). This phase has also formed by fumarolic activity (Varet 1970) from a precursor believed to have been hedenbergite. However, melanite is also stable relative to olivine or clinopyroxene during low-temperature aqueous alteration, so could also be a residual earlier phase.

Pentlandite veins, which are necessarily of parent body origin, crosscut the melanite in one complex aggregate, and must be later or roughly contemporaneous with the latter. Experimental work indicates that hydrothermal pentlandite requires fluid temperatures on the order of 450 °C (Godlevskiy et al. 1971). This would be consistent with the simultaneous formation of melanite (Deer et al. 1982). This must have occurred below the surface of the hydrous asteroid parent body. It seems probable that such a fluid would have generated significant pressure, which could have been vented explosively to space (e.g., Bourcier and Zolensky, 1991, 1992; Wilson et al. 1999). The altered materials could then have been transported during the explosion to another location on the surface of the same asteroid (if the diameter and therefore gravitational field was sufficiently large) or a neighboring asteroid.

The framboidal magnetites, in close association with the exposed ends of pyrrhotite crystals, probably formed through the late-stage oxidation of the latter. Previous work indicates that this would require log fO_2 higher than –60 to –65 (Eckstrand 1975). The widespread occurrence of pentlandite grains within the matrix could have a related origin. Experimental work indicates that melanite appears to require still higher fO_2 (>–25) to form from hedenbergite at 450 °C (Deer et al. 1982).

Finally, the isotopic composition of S in the acicular pyrrhotites and pentlandite in this lithology have been reported by McSween et al. (1997). These sulfides have very light compositions compared to basically all other chondrites, suggesting a relatively high-temperature hydrothermal origin.

We therefore conclude that this Kaidun CM1 lithology experienced prolonged, hydrothermal alteration, and that this could have occurred in a fumarolic vent on a hydrous asteroid. An explosive venting of steam to space could have transported the CM1 clasts to the asteroid regolith for mixture with the other diverse components of Kaidun.

CM1 Lithology B

This lithology is described here for the first time, although small pieces of it are very abundant in Kaidun. A large sample of this lithology is shown in Figure 19. The bulk of this lithology consists of fine-grained serpentine, saponite, and minor clinochlore (Fig. 19). Set within this matrix are submillimeter-sized complex aggregates containing phyllosilicates and sulfides (principally pyrrhotite).

Lithology CM1-B is immediately distinguishable from CM1-A by the appearance and distribution of pyrrhotite. Here the pyrrhotite is cryptocrystalline, forming masses within the altered chondrules, rather than forming rims as in the CM1-A lithology. Another difference is that the matrix contains practically no sulfides. High-magnification images

show how abrupt the boundary between pyrrhotite and host phyllosilicate can be (Fig. 19). Another unusual (but here typical) feature is the association of phyllosilicates and pyrrhotite in small rounded objects, which may be altered microchondrules (Fig. 19d).

- Classification and Genesis

We have obtained oxygen isotopic compositions for this lithology, and the results lie within the field of CM chondrites, suggesting a classification as CM1. Of course, the fields for CR and CM chondrites overlap to some degree on the oxygen three-isotope plot, and so this conclusion is rather tentative. The significant difference between this and the CM1-A lithology described above is that sulfides seem to have been sequestered within the altered chondrules. We have not observed this feature in other meteorites, but presume that it occurred during prolonged aqueous alteration.

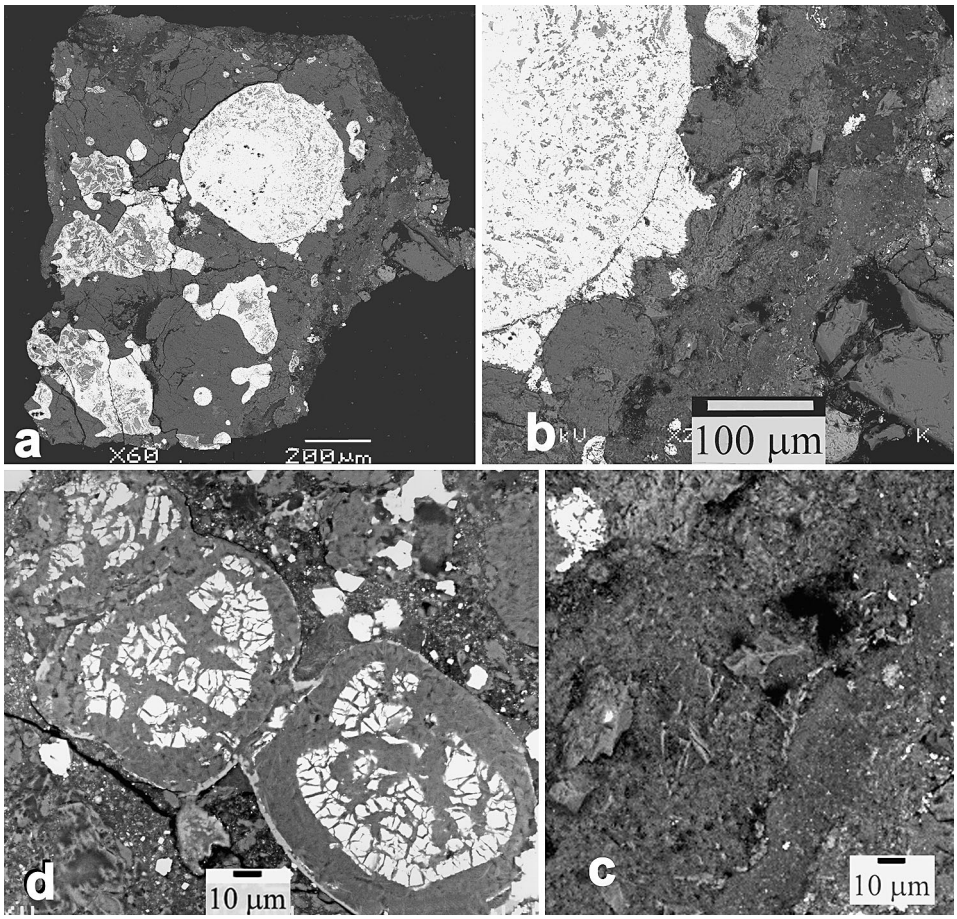

Fig. 19. BSE images of another type of CM1 lithology, Type 2. In this lithology pyrrhotite forms large blebs, which may be chondrule remnants, rather than acicular crystals. (a) Low- and (b) high-magnification images of the lithology, showing the abrupt boundary between pyrrhotite and host phyllosilicate. (c) High-magnification view of the matrix phyllosilicates, showing the almost complete absence of pyrrhotite. (d) Unusual (but here typical) association of serpentine and pyrrhotite in small rounded objects (altered chondrules?).

C2 Lithology A

This Kaidun lithology is described here for the first time, and is easily distinguished from lithology C2-B. The largest sample of this lithology is shown in Figure 20 (section 01.3.18A), a clast measuring 2 mm in longest dimension. This lithology consists of matrix of fine-grained serpentine, pyrrhotite and pentlandite with scattered larger crystals and rare lithic fragments (generally up to 0.1 mm). Only one larger component is observed – a mm-long fragment of chabazite-Na [$(Na_2,K_2,Ca,Mg)(Al_2Si_4O_{12})\cdot 6(H_2O)$], the first known occurrence of this zeolite phase in a meteorite. This particular chabazite-Na grain shows zoning of Na typical of heated material.

- Mineralogy and Petrography

The matrix consists of serpentine with fibrous, platy and cylindrical morphologies typical for serpentine-containing carbonaceous chondrites. We did not observe any saponite among the matrix. The compositional range of this serpentine, when displayed on a Fe-Mg-(Si+Al) diagram (Fig. 15), is rather Mg-rich, with a Mg/Fe ratio of ~4. Such a high Mg-content is typical for CM chondrites

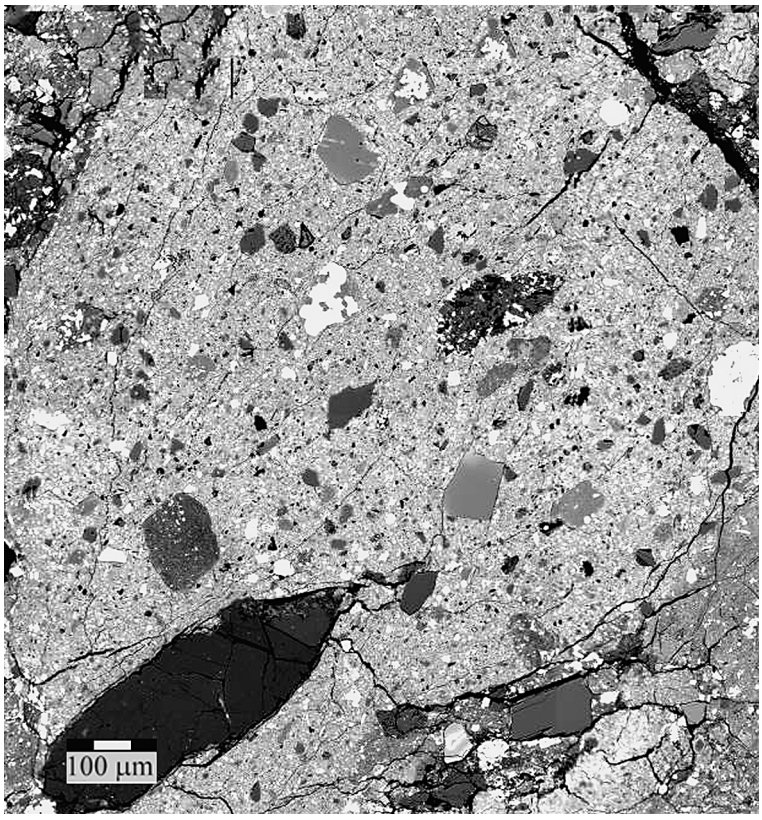

Fig. 20. BSE image of a single example of a unique C2 fragmental breccia. Numerous olivine, pyroxene, Ca-carbonate, pyrrhotite/pentlandite, and lithic fragments can be seen. At the lower left is a large zeolite fragment (black – under the scale bar).

that have experienced an advanced degree of aqueous alteration (McSween 1987; Zolensky et al. 1993; Browning et al. 1993), although this clast is probably not CM chondrite material.

Pyrrhotite and pentlandite are very abundant in the matrix, appearing as individual grains and clusters, making it very difficult to obtain reliable microprobe analyses of matrix serpentine. We did not find any tochilinite, a mineral generally found in CM2 chondrites.

- Large Components

Set within the matrix-supported fabric are abundant crystal and rare lithic fragments. The crystal fragments include olivine (generally unzoned, Fa_{1-36} with a pronounced peak at Fa_1), low-Ca pyroxene (Fs_{1-24}), pyrrhotite, and pentlandite. The anhydrous silicates have rounded, embayed outlines, consistent with partial dissolution. Coarse-grained aggregates of serpentine are very abundant, with approximately the same composition as found in the matrix.

We did not observe any chondrules, although this could be a sampling artifact. However, there are no chondrule fragments either. A few small lithic clasts are present, but have not been analyzed.

The most interesting feature of the lithology is the presence, within one clast, of a rather large (1 mm long) splinter of heated chabazite-Na. This phase appears to be unique for meteorites and is suggestive of a wet history followed by heating.

- Classification and Genesis

This lithology is clearly a fragmental breccia of type C2, however, not much else is certain. We have not attempted to determine bulk compositional data for separated clasts of C2-A material, because of their small sizes. The ubiquitous presence of rather Mg-rich serpentine, but no saponite or other high temperature phyllosilicate, suggests prolonged exposure to low-temperature aqueous fluids for some components of the breccia. However, the presence of abundant residual olivine and pyroxene shows that alteration was far from complete, and that the assembled bits of this breccia had quite different histories.

C2 Lithology B

This lithology is described here for the first time. The largest sample of this lithology is shown in Fig. 21 (from section d3), and is a clast measuring about 1 mm across. The bulk of this C2 lithology consists wholly of fine-grained materials set within still finer-grained matrix. Matrix consists of sub-micron grain size serpentine, olivine, low-Ca pyroxene, pyrrhotite and Ca-carbonate. Scattered within the matrix are larger grains, measuring up to 40 µm, of the matrix minerals (Figs. 21a,b). Also set within this matrix are a couple of 300 µm-sized coarser-grained clasts (Fig. 21a). These appear to contain the same minerals as the matrix, although they have received limited characterization to date.

- Mineralogy and Petrography

The matrix phyllosilicates in this lithology are dominated by Fe-rich serpentine. This serpentine is *very* iron-rich (Fig. 15), lying at the extreme Fe-rich end of the serpentine compositional range observed for type 2 chondrites. Based upon our experience with CM2 chondrites (Browning et al. 1996), such Fe-rich compositions indicate a low degree of aqueous alternation. This is consistent with the extremely fine-grained size of olivine in the matrix, which would have been completely destroyed during prolonged alternation. Matrix serpentine displays, variously, fibrous, platy and cylindrical morphologies, as it does in most other serpentine-containing carbonaceous chondrites (Zolensky et al. 1993). Saponite, so common in aqueously-altered Kaidun lithologies, has not been

found. Pyrrhotite is intimately intergrown with the matrix serpentine, however, complicating compositional analysis.

Olivine and pyroxene are common in this lithology, but only as very small, somewhat rounded grains. Compositional variability is high – $Fa_{5–79}$, and $Fs_{3–20}$. We did not observe large crystals or chondrule fragments that are characteristic of all other C2 chondrites. It is of course possible that chondrules are very rare in this lithology, as they are in the Tagish Lake C2 chondrite (Zolensky et al. 2002a), in which case one might not expect to see even one chondrule in most randomly selected, small, mm-sized clasts. However, it is also possible that the lithology is simply uniformly fine grained, with no larger components.

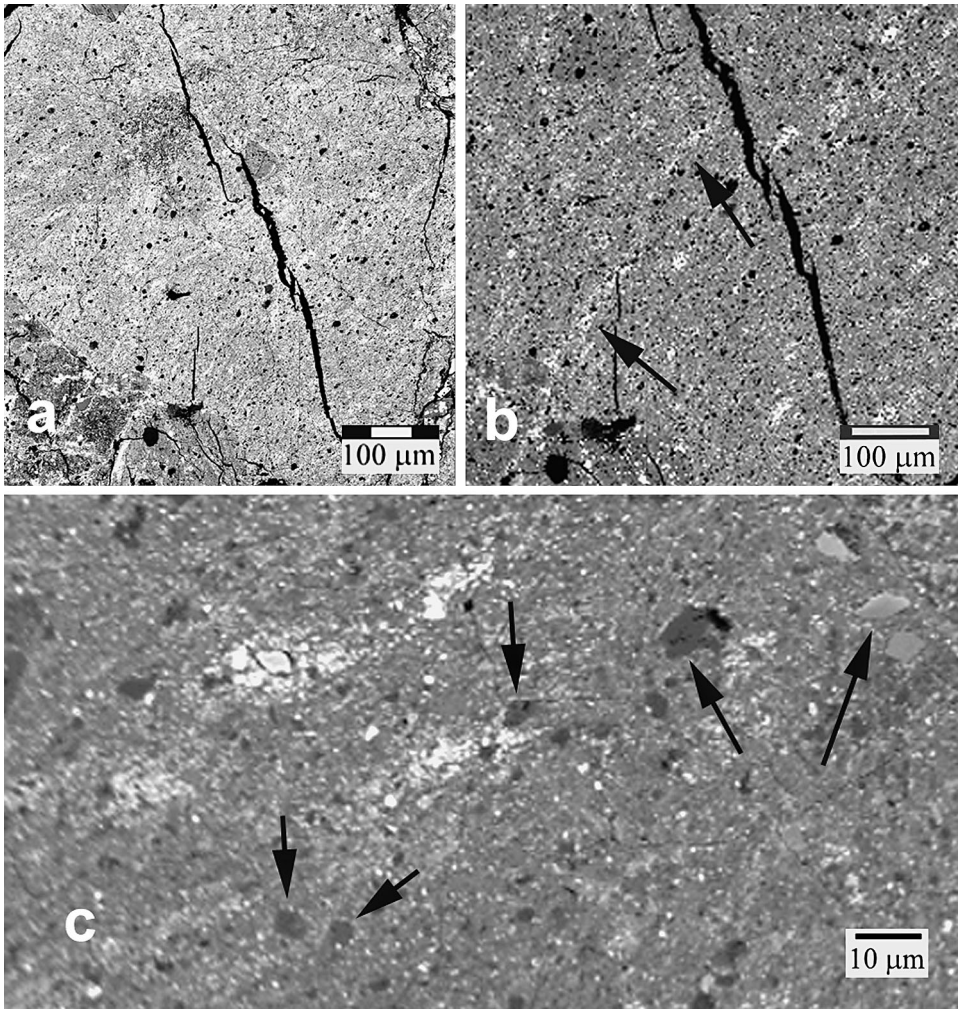

Fig. 21. BSE images of a common C2 lithology in Kaidun. (a and b) Slight foliation is imparted to this lithology by pyrrhotite strings [arrows in (b)]. The only exception to the overall fine-grained nature of this lithology is a slightly coarser-grained aggregate in the center of the image. (c) Higher magnification image from the center of (b), showing the strings of pyrrhotite grains (white) and numerous fine-grained olivine and pyroxene grains (arrows).

Pyrrhotite is very abundant and consistently contains 1–2 wt.% Ni. Irregular disk-shaped lenses of this mineral define a foliation (Fig. 21). These lenses could be due to shearing, but could also have arisen due to a sedimentary regolith process, as described below.

Sitting within matrix are abundant, though small (< 30 µm), grains of Ca-carbonate. We do not know if these are calcite or aragonite. This Ca-carbonate is very pure, with FeO less than 1 wt.%, and MgO below microprobe detection limits. Such carbonates are typical for most C2 chondrites.

- Classification and Genesis

We have no bulk chemical data for this lithology, and it may not be possible to obtain these. The presence of both abundant serpentine as well as common anhydrous silicates appears to require a classification as C2. However, the apparent lack of chondrules (or even altered chondrules) sets this material apart from any other known C2 material.

There are clasts of similarly fine-grained, though anhydrous, materials in CV3 and several unequilibrated ordinary chondrites, and Zolensky et al. (2002b) have suggested that these are samples of ponded deposits, as have been observed on the near-Earth asteroid Eros. The mechanism suggested for their formation is that seismic shaking (from impacting bodies) caused segregations of asteroid surface grains based upon grain density and size. With this mechanism, one would form layered deposits of fine-grained materials, with the layering being most apparent by thin beds of the smallest and densest grains. Discontinuous beds of dense pyrrhotite grains are observed in the Kaidun C2 lithology. It is interesting that such fine-grained materials are not observed in other C2 chondrites (M.E. Zolensky 2002, unpublished data).

Another possibility is that this lithology is related to the Tagish Lake C2 chondrite (Zolensky et al. 2002a). The carbonate-poor lithology of Tagish Lake is very similar to this Kaidun lithology in terms of mineralogy and structure. Tagish Lake also contains very few chondrules – about one per cm^2. The vast majority of masses of Tagish Lake the size of the clasts in Kaidun would not be expected to carry even a single chondrule. The proposed source of Tagish Lake is the D-class asteroids (Hiroi et al. 2001).

C1 Lithology

This lithology is described here for the first time. Typical examples of this lithology are shown in Fig. 22 (section d3), these are clasts measuring up to about 3 mm across. This C1 lithology consists wholly of fine-grained matrix. The only larger components are an occasional 100 µm sulfide grain or phyllosilicate aggregate. Matrix consists of submicron grain size serpentine, saponite, pyrrhotite, pentlandite and magnetite.

- Mineralogy and Petrography

The matrix phyllosilicates are dominated by Mg-rich serpentine and saponite, with a grain size so fine that separate phases cannot be distinguished at the 5um level. This phyllosilicate material thus plots at compositions intermediate between Mg-rich serpentine and saponite (Fig. 15), compositions typical of CR2 and CI1 matrix (Zolensky et al. 1993). Matrix serpentine displays variously fibrous, platy and cylindrical morphologies, and the saponite has its typically flaky morphology (Zolensky et al. 1993). Pyrrhotite, pentlandite, and magnetite are intimately intergrown with the matrix serpentine, complicating compositional analysis.

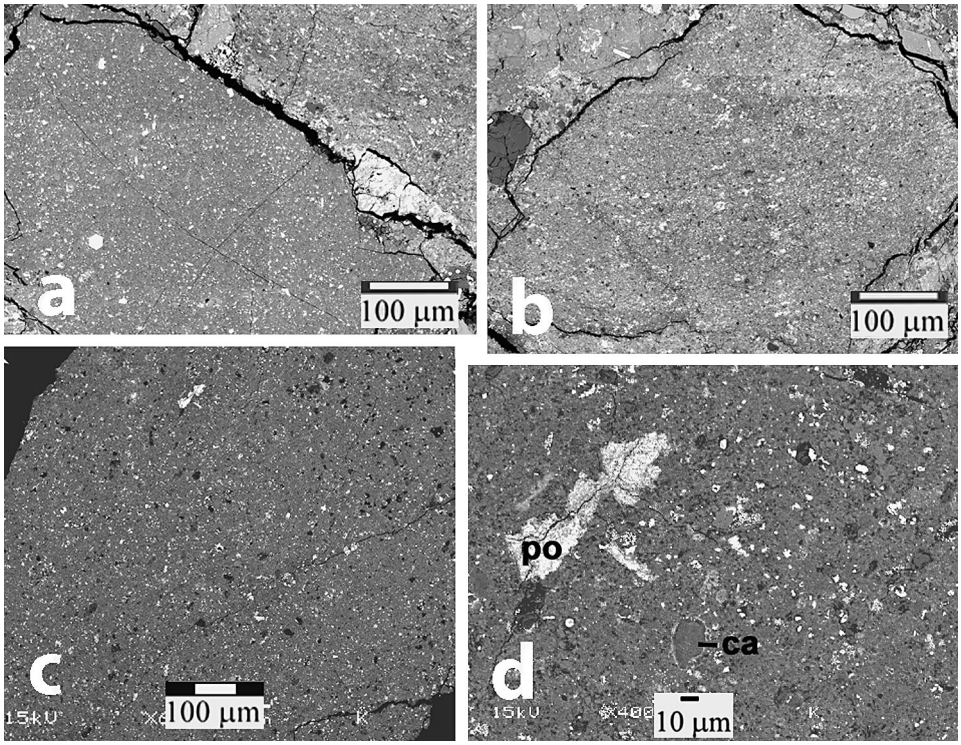

Fig. 22. BSE images of C1 lithologies in Kaidun, showing the subtle differences in these lithologies, despite essentially the same mineralogy. (a) Massive, rather homogeneous texture. (b) Slight foliation of the pyrrhotite. (c) High porosity, with pore spaces being black. (d) Closeup of lithology in (c), showing fine-grained Ca-carbonates (ca) and pyrrhotite aggregates (po).

Anhydrous silicates appear to be absent. There are no chondrules, aggregates, CAIs, crystal fragments, or even recognizable pseudomorphs of these. Pyrrhotite and pentlandite are very abundant and in places form thin rims about phyllosilicate and carbonate aggregates (Fig. 22d).

- Classification and Genesis

We have no bulk composition for this lithology, and it may not be possible to obtain this. However, identical material (Kaidun 40.23) was analyzed for O isotopes and bulk chemistry. The O isotope composition of 40.23 lies among CI chondrites on the 3-isotope oxygen plot. However, the bulk composition of 40.23 is more consistent with CM and CR material. The presence of both abundant phyllosilicates as well as the complete absence of anhydrous silicates, or even evidence of pseudomorphs after these suggest classification as C1, and probably CI1. However, the unusual bulk composition must set this material apart from known CI1 materials.

About all that may be said here is that aqueous alteration has completely altered whatever the precursor material must have been. Presence of saponite suggests relatively high temperatures during alteration, on the order of 100–125 °C (Zolensky et al. 1993).

R Chondrite Lithology

A single clast from Kaidun has been described by Brandstätter et al. (1996) as a probable R chondrite. The fragment measures 0.6 by 3.5 mm and has a sharp contact with the host meteorite. The lithology appears to be a fragmental breccia, with recognizable fragments of porphyritic olivine, porphyritic pyroxene, and barred olivine chondrules, set within a granular matrix of, predominantly, olivine (Fig. 23). Lithic fragments are also present, some with fine-grained igneous textures containing olivine, pentlandite, pyrrhotite and chromite.

Matrix and chondrule olivine is uniformly Fe-rich, with a mean composition of Fa_{33}, with 0.44 wt.% MnO, 0.08 wt.% NiO and concentrations of CaO, Al_2O_3 and Cr_20_3 below 0.1 wt. Low-Ca pyroxene ($Fs_{12}Wo_1$ to $Fs_{26}Wo_1$) and diopside ($Fs_{11}Wo_{47}$) are abundant. Additional Ca-pyroxenes with widely varying compositions ($Fs_{20–26}\,Wo_{7–23}$) are present in low abundance. Chondrule mesostasis is predominantly albite ($An_8Ab_{87}Or_5$) and pyroxene, though small amounts of anorthite ($An_{85}Ab_{15}$) are also present.

Although this lithology appears to lack typical fine-grained matrix, the presence of chondrules and mineral compositions permit classification as R3 chondrite. As is typical for R3 chondrites, equilibrated olivine is present with unequilibrated pyroxene. This classification is tenuous due to the small sample available for study, and the unusual granular matrix that imparts the appearance of being an igneous rock.

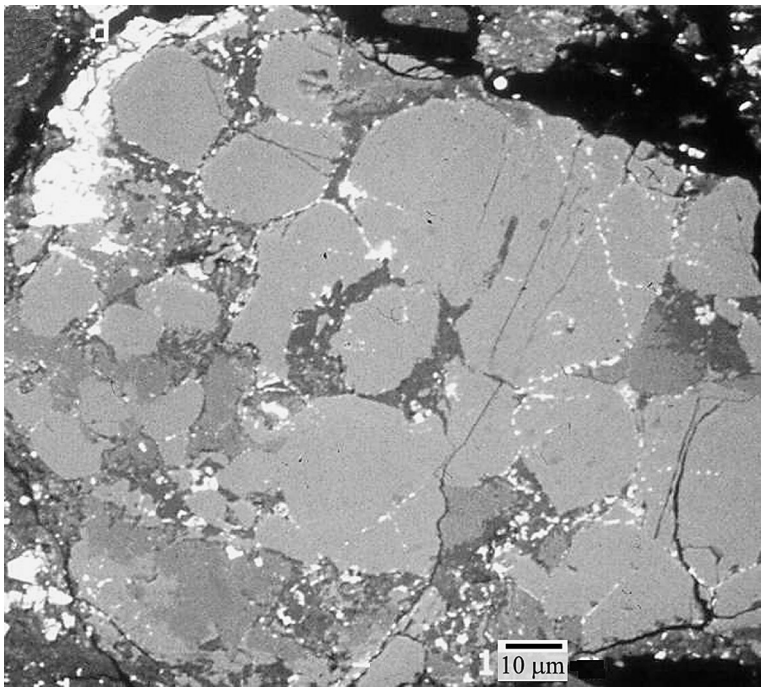

Fig. 23. BSE image of the single recognized R chondrite clast in Kaidun, showing characteristic Fe-rich olivine and enclosed metal grains.

Ca-rich Achondrite Fragment

Mineralogy and Petrography

Clast #58.08 has been studied exhaustively because of its unusual nature (Migdisova et al. 2000). This lithology contains 97 vol.% silicate minerals and only 3 vol.% Fe-Ni metal + troilite. The size of silicate grains varies from 50–80 to 200–300 µm. Metal and troilite form a net of thin stringers along microfractures between and within grains of silicate minerals. The fragment has an ophitic, locally poikilitic, texture. It is devoid of any evidence of shock.

The modal mineralogical composition (vol.%) is: diopside 32.2, enstatite 30.9, olivine 21.4, plagioclase 12.4, metal 2.3, and troilite 0.8. All silicate phases are compositionally homogeneous: diopside ($Fs_{2.6}Wo_{42.3}$), enstatite ($Fs_{5.5}$ $Wo_{3.6}$), olivine ($Fa_{5.5}$), and plagioclase ($An_{29.5}$ $Or_{1.2}$) (Migdisova et al. 2000). According to two-pyroxene thermometry (Lindsley 1983), the equilibrium temperature of this fragment is estimated at 1000–1100 °C, though with large error bars. The equilibrium composition of the mineral phases suggests post-accretion annealing.

Point counting was used to calculate the following whole-rock composition (wt.%) of this lithology: SiO_2 50.5, TiO_2 0.24, Al_2O_3 2.9, Cr_2O_3 0.52, FeO 2.8, MnO 0.33, MgO 27.4, CaO 7.8, Na_2O 1.0, K_2O 0.02, Fe_{met} 4.9, Fe_{sulf} 0.78, Ni 0.58, Co 0.05, P 0.04, S 0.38.

Discussion

Silicates compose 97 vol.% of the Kaidun fragment. A similarly high proportion of silicate phases is found only in silicate inclusions in the Odessa anomalous iron (99 vol%, on the average) (Marshall and Keil 1965). The fragment is comparable with other types of meteorite materials in plagioclase proportion, but has a rather large Px/Ol ratio. The ratio of low-Ca to high-Ca pyroxene is similar only to that of silicate inclusions in the Odessa meteorite.

This lithology differs from meteorite material mentioned above in its plagioclase composition – $An_{30}Or_1$. Compositionally similar plagioclase is found only in a silicate inclusion in the Kendal County anomalous iron meteorite (Bunch et al 1970).

- Classification and Genesis

The mineralogical characteristics of this lithology, being intermediate between enstatite and ordinary chondrites, suggest that it was formed in a more reducing environment than ordinary chondrites. The mineral assemblage, mineral and bulk compositions suggest close similarities to winonaites and silicate inclusions in IAB iron meteorites, which represent the primitive achondrites.

Alkaline-Enriched Lithologies

Two clasts enriched in alkaline elements were found in Kaidun that may be related genetically, as explained below.

Clast #d4A

This clast is a twinned albite crystal 1.2 × 0.7 mm in size (Ivanov et al. 2001a, 2002a). The crystal contains small (30–40 µm) inclusions of fluorapatite and a polymineralic inclusion

consisting of aenigmatite, wilkinsonite and arfvedsonite. This is the first time aenigmatite and wilkinsonite have been found in meteorites and only the second time wilkinsonite has been found in nature.

Albite ($Ab_{90.3}Or_{6.8}$) shows weak chemical zoning. It appears to be among the largest albite grains detected in meteorites. Aenigmatite is present in two settings – within a multiphase inclusion and in an intergrowth with a relatively large fluorapatite crystal. The composition of the two varieties is somewhat different:

$$Na_{2.0}(Fe^{2+}_{4.1},Mg_{0.8},Ca_{0.1},Mn_{0.1})Ti_{1.0}(Si_{5.9},Al_{0.2})O_{20} \text{ and}$$
$$Na_{2.1}(Fe^{2+}_{3.4},Mg_{1.4},Ca_{0.1},Mn_{0.1})Ti_{1.0}(Si_{5.9},Al_{0.1})O_{20}.$$

The compositions of both aenigmatites differ noticeably from the composition of terrestrial aenigmatites in MgO and also MnO contents. The content of MgO in terrestrial aenigmatite never exceeds 3 wt.% and is usually smaller that 1.5 wt.% (e.g., Mitrofanova and Afanas'eva 1966; Jones 1984; Stolz 1986), whereas the MgO contents in aenigmatite from the Kaidun clast are 3.6 and 6.8 wt.%. The MnO content in terrestrial aenigmatite usually exceeds 1 wt.% and quite often exceeds 2 wt.%, whereas MnO content in Kaidun aenigmatite is 0.5–0.8 wt.%.

Wilkinsonite occurs as very small grains, no more than 5 µm in size. Its composition $[(Na_{2.0}(Fe^{2+}_{3.6}Mg_{0.2},Mn_{0.1},Ca_{0.1})(Fe^{3+}_{1.9},Al_{0.1},)Si_{5.97}O_{20})]$ has a noticeably higher MgO content and lower MnO content in comparison with the only known terrestrial wilkinsonite found in an Australian trachyte which contains MgO <0.1 wt.% and MnO >1.0 wt.% (Duggan 1990). Arfvedsonite is represented by a magnesia-rich variety.

Clast #d4A does not show evidence of significant secondary changes and appears to have retained its initial mineralogy. The mineral association – albite, apatite, aenigmatite, wilkinsonite and arfvedsonite – clearly indicates its nature as an alkaline rock and suggests formation by parent body differentiation.

Clast #d4A is the second alkaline rock found in meteorites. Previously, four clasts of alkaline rocks have been found in the LL3-6 chondritic breccia Adzhi-Bogdo (Bischoff et al. 1993). Kaidun clast #d4A and the alkali-granitoid clasts of Adzhi-Bogdo are similar in some respects (Ivanov et al. 2001b, 2002a).

Clast #d(3–5)D

This clast measures only ~3 mm in size. Its overall texture is defined by an ophitic main mass speckled with large pyroxene (up to 400 µm in size) and fluorapatite (up to 120 µm) grains (Ivanov et al 2001b). The pyroxene grains are characteristically rounded and fluorapatite grains are subhedral. Eight of the nine pyroxene grains found in the thin sections are high-Ca and one (190 × 80 µm) is low-Ca. The main mass of the clast consists of skeletal to rectangular plagioclase crystals submerged in a finely-crystalline to glassy mass of complex composition (Fig. 25). The plagioclase crystals are commonly lath-shaped, ~400 × 40 µm in size and are skeletal to rectangular. They are usually surrounded by thin pyroxene crystals. Potassium-rich grains with anorthoclase composition are ubiquitous in the matrix. No opaque phases were found in the clast.

One section #d3D contains a rounded, amoebae-shaped piece of Kaidun's carbonaceous matrix in contact with the clast material, which at this site is a uniform, crystal-free glassy mass (Fig. 25b). The unusual feature of clast #d(3–5)D is the presence of cavities with thin coatings on their walls. These cavities will be discussed separately below.

All large grains of high-Ca pyroxene in this lithology are of nearly constant major element compositions (augite $Fs_{21.6}Wo_{36}$). The only low-Ca pyroxene grain we found has a pigeonite composition ($Fs_{42.9}Wo_{9.9}$). Chemical zoning is not present in the crystals.

Matrix plagioclase varies widely in composition ($An_{16.0–34.5}$ $Ab_{64.6–82.1}$ $Or_{0.8–1.2}$, average $An_{21.8}$ $Ab_{76.7}$ $Or_{1.5}$) and usually has a high content of foreign components. Wide variation in compositions also were noted in the fine subcalcic augite crystals of the matrix ($Fs_{36–54}Wo_{15–27}$). Some portions of the matrix have potassium-rich anorthoclase compositions.

In normalized composition, the matrix of the clast is more than 83.5 vol.% plagioclase ($Ab_{82.2}$ $An_{14.2}$ $Or_{3.6}$), 9 vol.% pyroxene, and 5.8 vol.% olivine. The texture of the main mass of the clast is finely crystalline to glassy, containing skeletal and subangular plagioclase crystals. This texture probably formed by rapid cooling of a melt. According to an experimental study of the morphology of plagioclase crystals during crystallization (Lofgren 1974; 1980), presence of skeletal subangular crystals indicates supercooling of the melt of ~150 °C, with a cooling rate of ~5–10 ˚C/h. A rounded contact between the body of the clast and an adjacent carbonaceous chondrite clast in #d3D clearly indicates that the former was plastic or in liquid form during the assembly of the meteorite.

It is possible that the formation of clast #d(3–5)D occurred during a high-velocity impact event during which the impactor was heavily melted. However the smooth, rounded edges of most of the large mineral grains in clast #d(3–5)D are incompatible with formation by crystallization of this melt, instead suggesting the opposite process of resorption of crystals in the melt. The large mineral grains of the clast appear to be the remains of a previously existing fragment that has undergone melting.

The formation of the phyllosilicate coatings within this lithology's vesicles requires the presence of a late-stage aqueous fluid. The presence of the fluid can be connected with contamination of water and other volatile components from the carbonaceous matrix of the meteorite. However, the melting and crystallization of clast #d(3–5)D must have occurred on or near the surface of the parent body. There are no reasons to expect intensive diffusion of water and other volatile components from the matrix. The nearly complete lack of sulfur in the matrix and the low iron content (typical components of carbonaceous chondrite matrix) supports this supposition. The clasts' vesicles require a high content of volatile components in the clast precursor.

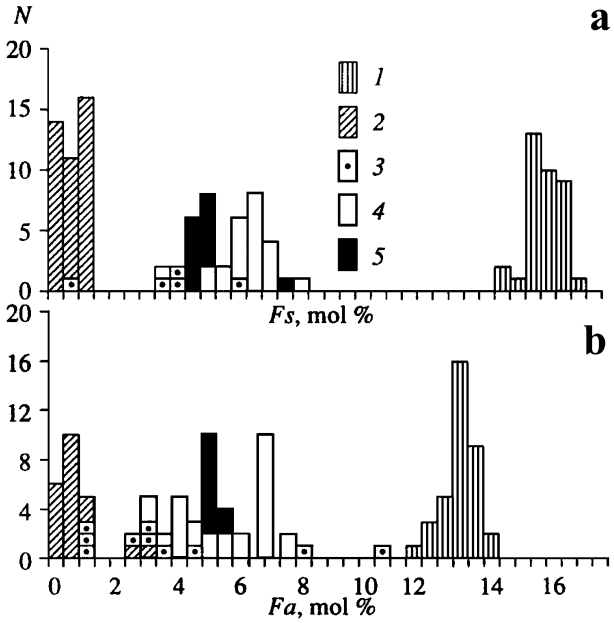

Fig. 24. Comparison of the composition of low-Ca pyroxenes (**a**) and olivines (**b**) from the Kaidun #58.08 fragment and type of meteorite materials: 1 – H chondrites, 2 – E chondrites, 3 – winonaites, 4 – IAB silicate inclusions, 5 – Kaidun fragment.

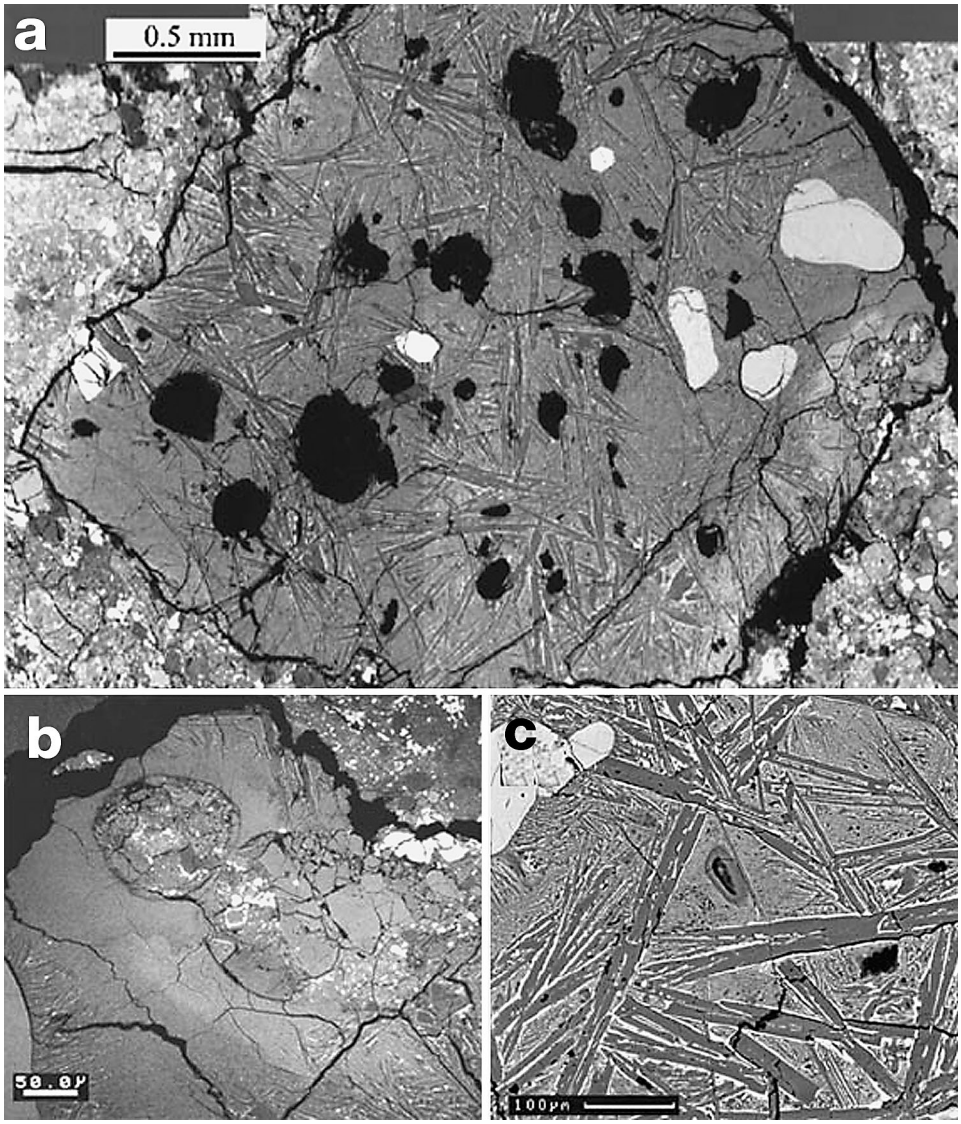

Fig. 25. (**a**) BSE images of a subalkaline fragment #d(3–5)D, section #d3. Dark areas of irregular shapes are cavities. Light-gray roundish grains are Ca-rich pyroxenes, small light grains are apatite. (**b**) BSE images of margin zone of the fragment #d(3–5)D, section #d3, with roundish inclusion of carbonaceous matrix of the meteorite. The region of the clast in contact with matrix has a glassy structure. (**c**) BSE images of central part of the fragment #d(3–5)D, section #d4. Elongated plagioclase laths are submerged in a fine-crystalline mass. A cavity with colloform coating is in center. A part of a rather large Ca-rich pyroxene grain is in upper left.

The matrix of clast #d(3–5)D, as mentioned above, has been insignificantly contaminated by material from the matrix of the meteorite (if at all), which permits us to evaluate the character of the precursor material that underwent melting. When determining the nature of the melted primary material, key parameters appear to be: (1) relict character of the large grains of the clast under study – two different pyroxenes and fluorapatite, (2) the high content of alkali plagioclase in the clast, and (3) the lack of significant amounts of olivine. These parameters indicate a strongly differentiated character for the melted material. Based on the bulk SiO_2 content and the sum of Na_2O+K_2O in clast #d(3–5)D, in reference to terrestrial rocks, the clast falls among the intermediate rocks of the subalkaline series, in the family of trachyandesites.

The material of clast #d(3–5)D is similar in some characteristics to the material of the basaltic shergottites. The olivine content of clast #d(3–5)D, according to norm calculations, is less than 5 vol.%. The clast contains fairly large grains of augite and pigeonite, which is typical for shergottites. The clast's pyroxene compositions fall in fields corresponding to the pyroxenes of shergottites in the pyroxene prism (Meyer 1998). However, the average calcium content in clast augite is somewhat lower and that in pigeonite is somewhat higher in comparison with the calcium content of shergottite pyroxenes. This difference may be connected with the lower equilibration temperature of clast pyroxenes in comparison with the equilibration temperature of shergottite pyroxenes (Lindsley 1983).

Phosphide-Bearing Clasts

One Kaidun clast (#53.10) contains the new mineral florenskyite (FeTiP) (Ivanov et al. 2000a). This clast consists of extremely brecciated carbonaceous and enstatite chondrite material, showing various degrees of asteroidal alteration. Among these fragments are two rounded serpentine-dominated masses of similar mineralogy (masses 1 and 2, measuring 90 × 190 µm and 300 × 90 µm, respectively) (Fig. 26a). Both masses contain numerous laths of Fe-Cr phosphides measuring up to 1.0–1.5 µm in width and up to 5 µm in length. The laths often form extended chains up to 100 µm in length. Four dispersed anhedral to subhedral grains of florenskyite with a maximum dimension of 14 µm were discovered in phyllosilicate mass 1. The florenskyite composition can be approximated by the formula $Fe_{1.01}(Ti_{0.87}Ni_{0.13}Cr_{0.03}V_{0.02}Co_{0.01})_{1.06}(P_{0.97}Si_{0.03})$, which is very close to the ideal formula FeTiP.

The chemical compositions of the thinnest Fe-Cr-phosphide laths were calculated by subtraction of matrix compositions of immediately adjacent regions from multiphase microprobe analyses. They are different for phosphides from the two different masses but rather similar within each mass. The compositions of the laths can be calculated to formulas $(Fe,Ni,Co)_{4.79}(Cr,V)_{0.83}(P,Si)_3$ and $(Fe,Ni,Co)_{4.13}(Cr,Ti,V)_{1.80}(P,Si)_3$. The ideal formulas for these phosphides can be written: $(Fe,Ni,Co)_5(Cr,V)(P,Si)_3$ and $(Fe,Ni,Co)_4(Cr,Ti,V)_2(P,Si)_3$, respectively. The first of these phosphides is apparently similar to material found in the ALH85085 CH chondrite (Kimura and El Goresy 1989; Zanda 1992), whereas the second has not previously been reported.

The regular distribution of the Fe-Cr phosphide laths in the host serpentine masses suggests formation by alteration or recrystallization, possibly during cooling, of material enriched in Cr and P. The homogeneous distribution of the laths in both masses further suggests homogeneity of the precursors in P and Cr (and Ti in mass 2). Kaidun contains enstatite chondrite lithologies displaying varying degrees of aqueous alteration. The formation of such precursors could be explained as a result of remelting of a mineral

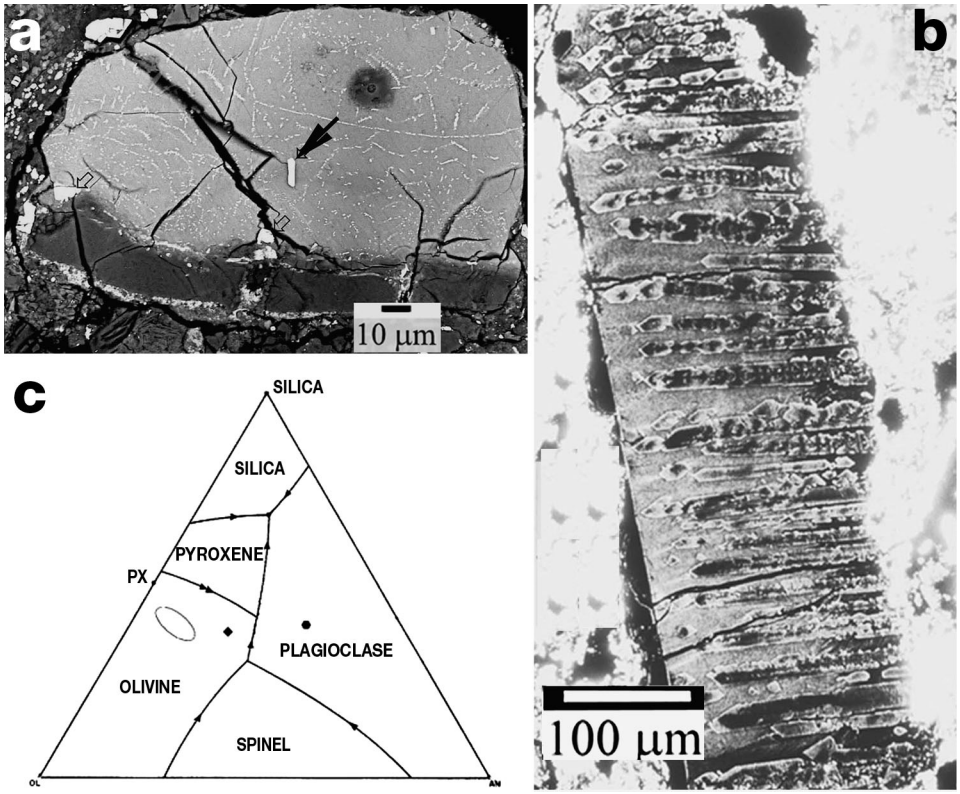

Fig. 26. (**a**) BSE images of the phosphide-containing grain #53.10. The grains of florenskyite FeTiP are indicated by arrows. Fe-Cr phosphide are present as white linear arrays throughout the matrix. (**b**) BSE images of a fragment #d3C whose structure indicates fast crystallization from a superheated melt. (**c**) The composition of the phases of the fragment #d3C, shown in **(b)**, on the three-component diagram Q–An–Ol (Walker et al. 1972). The ellipse is the area of composition of pyroxene crystals, dot is composition of interstitial glass, and rhomb is a calculated average composition of the fragment.

assemblage including Fe-Ni metal, schreibersite, daubreelite, osbornite and/or heideite. Partial loss of volatile components such as S or N would have accompanied the hypothesized melting. It is also possible that these chains have recrystallized from impact melt veins of metal. Rubin (2003) has recently proposed that such veins are rather more common in chondrites than has been previously realized. Florenskyite could have formed as a result of cooling and crystallization of a melted precursor consisting mainly of Fe-Ni metal enriched in P, Ti, and Cr.

These phosphide-containing masses experienced aqueous alteration on the parent body, which resulted in complete alteration of the metal matrix and production of the serpentine. Ti-Cr rich phosphides should have been stable during such alteration.

Note the florenskyite is the first natural phosphide of a lithophile element (Ti). This mineral is thus the first example of a new mineral group – phosphides of lithophile elements.

Melt Features

Kaidun contains many variously melted fragments. In this respect the meteorite differs appreciably from carbonaceous and enstatite chondrites in which such fragments are very rare to unknown.

Splashes

Splashes are very common features on the surfaces of lunar regolith particles (Carter and MacGregor 1970; McKay et al. 1970; Florensky et al. 1974). They form by micrometeorite bombardment of the lunar surface, which is one of the main processes of regolith formation on atmosphereless bodies. One also encounters larger melted bodies in ordinary chondrites and howardites, which are due to the impact of larger objects. Melted bodies are also found as small fragments in Kaidun (Ivanov et al 1996a).

An open cavity with a glassy coating up to ~100 µm in thickness on one inner wall was found in Kaidun sample #53.02 (Fig. 27). There is a lithological difference between two walls of the cavity;

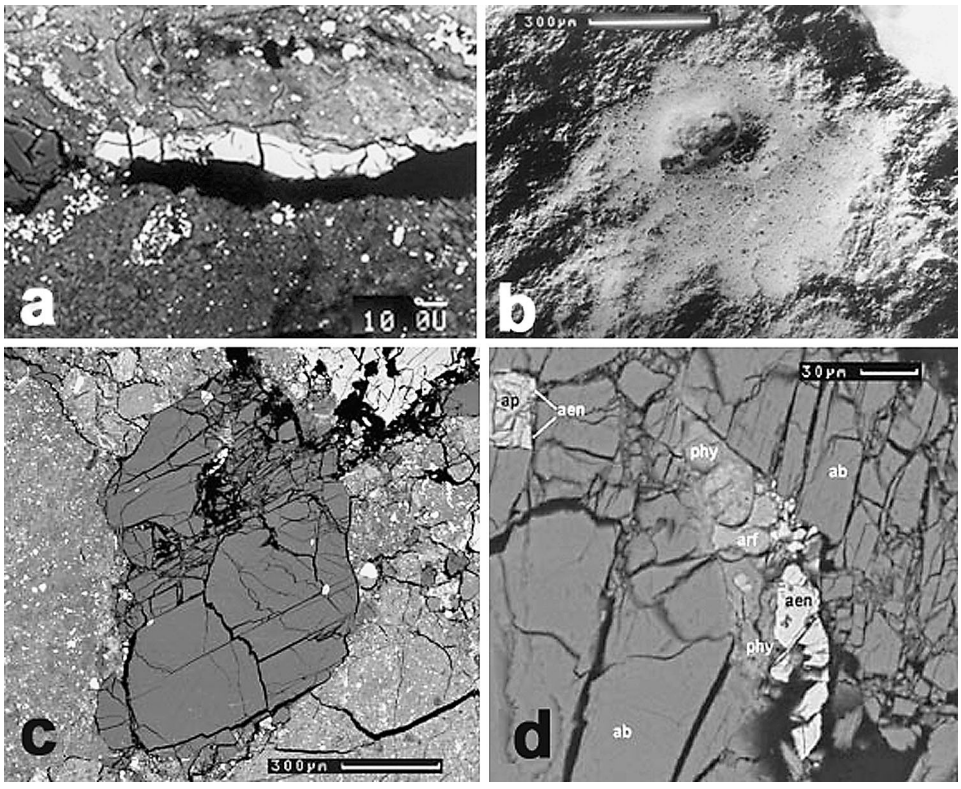

Fig. 27. (a and b) BSE images of glassy splashes inside (**a**) and on the surface (**b**) of Kaidun samples. (**c**) BSE images of albite crystal #d4A. The elongate light area in upper center is an inclusion of complex composition. Small white grains are apatite. (**d**) The inclusion of complex composition from albite (ab) crystal. A rather large apatite (ap) grain with two small aenigmatite (aen) grains is upper left. Arfvedsonite (arf) and phyllosilicates (phy) are also present in this image.

the coated wall has an olivine composition while the opposite wall is a carbonaceous chondrite breccia. The contact of the coating with the olivine clast shows evidence of an interaction of materials whereas the contact with a carbonaceous material is sharp. A similar feature was found in sample #58.02. In this sample there is an elongated cavity; two walls of the cavity consist of carbonaceous chondrite material of different lithologies, and one wall has a coating with thickness up to 15 µm. These coatings are essentially iron oxide (62 and 77 wt.% FeO) with admixture of lithophile components. They are very similar to products of parent body aqueous alteration of Fe-Ni metal that were studied in detail in enstatite chondrite lithologies in Kaidun.

The characteristics of the coatings in #53.02 and #58.02 are: (1) presence in cavities on one of the walls, (2) different lithologies of coated vs. non-coated walls, (3) the traces of a complex interaction between coating and wall in #53.02. These characteristics suggest that the coatings were applied to regolith before the final consolidation of the meteorite. The present composition of the splashes can be interpreted as resulting from aqueous alteration of metal.

A component in Kaidun that appears identical to lunar splashes was found in sample #53.15 (Fig. 27b). The size of this splash is ~0.6 mm. The character of interaction of splash material with a small hillock on the surface of the target shows the direction of movement of melted material during splash formation. This splash is very iron-rich and is probably also altered metal.

Morphologic evidence of regolith processes are relatively uncommon in meteorites. The presence of splashes in Kaidun could provide an important glimpse into regolith forming processes occurring on small bodies.

Fast crystallization of a fragment from a superheated melt

Kaidun clast #d3C was found within a carbonaceous matrix in a large thin section and demanded attention owing to its rather unusual texture (Ivanov et al. 2000b). The fragment is ~1.0 × 0.28 mm in size and has a subregular rectangular shape (Fig. 26b). One long side forms an uneven, wave-shaped boundary with the matrix; the other has a smooth, straight boundary with a thin (~30 µm) olivine strip. The fragment shows no visible traces of interaction with the olivine. The fragment is dominated by skeletal layered pyroxene crystals growing perpendicularly from the uneven long side, parallel to each other. The crystals are 220–270 µm long and 15–40 µm wide. The spaces between the crystals are 15–45 µm wide and filled with partially devitrified glass, which contains faint traces of crystals growing from the side touching the olivine strip.

The skeletal pyroxene crystals show zoning and large compositional variations ($Fs_{6.9–11.6}Wo_{8.4–41.4}$). The crystals' cores are usually Mg-rich, and the rims Ca-rich. The interstitial glass is almost uniform in composition. In the An–Ol–SiO_2 system it may be represented as $2An \cdot Ol(Fa_{37}) \cdot 2SiO_2$. The olivine strip next to the studied fragment has an average composition of $Fa_{7.3±0.4}$.

On a An–Ol– SiO_2 diagram for mole ratio Fe/(Fe+Mg)~0.3 (Walker et al. 1972), the fragment's bulk and pyroxene compositions fall in the olivine field, while the glass composition falls in the plagioclase field rather far from the Ol–An boundary (Fig. 26c). Thus the fragment did not crystallize under equilibrium conditions. Occurrence of this nonequilibrium phase assemblage may be explained from dynamic crystallization experiments (Grove and Bence 1979), which show that the change of phase appearance is coupled with high over-saturation of glasses with plagioclase during fast cooling. The skeletal morphology and high Al_2O_3 contents of the pyroxene in the fragment also suggests rapid cooling. According to experimental data (Grove and Bence 1979), the cooling rate appears to have been several hundred degrees per hour. Phase equilibrium calculations suggest the fragment's glass was annealed at temperatures above 1250–1270 °C (Ariskin et al. 1997). The upper limit of the temperature of the melt is ~1850 °C, as follows from the melting temperature for $Fa_{7.3}$.

There are two possible formation mechanisms for this fragment. It may be a crystallized splash formed during an impact event on a parent asteroid. However, in such a case it is difficult to imagine the presence in the regolith of a smooth, unaltered strip of olivine. It seems more realistic

to suppose the studied fragment and the adjacent olivine strip have a common origin and may be a fragment of a barred chondrule destroyed by a shock and heating event. In this case the basalt-like mesostasis was melted whereas the olivine bar remained unmelted – a common occurrence (Gary Lofgren, personal communication, 2003). The unusual composition of the fragment's glass, characterized by almost constant stoichiometric proportions, suggests clustering of the melt before crystallization.

Melted features in the Kaidun meteorite are not limited to the two clasts described above. Formation of florenskyite-containing small phyllosilicate masses as well as of the subalkaline clasts are also connected with melting of material. The study of melted fragments in Kaidun is only just now beginning.

Crystals in Cavities

Some samples of the Kaidun meteorite contain cavities filled with crystals. Compositions of the crystals are very different from clast to clast, requiring mother fluids of different compositions.

Geode of Iron Crystals

The initial study of the main body of the Kaidun meteorite on a fracture surface apparently opened during terrestrial impact revealed a cavity about 2 mm in diameter, filled with isometric-appearing and elongated black crystals with lengths up to 0.35 mm (Fig. 28a). The crystals are weakly bound to one another and to the wall of the cavity and most of them were lost before the sample was subjected to detailed examination.

The crystals in the cavity are α-Fe with a distorted structure (Ivanov et al 1988; Ivanov 1989b), i.e. α_2-Fe which is martensite. Their composition is rather constant (wt.%): Fe 85.3–86.7, Ni 11.7–12.0, Co 0.54–0.68, Cr 0.03–0.09, Mn 0.03–0.08, P 0.63–0.68, S 0.05–0.08, Si 0.05–.08, total 98.8–99.8. On the rim of the crystals metallic iron is replaced by a complex mixture of oxides, oxyhydroxides and sulfates.

Euhedral crystals of metal iron were previously found in the pores of recrystallized lunar breccias (McKay et al. 1972; Clanton et al. 1973, 1974) and in the pores of several shocked ordinary chondrites (Olsen 1981). There are similarities to the crystals described here. In both cases the crystals are isolated, not forming clusters, intergrowths or druses. As a rule their size is limited to from a few to several tens of microns. The metal from ordinary chondrites is kamacite (Olsen 1981). Metal crystals in lunar breccias contain <0.5 wt.% Ni (Clanton et al. 1973, 1974). The formation of such iron crystals is explained by growth from a gas phase produced during the impact heating of the material (McKay et al. 1972; Clanton et al. 1973, 1974; Olsen 1981). Thus the metallic iron crystals found in lunar breccias and in ordinary chondrites differ in many respects from the metal crystals from Kaidun. The only report of iron crystals similar to those in Kaidun is from the ordinary chondrite Gao, and these have received no detailed characterization (Marvin Kilgore, personal communication, 2003).

As shown in the phase diagram of the Fe-Ni system, iron alloys with 12 wt.% Ni at temperatures below ~750 °C fall into the double-phase (α+β) area. The presence of phosphorus lowers the double-phase area slightly (Romig and Goldstein 1981), but this does not apply to the compound under consideration. At temperatures above ~750 °C, the compound is in the mono-phase (γ) area. This situation is well illustrated in natural – lunar and meteorite – nickel-iron minerals. It should also be noted that the diagram under consideration shows stable compounds and phase characteristics of Fe-Ni alloys as they formed from melt or from an alloys heated to a high temperature and then cooled.

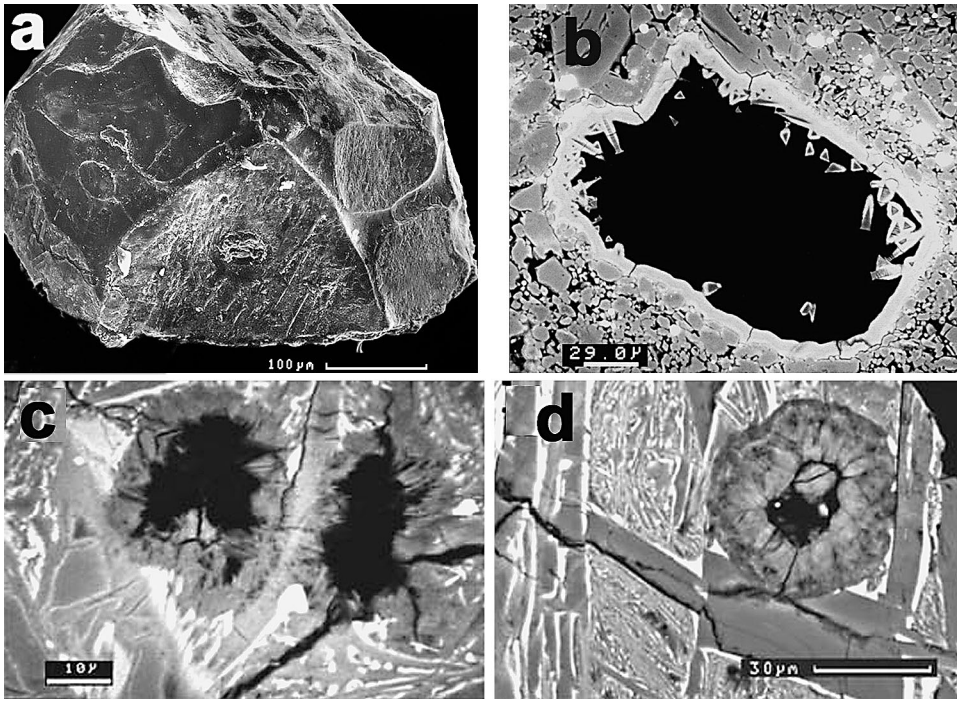

Fig. 28. (**a**) BSE images of martensite crystal from a geode. (**b**) BSE images of a cavity from a fragment #d3A. The walls of the cavity are covered by phyllosilicate coatings containing elongate crystals. (c) and (d) BSE images of cavities in #d(3–5)D with different types of coatings: crystalline (**c**) and colloform (**d**).

Under fast cooling and high supercooling the γ-phase undergoes diffusionless transformation with formation of martensite – α_2-phase with a distorted α-lattice (Gulyaev 1977). This situation frequently occurs in impact-heated ordinary chondrites. It is important that due to the nature of the formation of martensite it never forms single crystals, rather always forming thin, needlelike growths.

Metallic iron crystals from the Kaidun cavity are single crystals of α_2-Fe containing 12 wt.% Ni. In light of the above it is clear that crystal formation is unconnected with crystallization from melt and generally is not connected with high-temperature processes. The position of the crystals in the meteorite points to their formation *in situ* and thus from "local" material.

The composition of the metal crystals does not yet permit identification of a definite source for the material. The Fe/Ni ratio (7.2) suggests fractionation of material during crystal formation since this ratio contrasts sharply with the ratio of metal of the main mass of the meteorite (15–17). Taking into consideration that the crystals found in the meteorite which are a mixture of carbonaceous and enstatite chondrites and were not found in any "pure" carbonaceous chondrites, and further taking into account the alteration of metal iron in enstatite fragments of Kaidun, it appears likely that the sources of metal in the process under consideration were enstatite components of the meteorite.

Apparently the formation of the metal crystals is connected with mobilization of iron, nickel and other components from meteorite material, transport of the component in a fluid or gaseous form and subsequent deposition of the materials. The composition of such a fluid is determined by the composition of parent body material. Transport of the iron in the more usual form in terrestrial

environment – as chloride complexes in an aqueous fluid – would not be expected due to the very low chlorine content of meteorites (Anders and Grevesse 1989). Transport in the form of oxides or sulfides requires some local reduction of the metal, the mechanism of which is totally unknown. Transport of the metal in gaseous form is excluded both by the overall low temperature of the process as well as the differences in composition between Kaidun crystals and those found in the pores of lunar breccias and ordinary chondrites as shown above.

It is clear that we are dealing with an unusual geochemical process here. The process must take place at a relatively low temperature (< 350 °C) and must result in the formation of Fe,Ni crystals with unusual Fe/Ni ratio. It is proposed that the most probable form of transport of the metal is as carbonyl compounds such as $Fe(CO)_5$ and $Ni(CO)_4$. Iron pentacarbonyl $Fe(CO)_5$ forms in a rather wide range of temperature and pressure (Syrkin 1983) as a result of a reaction between carbon monoxide with pure metal or with iron oxides and salts. The presence of admixtures has a major effect on the process of forming iron pentacarbonyl. So, the presence of ammonia, water steam, hydrogen, hydrogen sulfide and sulfur contribute to carbonyl formation. The presence of hydrocarbon and oxygen has the opposite effect. A reaction of carbonyl formation is a reversible one. Since there is large increase in volume in the process of dissociation of carbonyls, reduction of pressure leads to its decay. The size of particles formed during the decay of carbonyls is reduced as the temperature rises. At a certain optimal temperature single crystals of metal can form (Syrkin 1983).

The follow general scheme can be postulated for formation of Fe,Ni crystals in the geode in Kaidun. Heating of the parent body material (during an impact?) led to thermal destruction of a carbon-bearing substance. One of the main decay products was carbon monoxide. The interaction of carbon monoxide with iron metal, and possibly with other mineral phases of the meteorite, led to the formation of highly volatile metal carbonyl complexes. Thermal decay of carbonyls due to pressure decrease during floe through a narrow crack in the meteorite led to the formation of Fe,Ni crystals.

Oxide Crystals in Cavities

Cavities with encrustations of small oxide crystals were found in two quite different clasts. The crystals are different in morphology but show a similar composition and appear to have a similar genesis.

Clast #d3A is ~2 mm in size and has a brecciated texture. Porosity varies noticeably across the clast (Ivanov et al. 2000c). The clast's main minerals are olivine and pyroxene with high variation in minor elements. Olivine ($Fa_{0.4–9.2}$, average $Fa_{5.5}$) has a variable FeO/MnO ratio (8.7–49.2, average 14.3). Pyroxenes vary from enstatite to low-Ca augite ($Fs_{0.7–11.4}Wo_{0.3–25.8}$), with FeO/MnO ratios of 3.5 to 27.6, average 9.8. Some olivine grains are enclosed within pyroxene crystals. Rounded aggregates of kamacite, taenite and tetrataenite are rimmed by troilite and pentlandite. The clast itself has a discontinuous Fe-Ni sulfide rim.

The special feature of this clast is the presence of three cavities up to 0.3 mm in size, whose shapes are close to rectangular. Large olivine crystals form the cavities' walls (Fig. 28b) creating a thin low-porosity zone. One of the cavities is partially surrounded by elongated olivine crystals whose shape conforms to the cavity walls. A thin (up to 25 µm) zoned coating covers the walls of all cavities. Two cavities contain long, thin, striped crystals (length up to 25 µm, thickness no more then 4 µm) growing inward from the walls. A shell with thickness about 4 µm covers the crystals. Some of the thin crystals lie entirely within the cavities' coatings.

The wall coatings have a low analytical total (85–90 wt.%) and their chemical compositions vary both for different cavities and for the same cavity with a trend of increasing of SiO_2, MgO and MnO contents and decreasing of TiO_2, Al_2O_3, Cr_2O_3, FeO, Na_2O, K_2O and S from the wall towards the center of cavities. As a whole, coating compositions corresponds to Al-rich serpentines. The largest striped crystal has a low analytical total of 88–89 wt.%. Its chemical composition, after

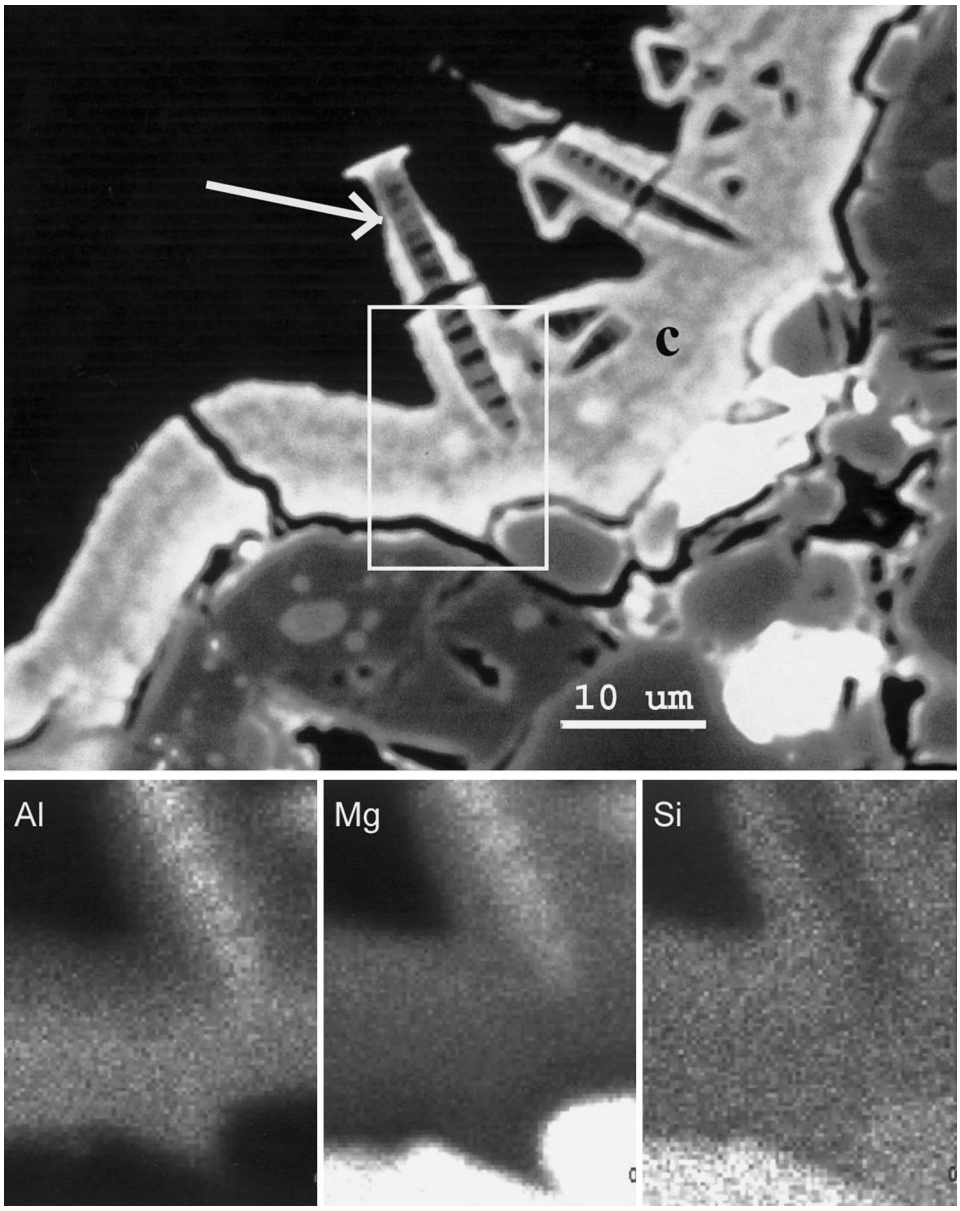

Fig. 29. BSE image of the largest crystal from the cavity shown on Fig. 28. Bladed crystal (arrow) is overgrown with a colloform coating (**c**). Also shown are Al, Mg and Si elemental maps of the area in the box indicated on the BSE image. The crystal is enriched in Al and Mg and depleted in Si.

subtracting the cavity shell material admixture, can be approximated by the formula $Mg_{11}Fe_4Al_6O_{24}{\cdot}nH_2O$. The mineral phase with this composition has not been previously observed in nature.

The cavities' large sizes and rectangular shapes appear to exclude their formation during clast agglomeration. However, the cavity characteristics suggest that the cavities may have been filled with some crystals, which were later lost. Aqueous alteration was a common process for Kaidun components. It is probable that aqueous alteration could account for the disappearance of the primary crystals, leaving the cavities, and the formation of the new thin crystals and the cavity coatings. The textural relationships indicate that the thin crystals began forming before the precipitation of the cavity coatings. The zoned structure of cavity coatings is due to changes in fluid composition over time.

Clast #d(3–5)D crystallized from a melt of essentially plagioclase composition and contains relict grains of high-Ca and low-Ca pyroxenes and fluorapatite (Ivanov et al. 2003). The textural relationship of the clast with the surrounding carbonaceous matrix indicates that clast material was plastic, or possibly even liquid during formation of clast-matrix contact. There is evidence to suggest that clast formation occurred as the result of high-velocity impact and consequent melting. A detail description of the clast #d(3–5)D was given above, so here we discuss only the features connected with clast cavities and crystals.

The cavity sizes vary from 0.5 mm down to a few tens of microns (Figs. 28c,d, 29). A thin (usually about 10 μm) coating often covers the walls of smaller cavities. The coating has two structural types – in some cases the coating is made of a brushy mass of thin needle-shaped crystals, and in others it is colloform (Fig. 29). Both coatings are commonly present in each cavity, with the colloform coating overlapping the brushy mass.

The colloform coatings have a consistently low analytical sum (85–92 wt.%) and appear to consist, according to their composition, of phyllosilicates of the serpentine group. The composition of these coatings is substantially different in different voids, but fairly constant within a given void. No chemical zoning was found in these coatings. The calculated composition of the finely crystalline coating, obtained by subtracting the suspected contribution of the colloform coating, is approximated by the formula $(Mg,Fe,Mn)_5Al_2O_8{\cdot}nH_2O$.

The formation of the clast cavities appears to be related to the presence of a fluid phase and occurred during cooling and crystallization of the melt. The presence of a fluid phase may be related to contamination by water and other volatiles from the carbonaceous matrix of the meteorite. The formation of the coatings on the cavities walls must have occurred during the final stage of formation of the clast, with the formation of the colloform coatings following that of the crystalline coatings.

Comparisons and Conclusions

The composition of the crystalline coatings of the cavities of clast #d(3–5)D – $(Mg,Fe,Mn)_5Al_2O_8{\cdot}nH_2O$ – is very similar to the $Mg_{11}Fe_4Al_6O_{24}{\cdot}nH_2O$ composition of the thin, elongated individual crystals found in the cavities of the chondritic clast #d3A. The formation of crystals of this phase in both cases appears to have occurred from a fluid of identical or extremely similar composition, and they could share a single process of formation. The difference in morphology of this phase in clasts #d3A and #d(3–5)D – elongated individual crystals in the first case and a finely crystalline brush in the second case – could reflect differences in formation temperature, but could also be due to differing crystallization rates. If it turns out that formation of this phase in clast #d(3–5)D occurred at a higher temperature than for clast #d3A, then the latter may have formed from the same fluid after its further cooling during filtration through meteorite material.

Evidence for Shock Melting

One clast from Kaidun contains large features which superficially resemble veins (Fig. 30). These areas consist of fine-grained Fe-rich phyllosilicates surrounding zoned phyllosilicate laths (Fig. 31c). The lath sizes decrease towards the boundaries of the veins. These phyllosilicates are all mixtures of serpentine and saponite. Representative microprobe analyses reveal that the lath phyllosilicates have atom Mg/Fe ratios twice as high as the surrounding groundmass phyllosilicates. This conflicts with an interpretation that groundmass phyllosilicates have replaced lath phyllosilicates, since the universal trend in C-chondrites is for second-generation phyllosilicates to be more Mg-rich than those they replace. Also, the phyllosilicate laths are compositionally zoned, with Mg-rich cores and Fe-rich rims, and contain unusually low amounts of minor elements compared to phyllosilicates in other meteorites and Kaidun lithologies.

There is a resemblance of these areas in Kaidun to shock melt veins in meteorites, where olivine and/or pyroxene skeletal/lath crystals are observed to project into a glassy mesostasis. Accordingly, we examined several shocked meteorites for comparison. In ALHA 79005 (a Martian lherzolite), the veins consist of laths of olivine exhibiting normal compositional zoning, set within a mesostasis of glass. Small grains of opaques are also present within the mesostasis. Our results from these shock melt veins are entirely consistent with previous work (McSween et al. 1979). Allowing for the very different starting materials (ALHA 79005 is a lherzolite), the petrographic similarities are striking, and the Mg/Fe trend of lath crystals/mesostasis are also similar (as would be expected for any shock melt). The major difference between the veins in Kaidun vs ALHA 79005 is that the lath crystallites in the latter are about twice as large. We therefore suggest that the Kaidun features resulted from shock melting of chondrite material (of problematic nature). Laths of zoned olivine formed within the cooling melt, with the lath grain size decreasing towards the boundaries of the veins due to faster cooling there. Melt blobs of sulfides crystallized to form pyrrhotite and pentlandite. Subsequent aqueous alteration transformed all silicates to an assemblage of serpentine and saponite, while perfectly preserving the preexisting chemical zoning and crystallite outlines (Fig. 31e). The low minor element composition of the Kaidun laths is a probable result of its formation from fairly pure olivine.

Why are shock-melting or heating textures not more commonly observed in C chondrites? Perhaps because post-heating (retrograde) aqueous alteration has generally erased the evidence of shock. Once everything has been replaced by serpentine and other hydrous materials one impact is probably all it takes to erase all petrographic evidence of shock. Also, impacts into already aqueously-altered materials would produce water vapor which would disrupt the target (Zolensky and Buchanan 1995).

Fig. 30. BSE images of a probable aqueously-altered shock melt vein in a Kaidun C2 lithology (left side), compared side by side to a shock melt vein in the shergotite ALHA 77005 (right side). (**a** and **b**) Low-magnification views of the veins. (**c** and **d**) Higher-magnification views of the arrowed regions in (**a**) and (**b**). The white phases in the Kaidun clast are pyrrhotite. (**e** and **f**) High-magnification views showing the zoned acicular crystals at the center of the veins. In ALHA 77005 (**f**)

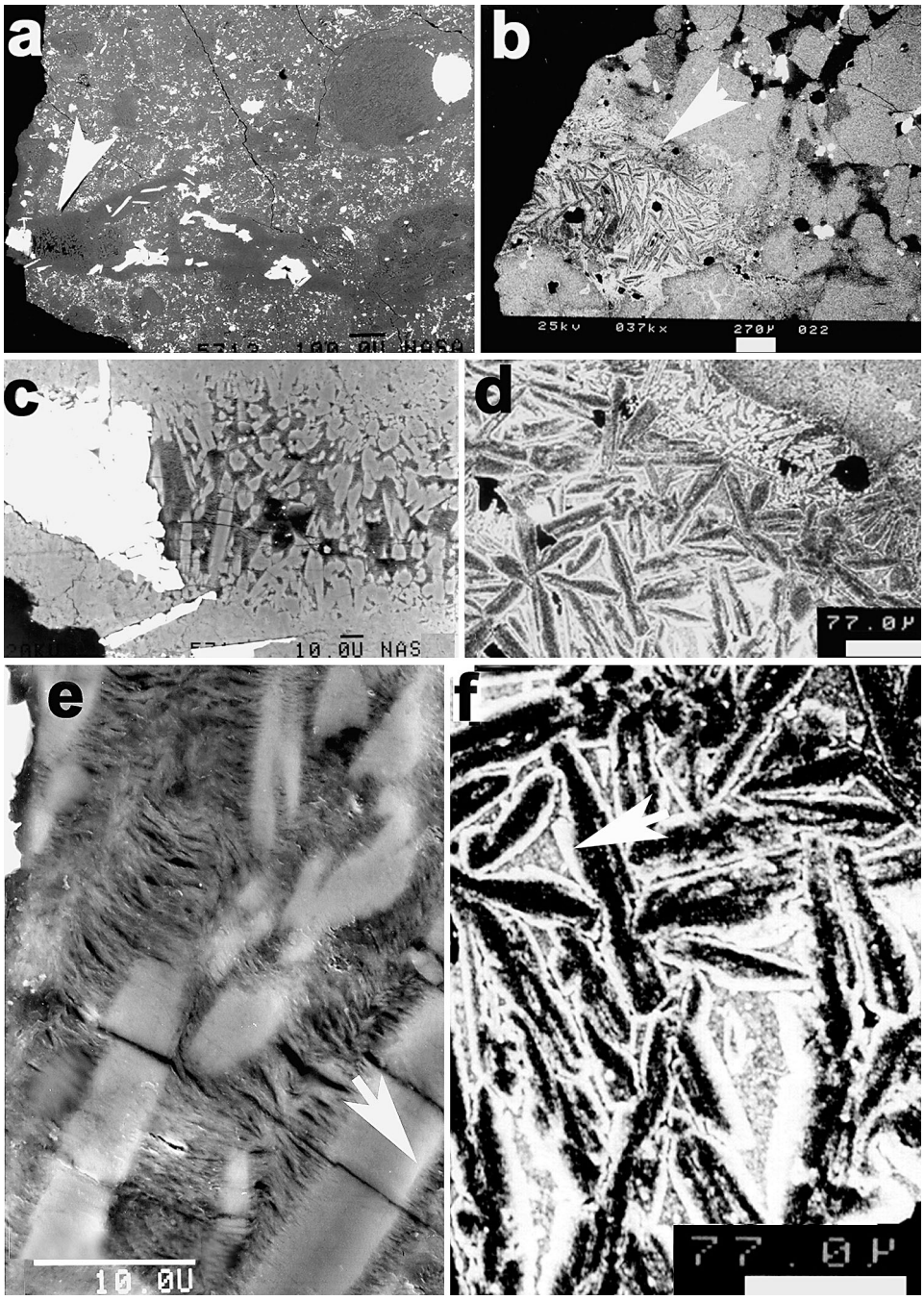

these crystals are olivine, and the mesostasis is pyroxene. In Kaidun (**e**) the crystals and mesostasis are phyllosilicates, which amazingly have preserved the original compositional zoning of the precursor shock melt veins phases (arrowed).

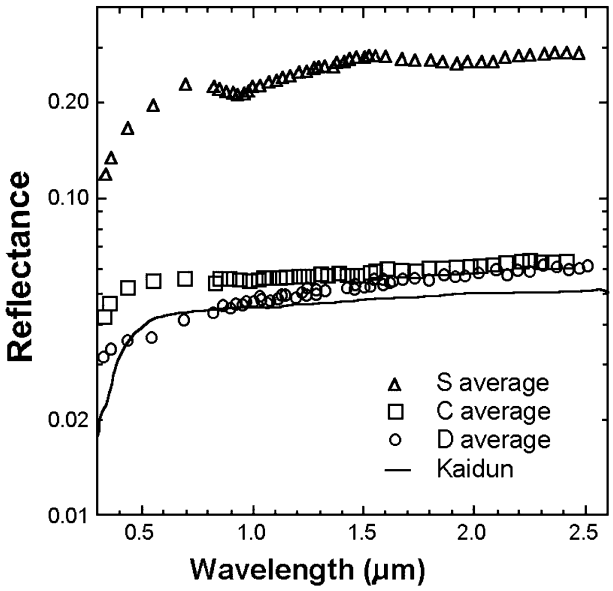

Fig. 31. Comparison of IR reflectance spectra of powdered Kaidun sample with three averaged types of asteroids: S, C and D types (Takahiro Hiroi, unpublished data). The Kaidun spectra is most similar to that of the average C type.

What Was the Parent Object of Kaidun?

It is fascinating that the Kaidun meteorite contains such a disparate assemblage of materials, ranging from CM2, CM1 to various enstatite chondrite clasts. These materials exhibit the complete range of alteration state, from fully anhydrous materials through completely altered on a very fine scale. There are even clasts which are frozen in a state of half-altered and half-unaltered. This observation requires aqueous alteration to have occurred at a different location than the place of final assembly of Kaidun. Indeed, much if not most of the materials within Kaidun must have formed on many different asteroids, and possibly other bodies as well. There is evidence that E, C, and D asteroids, at the very least, provided the various materials now in Kaidun. The mechanism for transport of these diverse materials to a single site on one parent body must have involved numerous impacts. A record of some of these impact events remains in Kaidun in the form of melt clasts and shock melt veins. Finally, some Kaidun lithologies, including the EH ones as well as some melt clasts, show evidence of incomplete, late-stage aqueous alteration otherwise unknown from these classes of materials. This observation suggests that either (1) Kaidun samples some rather unusual E-class asteroids, or else that (2) some aqueous alteration occurred on the final Kaidun parent body. Although the highly reduced nature of typical enstatite chondrites suggests that aqueous alteration was an improbable process on any E asteroid, there are spectroscopic observations of several E-class asteroids that suggest the presence there of hydrated phases (Rivkin et al. 1995).

Alkaline-rich fragments are extremely rare in meteorites, having been found only in the Adzhi-Bogdo LL3–6 chondrite (Bischoff et al. 1993) and now in Kaidun. Kaidun contains two different alkaline-rich clasts, which may be genetically related, but which differ noticeably, and probably arrived at the final assembly site for Kaidun at different times. It is therefore possible that the final Kaidun parent body lay near a source of alkaline-rich differentiated material.

Infra-red reflectance spectra of powdered bulk Kaidun are compared to the average reflectance spectra of S, C and D asteroids in Fig. 31. The spectrum of Kaidun is most similar to the C asteroids, and this is consistent with the mineralogical work we have summarized here – Kaidun consists predominantly of carbonaceous chondrite materials whose mineralogy generally masks the less abundant enstatite chondrite components. Therefore, Kaidun may have derived from an object with a C-type spectral signature.

Kaidun is important because it contains many asteroidal materials we have not seen before, providing a more complete view of the diversity of materials in the asteroid belt than has been provided by other meteorites. The Kaidun parent body must have been large in order to have accumulated clasts of many unrelated asteroids. This is possible because of the small, generally sub-millimeter-size of the component clasts in Kaidun – it is far easier for these smaller objects to scatter throughout the solar system than it is for larger, conventional-sized meteorites.

There is abundant mineralogical evidence of post-accretion aqueous alteration, requiring the final parent body to have been sufficiently large to have supported liquid water for a prolonged period. We have observed aqueously-altered enstatite chondrite clasts, as well as altered shock melt veins. Finally, Kaidun contains numerous impact shock-melt veins in carbonaceous chondrite materials, as well as completely melted clasts, which we have only just begun to recognize. These must result from collisions with higher velocities than those witnessed by typical carbonaceous chondrite asteroids. All of these attributes suggest that the parent asteroid for Kaidun was unusually large and carbonaceous, or at least has a C-type asteroid spectral signature. Such objects include the asteroid 1-Ceres, and Phobos, the large moon of Mars. If the source is indeed Phobos then perhaps the alkaline-rich clasts in Kaidun derive from the early Martian crust.

A further clue to the source of Kaidun is probably the list of asteroidal materials that are *not* included within it. The most notable omission is the ordinary chondrites. It seems very strange that Kaidun should contain samples of materials from the inner-most (E-type) and outer-most (C- and D-type) portions of the asteroid belt, but nothing from its dominant intermediate regions and the most abundant meteorite types.

Perhaps only one thing about Kaidun is certain: additional work on this meteorite will reveal new types of extraterrestrial materials we have never yet seen. As meteoritical laboratories around the world prepare for the return of nanogram-sized samples from comet Wild II, near-Earth asteroid Itokawa and the sun, courtesy of the Stardust, Hayabusa and Genesis Missions, the mm-sized clasts within Kaidun will become very attractive targets for further exploration.

Acknowledgements

The authors gratefully acknowledge unpublished data, discussions, and other assistance from many scientists from many countries, especially Franz Brandstätter, Gero Kurat, Glenn MacPherson, Duck Mittlefehldt, Natasha Kononkova, Sasha Ulyanov, Ludmila Migdisova, Taki Hiroi, Loan Le, Vincent Yang, Kazumasa Ohsumi, Doug Ming, Charlie Galindo, and Mike Weisberg and for their valuable contribution to investigations of this unique meteorite. Our Kaidun investigations were supported by NASA's Cosmochemistry Program to MEZ and the Russian Foundation for Basic Research to AVI. Finally, we thank Klaus Keil for inviting this review, thereby providing the ideal opportunity for us to harvest many years worth of unpublished data and ideas.

Appendix: Kaidun mineralogy.

Mineral or mineral phase	Formula, chemical features	Type of occurrence	Source
Graphite	C	Metal grains in EH fragments	1
Diamond	C	Carbonaceous chondrite material	2
Kamacite	α-Fe,Ni (Si <0.1 wt %)	CR material	3
Kamacite	α-Fe,Ni (Si 0.5–3.5 wt %)	Enstatite chondrite fragments	3
Martensite	α_2-Fe,Ni	Geode	4
Taenite	γ-Fe,Ni	Chondritic fragment	5
Tetrataenite	FeNi	Chondritic fragment	5
Perryite	$(Ni,Fe)_5(Si,P)_3$	Metal grains in EH fragments	1
Schreibersite	$(Fe,Ni)_3P$	Enstatite chondrite fragments	3
Florenskyite♦	FeTiP	Small grains in an elongate phyllosilicate grain	6
Fe,Cr-phosphide♦*	$(Fe,Ni)_5(Cr,V)_1(P,Si)_3$	Small laths in an elongate phyllosilicate grain	6
Fe,Cr-phosphide*	$(Fe,Ni)_4(Cr,V,Ti)_2(P,Si)_3$	Small laths in an elongate phyllosilicate grain	6
Troilite	FeS	Common	–
Pyrrotite	$(Fe,Ni)_{1-x}S$	Carbonaceous chondrite material	7
Pentlandite	$(Fe,Ni)_9S_8$	Carbonaceous chondrite material	7
Cubanite	$CuFe_2S_3$	A grain in carbonaceous matrix	8
Niningerite	(Mg,Fe,Mn)S (Ca < 1, Mn 10–13 wt %)	EH fragments	3
Ca,Mn-niningerite♦	(Mg,Mn,Fe,Ca)S (Ca~5, Mn~18 wt %)	Sulfide nodules in enstatite aggregates	9
Alabandite	(Mn,Fe,Mg)S	EL fragments	3
Oldhamite	CaS	Small grains in EH fragment	10
Sphalerite	ZnS	A grain in EH fragment	10
Heideite	$(Fe,Cr)(Ti,Fe)_2S_4$	Sulfide nodules in enstatite aggregates	9
Djerfisherite	$K_5(Cu,Na)(Fe,Ni)_{12}(S,Cl)_{14}$	One grain in one EH fragment	3
Na-sulfide♦*	Na_2S_2	Small inclusion in metal nodule in one EH fragment	11
Schöllhornite	$Na_{0.3}(H_2O)[CrS_2]$	Small inclusion in metal nodule in one EH fragment	11
Daubreelite	$FeCr_2S_4$	A grain in one EH fragment	19
Iron-chromium sulfide♦*	$FeCr_2S_4.nH_2O$	EH fragments	3
Fluorapatite	$Ca_5(PO4)_3(F)$	Alkaline enriched fragments	12
Hydroxylapatite	$Ca_5(PO4)_3(OH)$	CM1 fragment	7
Calcite	$CaCO_3$	Carbonaceous chondrite material mainly	13
Dolomite	$CaMg(CO_3)_2$	Carbonaceous chondrite material	13
Magnetite	Fe_3O_4	Carbonaceous chondrite material	7
Chromite	$FeCr_2O_4$	Chondritic fragment	16

Spinel	$MgAl_2O_4$	CAI	14
Hibonite	$CaA_{12}O_{19}$	CAI	14
Perovskite	$CaTiO_3$	CAI	14
Mg,Al-hydroxide♦*	$5(Mg,Fe)O \cdot Al_2O_3 \cdot nH_2O$	Small crystals in cavities in different fragments	5
Melilite	$Ca_2(Mg,Al)(Si,Al)_2O_7$	CAI	14
Andradite	$Ca_3Fe_2(SiO_4)_3$	Serpentine lump in carbonaceous matrix	15
Melanite (Ti-andradite)	$Ca_3Fe_2(SiO_4)_3$ (TiO_2 ~3 wt %)	CM1 fragment	7
Quartz	SiO_2	EH fragments	10
Cristobalite	SiO_2	EH fragments	19
Olivine	$(Mg,Fe)_2SiO_4$	Common	–
Forsterite	Mg_2SiO_4	Common	–
Enstatite	$Mg_2Si_2O_6$	Common	–
Diopside	$CaMgSi_2O_6$	Common	–
Endiopside	En68Wo32	CM1 fragment	7
Pigeonite	En47Fs43Wo10	Melted alkaline enriched fragment	17
Augite	En24Fs32Wo36	Melted alkaline enriched fragment	17
Roedderite	$(Na,K)_2Mg_5Si_{12}O_{30}$	Small inclusion in metal nodule in one EH fragment	11
Albite	$NaAlSi_3O_8$	Large single crystal and small grains in EH fragments	12
Anorthoclase	$(Na,K)AlSi_3O_8$	Small grains in melted alkaline enriched fragment	12
Plagioclase	Ab_nAn_{1-n}	Lamellae in melted alkaline enriched fragment	12
Aenigmatite●	$Na_2Fe^{2+}{}_5TiSi_6O_{20}$	Large albite crystal	12
Chabazite-Na●	$(Na_2,K_2,Ca,Mg)(Al_2Si_4O_{12}) \cdot 6(H_2O)$	Heated fragment in a C2 clast	12
Wilkinsonite●	$Na_2Fe^{2+}{}_4Fe^{3+}{}_2Si_6O_{20}$	Large albite crystal	12
Arfvedsonite	$(Na,Ca)(Mg,Fe^{2+})Fe^{3+}Si_8O_{22}(OH)_2$	Large albite crystal	12
Serpentite	$(Mg,Fe)_6Si_4O_{10}(OH)_8$	Carbonaceous chondrite material	7
Cronstedtite – greenalite	$Fe^{2+}{}_2Fe^{3+}(SiFe^{3+})O_5(OH)_4$ – $-(Fe^{2+},Fe^{3+})_{2-3}Si_2Fe^{3+})O_5(OH)_4$	Altered parts of metal iron in enstatite chondrite fragments	3
Saponite	$(Ca,Na)_{0.3}(Mg,Fe)_3(Si,Al)_4O_{10}(OH)_2.H_2O$	Carbonaceous chondrite material	7
Talk	$(Mg,Fe)_3Si_4O_{10}(OH)_2$	Carbonaceous chondrite material	12
Clinochlore	$(Mg,Fe^{2+})_5Al(Si_3Al)O_{10}(OH)_8$	CM1 fragment	7
"Hydro-ferrosilite"♦	$FeSiO_3 \cdot nH_2O$	Grains in one EH fragment	18

● the first find in meteorites; ♦ the first find in nature, * previously undescribed phase

Sources: 1 – Grokhovsky and Ivanov 1986; 2 – Fisenko et al 2000; 3 – Ivanov et al 1986; 4 – Ivanov 1989a; 5 – Ivanov et al 2000c; 6 – Ivanov et al 2000a; 7 – Zolensky et al 1996; 8 – Kurat private communication; 9 – Kurat et al 1997; 10 – Ivanov et al 1997; 11 – Ivanov et al 1996; 12 – Ivanov et al 2003; 13 – Weisberg et al 1994; 14 – MacPherson et al 1994; 15 – Brandstätter et al 1998; 16 – Brandstätter et al 1996; 17 – Ivanov et al 2001a; 18 – Ivanov et al 1998; 19 – Ivanov unpublished data; 20 – Zolensky unpublished data.

References

Akai J (1990) Mineralogical evidence of heating events in Antarctic carbonaceous chondrites, Y-86720 and Y-82162. Proc NIPR Symp Antarctic Meteorit, No. 3, 55–68

Akai J (1992) T-T-T diagram of serpentine and saponite, and estimation of metamorphic heating degrees of Antarctic carbonaceous chondrites. Proc NIPR Symp Antarctic Meteorit, No. 5, 120–135

Anders E, Grevesse N (1989) Abundances of elements: Meteoritic and solar. Geochim Cosmochim Acta **53**, 197–214

Ariskin AA, Petaev MI, Borisov AA, Barmina GS (1997) METEOMOD: A numerical model for the calculation of melting-crystallization relationships in meteoritic igneous systems. Meteorit Planet Sci **32**, 123–133

Barnhisel RI, Bertsch PM (1989) Chlorites and hydroxy-interlayered vermiculite and smectite. In Minerals in Soil Environments, Soil Sci. Soc. Amer

Binns RA (1967) Structure and evolution of non-carbonaceous chondritic meteorites. Earth Planet Sci Lett **2**, 23–28

Bischoff A, Geiger T, Palme H, Spettel B, Schultz L, Scherer P, Schluter J, Lkhamsuren J (1993) Mineralogy, chemistry, and noble gas contents of Adzhi-Bogdo – an LL3–6 chondritic breccia with L-chondritic and granitoidal clasts. Meteoritics **28**, 570–578

Bourcier WL and Zolensky ME (1991) Aqueous alteration on the parent bodies of carbonaceous chondrites: Computer simulations of late-stage oxidation (abstract). Meteoritics **26**, 321–322

Bourcier WL and Zolensky ME (1992) Computer modeling of aqueous alteration on carbonaceous chondrite parent bodies (abstract). Lunar Planet Sci **23**, 143–144

Brandstätter F, Ivanov AV, Kurat G (1996) An ordinary chondrite fragment (R3) in the Kaidun carbonaceous chondrite (abstract). Meteorit Planet Sci **31**, A20

Brandstätter F, Ivanov A, Kurat G (1998) The Kaidun meteorite: Postaccretionary andradite-magnetite-serpentine precipitation (abstract). Meteorit Planet Sci **33**, A22–A23

Browning LB, McSween HY Jr, Zolensky ME (1993) Determining the relative extent of alteration in CM chondrites (abstract). Lunar Planet Sci **24**, 203–204

Browning L, McSween HY Jr, Zolensky ME (1996) Correlated alteration effects in CM carbonaceous chondrites. Geochim Cosmochim Acta **60**, 2621–2633

Bunch TE, Keil K, Olsen E (1970) Mineralogy and petrology of silicate inclusions in iron meteorites. Contrib Miner Petrol **25**, 297–340

Carter JL, MacGregor ID (1970) Mineralogy, petrology and surface features of some Apollo 11 samples. Proc Apollo 11 Lunar Sci Conf **1**, 247–265

Clanton US, McKay DS, Laughon RB, Ladle GH (1973) Iron crystals in lunar breccias. Proc Lunar Sci Conf **4**, 925–931

Clanton US, McKay DS, Laughon RB, Ladle GH (1974) Vapor-phase crystallization of iron in lunar breccias. Proc Lunar Sci Conf **5**, 621–626

Clayton RN, Mayeda TK, Ivanov AV, MacPherson GJ (1994) Oxygen isotopes in Kaidun. Lunar Planet Sci **25**, 269–270

Crozaz G, Lundberg LL (1995) The origin of oldhamite in unequilibrated enstatite chondrites. Geochim Cosmochim Acta **59**, 3817–3831

Deer WA, Howie RA, Zussman J (1962) Rock-Forming Minerals. Vol. 3. Sheet Silicates. J. Wiley and Sons, New York

Deer WA, Howie RA, Zussman J (1982) Rock-Forming Minerals. Vol. 1A. Orthosilicates. Longman, London

Duggan MB (1990) Wilkinsonite, $Na_2Fe^{2+}{}_4\ Fe^{3+}{}_2Si_6O_{20}$, a new member of the aenigmatite group from the Warrumbungle Volcano, New South Wales, Australia. Am Mineral **75**, 694–701

Eckstrand OR (1975) The Dumont serpentinite: A model for control of nickeliferous opaque mineral assemblages by alteration reactions in ultramafic rocks. Economic Geology **70**, 183–201

Ehlers K, El Goresy A (1988) Normal and reverse zoning in niningerite: A novel key parameter to the thermal histories of EH-chondrite. Geochim Cosmochim Acta **52**, 877–887

Fisenko AV, Verchovsky AB, Semjonova LF, Ott U, Pillinger C, Ivanov AV (2000) Presolar diamond in CR and CI clasts of the Kaidun meteorite (abstract). Lunar Planet Sci **31**, #1834 (CD-ROM)

Florensky KP, Ivanov AV, Tarasov LS, Stakheev YuI, Rode OD (1974) Morphology and types of particles of the regolith sample from Mare Foecunditatis. In: Lunar sample from Mare Foecunditatis. Nauka Press, Moscow

Frondel JW (1975) Lunar Mineralogy. J.Wiley and Sons, New York

Godlevskiy MN, Likhachev AP, Chuvikina NG, Andronov AD (1971) Hydrothermal synthesis of pentlandite. Doklady Akad Nauk SSSR **196**, 146–149

Gooding JL, Zolensky ME (1987) Thermal stability of tochilinites (abstract). Lunar Planet Sci **18**, 343–344
Greshake A, Bischff A, Putnis A, Palme H (1996) Corundum, rutile, periclase, and CaO in Ca,Al-rich inclusions from carbonaceous chondrites. Science **272**, 1316–1318
Grokhovsky VI, Ivanov AV (1986) Kamacite-perrtite-graphite assemblages in the Kaidun III meteorite (abstract). Lunar Planet Sci **17**, 291–292
Grove TL, Bence AE (1979) Crystallization kinetics in a multiply saturated basalt magma: An experimental study of Luna 24 ferrobasalt. Proc Lunar Planet Sci Conf **10**, p. 439–478
Gulyaev AP (1977) Metallurgical Science. Metallurgy Press, Moscow, 258–269
Hiroi T, Zolensky M, Pieters C (2001) The Tagish Lake Meteorite: A Possible Sample from a D-Type Asteroid**.** Science **293**, 2234–2236
Hsu W (1998) Geochemical and petrographic studies of oldhamite, diopside, and roedderite in enstatite meteorites. Meteorit Planet Sci **33**, 291–301
Hutcheon I, Weisberg MK, Phinney DL, Zolensky ME, Prinz M, Ivanov AV (1999) Radiogenic ^{53}Cr In Kaidun Carbonates: Evidence For Very Early Aqueous Activity (abstract). Lunar Planet Sci **30**
Ikeda Y (1989) Petrochemical study of the Yamato-691 enstatite chondrite (E3). IV: Descriptions and mineral chemistry of opaque-mineral nodules. Proc NIPR Symp Antarct Meteorit **2**, 109–146
Ivanov AV, Skripnic AYa, Ulyanov AA, Barsukova LD, Kolesov GM, Kononkova NN (1986) Chemical composition, mineralogy and geochemical characteristics of the Kaidun new meteorite. Meteoritika **45**, 3–19 (in Rus)
Ivanov AV, Khisina NR, Kononkova NN, Petushkova LV (1988) Iron crystal in the Kaidun meteorite: A process of new type? (abstract) Lunar Planet Sci **19**, 529–530
Ivanov AV (1989a) The Kaidun meteorite: Composition and history. Geochem Internat **26 (9)**, 84–91
Ivanov AV (1989b) Formation of nickel-iron crystals in the Kaidun meteorite: The role of carbonyl compounds. Doklady AN SSSR **308**, 712–716 (in Rus)
Ivanov AV, Kononkova NN, Guseva YeV (1993) Hydrothermal alteration of schreibersite and metallic iron in Kaidun III meteorite (EH5). Geochem Internat **30**, 11–19
Ivanov AV, Brandstätter F, Zolensky ME, Kononkova NN (1996a) The Kaidun meteorite: Melt deposits on the surface of some particles (abstract). Lunar Planet Sci **27**, 585–586
Ivanov AV, MacPherson GJ, Zolensky ME, Kononkova NN, Migdisova LF (1996b) The Kaidun meteorite: Composition and origin of inclusions in the metal of the enstatite chondrite clast. Meteorit Planet Sci **31**, 621–626
Ivanov AV, Migdisova LF, Zolensky ME, MacPherson GJ, Kononkova NN (1997) The Kaidun meteorite: An enstatite chondrite fragment with unusual inclusion in the metal. Geochem Internat **35**, 318–328
Ivanov AV, Kurat G, Migdisova LF, Brandstätter F, Kononkova NN (1998) The Kaidun meteorite: Pre- and postaccretionary aqueous alterations of metal in an enstatite chondrite fragment. Geochem Internat **36**, 101–106
Ivanov AV, Zolensky ME, Saito A, Ohsumi K, Yang SV, Kononkova NN, Mikouchi T (2000a) Florenskyite, FeTiP, a new phosphide from the Kaidun meteorite. Am Mineral **85**, 1082–1086
Ivanov AV, Zolensky ME, Yang SV, Ariskin AA (2000b) The Kaidun meteorite: Fast crystallization of a fragment from a superheated melt (abstract). Meteorit Planet Sci **35**, A82–A83
Ivanov AV, Zolensky ME, Yang SV (2000c) The Kaidun meteorite: Evidence for aqueous alteration and precipitation (abstract). Meteorit Planet Sci **35**, A82
Ivanov AV, Kononkova NN, Zolensky ME, Migdisova LF, Stroganov IA (2001a) The Kaidun meteorite: A large albite crystal – fragment of an alkaline rock (abstract). Lunar Planet Sci **32**, #1386 (CD-ROM)
Ivanov AV, Zolensky ME, Kononkova NN, Yang SV, Migdisova LF (2001b) The Kaidun meteorite: A melted clast of subalkaline rock (abstract). Meteorit Planet Sci **36**, A87
Ivanov AV, Kononkova NN, Zolensky ME, Migdisova LF, Stroganov IA (2002a) Kaidun meteorite: An alkaline rock fragment. Geochem Internat **40**, 694–697
Ivanov AV, Kurat G, Brandstätter F, Kononkova NN, Migdisova LF (2002b) The Kaidun meteorite: An enstatite aggregate with sulfide-oxide inclusions. Geochem Internat **40**, 1139–1145
Ivanov AV, Kononkova NN, Yang SV, Zolensky ME (2003) The Kaidun meteorite: Clasts of alkaline-rich fractionated materials. Meteorit Planet Sci **37**, (in press)
Jones AP (1984) Mafic silicates from the nepheline syenites of the Motzfeld centre, South Greenland. Min Mag **48**, 1–12
Keil K (1968) Mineralogical and chemical relationships among enstatite chondrites. J Geophys Res **73**, 6945–6976
Keil K, Brett R (1974) Heideite, $(Fe,Cr)_{1+x}(Ti,Fe)_2S_4$, a new mineral in the Bustee enstatite achondrite. Am Min **59**, 465–470

Keil K (1982) Composition and origin of chondritic breccia. In: Workshop on lunar breccias and soil and their meteoritic analogs, LPI Tech. Rep. 82–02, 65–83
Keil K, Ntaflos Th, Taylor GJ, Brearley AJ, Newsom HE, Roming AD Jr. (1989) The Shallowater aubrite: Evidence for origin by planetesimal impacts. Geochim Cosmochim Acta **53**, 3291–3307
Kerridge JF (1985) Carbon, hydrogen and nitrogen in carbonaceous chondrites: Abundances and isotopic compositions in bulk samples. Geochim Cosmochim Acta **49**, 1707–1714
Kimura M (1988) Origin of opaque minerals in an unequilibrated enstatite chondrite Yamato-691. Proc NIPR Symp Antarct Meteorit **1**, 51–64
Kimura M, El Goresy A (1989) Discovery of E-chondrite assemblages, SiC, and silica-bearing objects in ALH85085: Link between E- and C-chondrites (abstract). Meteoritics **24**, 286
Kimura M, Lin Y-T, Ikeda Y, El Goresy A, Yanai K, Kojima H (1993) Mineralogy of antarctic aubrites Yamato-793592 and Allan Hills-78113: Comparison with non-antarctic aubrites and E-chondrites. Proc NIPR Symp Antarct Meteorit **6**, 186–203
King TVV, King EA (1978) Grain size and petrography of C2 and C3 carbonaceous chondrites. Meteoritics **13**, 47–72
Klock W, Thomas KL, McKay DS, Palme H (1989) Unusual olivine and pyroxene composition in interplanetary dust and unequilibrated ordinary chondrites. Nature **339**, 126–128
Krot AN, Scott ERD and Zolensky ME (1995) Mineralogic and chemical variations among CV3 chondrites and their components: Nebular and asteroidal processing. Meteoritics **30**, 748–775
Kurat G, Zinner E, Brandstätter F (1992) An ion microprobe study of an unique oldhamite-pyroxenite fragment from the Bustee aubrite (abstract). Meteoritics **27**, 246–247
Kurat G, Zinner E, Brandstätter F, Ivanov A (1997) The Kaidun meteorite: An enstatite clast with niningerite and heideite as trace element carriers (abstract). Meteorit Planet Sci **32**, A76–A77
Leitch CA, Smith JV (1982) Petrography, mineral chemistry and origin of type I enstatite chondrites. Geochim Cosmochim Acta **46**, 2083–2097
Lin YT, Kimura M, El Goresy A (1990) Discovery of a new aqueous Fe-Cr-sulfide in some enstatite chondrites (abstract). Meteoritics **25**, 379
Lindsley DH (1983) Pyroxene thermometry. Amer Mineral **68**, 477–493
Lipschutz ME, Zolensky ME, Bell MS (1999) New petrographic and trace element data on thermally metamorphosed carbonaceous chondrites. Proc NIPR Symp Antarctic Meteorit, No. 12, 57–80
Lodders K (1996) Oldhamite in enstatite achondrites (aubrites). Proc NIPR Symp. Antarct Meteorites **9**, 127–142
Lofgren G (1974) An experimental study of plagioclase crystal morphology: Isothermal crystallization. Amer J Science **74**, 243–273
Lofgren G (1980) Experimental studies on the dynamic crystallization of silicate melt. In: Physics of Magmatic Processes. Princeton University Press, Princeton, New Jersey, 487–551
Lugmair GW, Shukolyukov A (1998) Early solar system timescales according to 53Mn–53Cr systematics. Geochim Cosmochim Acta 62, 2863
MacPherson GJ, Davis AM, Ivanov A (1994) Refractory inclusions in the Kaidun carbonaceous chondrite breccia (abstract). Meteoritics **29**, 494
Marshall R, Keil K (1965) Polymineralic inclusions in the Odessa iron meteorites. Icarus **4**, 461–479
McCoy TJ (1998) A pyroxene-oldhamite clast in Bustee: Igneous aubritic oldhamite and a mechanism for the Ti enrichment in aubritic troilite. Antarctic Meteorit Res **11**, 32–48
McKay DS, Greenwood WR, Morrison DA (1970) Origin of small lunar particles and breccia from Apollo 11 site. Proc Apollo 11 Lunar Sci Conf **1**, 673–694
McKay DS, Clanton US, Morrison DA, Ladle GH (1972) Vapor phase crystallization in Apollo 14 breccias. Proc Lunar Sci Conf 3rd **1**, 739–752
McSween HY Jr, Taylor LA, Stolper EM (1979) Allan Hills 77004: A new meteorite type found in Antarctica. Science **204**, 1201–1203
McSween HY Jr. (1987) Aqueous alteration in carbonaceous chondrites: Mass balance constraints on matrix mineralogy. Geochim Cosmochim Acta **51**, 2469–2477
McSween HY Jr., Riciputi LR, Paterson BA (1997) Fractionated sulfur isotopes in sulfides of the Kaidun meteorite. Meteorit Planet Sci **32**, 51–54
Meibom A, Clark BE (1999) Evidence for the insignificance of ordinary chondritic material in the asteroidal belt. Meteorit Planet Sci **34**, 7–24
Meyer C (1998) Mars Meteorite Compendium. NASA JSC, Houston, Texas
Migdisova LF, Ivanov AV, Kononkova NN, Brandstätter F, Kurat G (2000) The Kaidun meteorite: A fragment of a high-calcium primitive achondrite. Geochem Internat **38**, Suppl.3, S369–S374

Misra KC, Fleet ME (1973) The chemical composition of synthetic and natural pentlandite assemblages. Economic Geology **68**, 518–539
Mitrofanova FL, Afanas'eva LI (1966) Aenigmatite from alkaline syenites of Eastern Sayane. Doklady AN SSSR **166**, 444 (in Rus)
Nehru CE, Prinz M, Weisberg MK, Delaney JS (1984) Parsa: an unequilibrated enstatite chondrite (DEC) with an aubrite-like impact melt clast (abstract). Lunar Planet Sci **15**, 597–598
Olsen EJ, Bunch TE, Jarosewich E, Huss GJ (1976) Happy Canyon: An E7 enstatite chondrite. Meteoritics **11**, 348–349
Olsen EJ (1981) Vugs in ordinary chondrites. Meteoritics **16**, 45–59
Olsen EJ, Davis AM, Hutcheon ID, Clayton RN, Mayeda TK, Grossman L (1988) Murchison xenoliths. Geochim Cosmochim Acta **52**, 1615–1626
Patzer A, Hill DH, Boynton WV (2001) Itqiy: A metal-rich enstatite meteorite with achondritic texture. Meteorit Planet Sci **36**, 1495–1505
Perron C, Bourot-Denise M, Pellas P, Marti K (1990) Si-, P-, Cr-bearing inclusions in Fe-Ni of ordinary Chondrites (abstract). Meteoritics **25**, 398–399
Petaev MI, Skripnik AYa (1983) Mineral composition of the enstatite chondrites. Meteoritika **42**, 86–92 (in Rus)
Petaev MI, Wood JA (1998) The condensation with partial isolation (CWPI) model of condensation in the solar nebula. Meteorit Planet Sci **33**, 1123–1137
Prinz M, Nehru CE, Weisberg MK, Delaney JS (1984a) Type 3 enstatite chondrites: A newly recognized group of unequilibrium enstattite chondrites (UEC's) (abstract). Lunar Planet Sci **15**, 653–654
Prinz M, Nehru CE, Weisberg MK, Delaney JS, Yanai K (1984b) Yamato-691, a Type 3 enstatite chondrite: Relationship with other unequilibrium enstattite chondrites (UEC's). NIPR Symp Antarc Meteor **9**, 14–18
Rambaldi ER, Housley RM, Rajan RS (1983a) Unusual mineral assemblages and textures in Qingzhen enstatite chondrite (abstract). Meteoritics **18**, 380–381
Rambaldi ER, Rajan RS, Wang D (1983b) Chemical and textural study of Qingzhen, a highly unequilibrated enstatite chondrite (abstract). Lunar Planet Sci **14**, 626–627
Rivkin AS, Howell ES, Britt DT, Lebofsky LA, Nolan MC, Branston DD (1995) 3-µm spectroscopic survey of M- and E-class asteroids. Icarus **117**, 90–100
Romig AD Jr, Goldstein JI (1981) Low temperature phase equilibria in the Fe-Ni and Fe-Ni-P systems: Application to the thermal history of metallic phases in meteorites. Geochim Cosmochim Acta **45**, 1187–1197
Rubin AE (1983) The Atlanta enstatite chondrite breccia. Meteoritics **18**, 113–121
Rubin AE, Keil K (1983) Mineralogy and petrology of the Abee enstatite chondrite breccia and its dark inclusions. Earth Planet Sci Letts **62**, 118–131
Rubin AE (2003) Post-shock annealing and post-annealing shock: Implications for the thermal and shock histories of ordinary-chondrite parent bodies (abstract). Lunar Planet Sci **34**, #1263 (CD-ROM)
Samsonov GV, Drozdova SV (1972) Sulfides. Metallurgiya Press, Moscow (in Rus)
Skinner BJ, Luce FD (1971) Solid solutions of the type (Ca,Mg,Mn,Fe)S and their use as geothermometer for the enstatite chondrites. Am Mineral **56**, 1269–1295
Stolz AJ (1986) Mineralogy of the Nandewer Volcano, northeastern New South Wales, Australia. Min Mag **50**, 241–255
Syrkin VG (1983) Carbonyls of metals. Chemistry Press, Moscow (in Rus)
Ulyanov AA, Ivanov AV, Brandstätter F, Kurat G, Biryukov VV (1994) Spinel-rich metasomatized CAI from Kaidun (abstract). Meteoritics **29**, 542–543
Varet J (1970) The origin of fumarolic andradite at Menoyre, France and Fant'Ale, Ethiopia. Contr Mineral Petrol **27**, 321–332
Walker D, Lonhi J, Hays JF (1972) Experimental petrology and origin of Fra Mauro rocks and soil. Proc Lunar Sci Conf **3**,797–817
Weisberg MK, Prinz M, Clayton RN, Mayeda T.K. (1993) The CR (Renazzo-type) carbonaceous chondrite group and its implications. Geochim Cosmochim Acta **57**, 1567–1586
Weisberg MK, Prinz M, Zolensky ME and Ivanov AV (1994) Carbonates in the Kaidun chondrite. Meteoritics **29**, 549–550
Wheelock MM, Keil K, Floss C, Taylor GJ, Crozaz G (1994) REE geochemistry of oldhamite-dominated clasts from the Norton County aubrite: Igneous origin of oldhamite. Geochim Cosmochim Acta **58**, 449–458
Wilson L, Keil K, Browning LB, Krot AN, Bourcier WL (1999) Early aqueous alteration, explosive disruption, and reprocessing of asteroids. Meteorit Planet Sci **34**, 541–557
Zanda B, Bourot-Denise M, Perron C (1990) Inclusions in the metal of the Leoville CV3 chondrite (abstract). Meteoritics **25**, 422–423

Zanda B (1992) Inclusions in the metal of ALH85085: New clues to a condensation origin (abstract). Lunar Planet Sci **23**, 1569–1570

Zolensky ME, Bourcier WL, Gooding JL (1989) Aqueous alteration on the hydrated asteroids: Results of EQ3/6 computer simulations. Icarus **78**, 411–425

Zolensky ME, Lindstrom DJ (1992) Mineralogy of 12 large „chondritic" interplanetary dust particles. Proc Lunar Planet Sci Conf **19**. LPI, Houston, 161–169

Zolensky ME, Barrett RA, Browning L (1993) Mineralogy and composition of matrix and chondrule rims in carbonaceous chondrites. Geochim Cosmochim Acta **57**, 3123–3148

Zolensky ME, Barrett R (1994) Chondritic interplanetary dust particles: Basing their sources on olivine and pyroxene compositions. Meteoritics **29**, 616–620

Zolensky ME, Buchanan PC (1995) Evidence for shock melting and parent body heating in CR and CV chondrites (abstract). Lunar Planet Sci **26**, 1565–1566

Zolensky ME, Ivanov AV, Yang V, Ohsumi K (1996) The Kaidun meteorite: Mineralogy of an unusual CM1 clast. Meteorit Planet Sci **31**, 484–493

Zolensky ME, Mittlefehldt DW, Lipschutz ME, Wang M-S, Clayton RN, Mayeda T, Grady MM, Pillinger C, Barber D (1997) CM chondrites exhibit the complete petrologic range from type 2 to 1. Geochim Cosmochim Acta **61**, 5099–5115

Zolensky ME, Nakamura K, Gounelle M, Mikouchi T, Kasama T, Tachikawa O, Tonui E (2002a) Mineralogy of Tagish Lake: An ungrouped type 2 carbonaceous chondrite. Meteorit Planet Sci **37**, 737–761

Zolensky ME, Nakamura K, Cheng AF, Cintala MJ, Horz F, Morris RV, Criswell D (2002b) Meteoritic evidence for the mechanism of pond formation on asteroid Eros (abstract). Lunar Planet Sci **33** (CD-ROM)